COMENIUS UNIVERSITY IN BRATISLAVA

FACULTY OF MATHEMATICS, PHYSICS AND INFORMATICS

Mgr. Jozef Klimo

Properties and Production Possibilities of Exotic Nuclei

Academic Dissertation for the Degree of Doctor of Philosophy

Study Program:	4.1.5 Nuclear and Sub-Nuclear Physics
Educational institution:	Institute of Physics, SAS Bratislava
Head Supervisor:	Mgr. Martin Veselský, PhD

Bratislava, 2019

Protokol o kontrole originality

Kontrolovaná práca

Citácia	Percento*
Properties and production possibilities of exotic nuclei / autor Klimo Jozef, Mgr. - školiteľ Veselský Martin, Mgr., PhD. - FMFI / FMFI.KJFB. - Bratislava, 2019. - 112 *plagID: 1633902 typ práce: dizertačná zdroj : UK.Bratislava*	**0,25%**

* Číslo vyjadruje percentuálny podiel textu, ktorý má prekryv s indexom prác korpusu CRZP. Intervaly grafického zvýraznenia prekryvu sú nastavené na [0-20, 21-40, 41-60, 61-80, 81-100].

Informácie o extrahovanom texte dodanom na kontrolu

Dĺžka extrahovaného textu v znakoch: 239370
Počet slov textu: 24853

Početnosť slov - histogram

Dĺžka slova	3	4	5	6	7	8	9	10	11	12	13	14	15	16	17	18	19	20	21	22	23	24	25
Indik. odchylka	>>	>>	=	=	=	=	=	=	=	=	=	=	<<	=	=	=	=	=	=	=	=	=	=

* Odchýlky od priemerných hodnôt početnosti slov. Profil početností slov je počítaný pre korpus slovenských prác. Značka ">>" indikuje výrazne viac slov danej dĺžky ako priemer a značka "<<" výrazne menej slov danej dĺžky ako priemer. Výrazné odchylky môžu indikovať manipuláciu textu. Je potrebné skontrolovať "plaintext" !Priveľa krátkych slov indikuje vkladanie oddelovačov, alebo znakov netradičného kódovania. Privela dlhých slov indikuje vkladanie bielych znakov, prípadne iný jazyk práce.

Práce s nadprahovou hodnotou podobnosti

Dok.	Citácia	Percento*
1	**Vývoj zosilňovačov pre germániové detektory a zberový systém Pixie-16** / autor Bírová Monika - školiteľ Slugeň Vladimír, prof., Ing., DrSc. - oponent Petriska Martin, Ing., PhD. - FEI / ÚJFI (FEI). - Bratislava, 2019 *plagID: 1621731 typ práce: bakalárska zdroj : STU.Bratislava*	**0,18%**
2	**Použitie hmotnostnej spektrometrie v skúmaní jadrových reakcií vyvolaných ťažkými iónmi** / autor Motyčák Štefan, Ing. - školiteľ Kliman Ján, Ing., DrSc. - oponent Mudroň Ján, prof., Ing., CSc. - oponent Gmuca Štefan, Ing., CSc. - FEI / ÚJFI (FEI). - Bratislava, 2017 *plagID: 1538672 typ práce: dizertačná zdroj : STU.Bratislava*	**0,12%**
3	**Gamma-ray and conversion-electron spectroscopy at CERN-ISOLDE facility** / autor Sedlák Matúš, Ing. - školiteľ Venhart Martin, Mgr., PhD. - FMFI / FMFI.KJFB. - Bratislava, 2019. - 131 *plagID: 1609813 typ práce: dizertačná zdroj : UK.Bratislava*	**0,08%**
4	**http://matesfamily.org/bz2/Readme13.pdf** / Stiahnuté:07.12.2012; Veľkosť: 51,35kB. *plagID: 3493604 typ práce: application/pdf zdroj : internet/intranet*	**0,07%**
5	**http://larryjulian.com/download/God_ismy_CEO.pdf** / Stiahnuté:07.12.2012; Veľkosť: 57,90kB. *plagID: 3523793 typ práce: application/pdf zdroj : internet/intranet*	**0,07%**

* Číslo vyjadruje percentuálny prekryv testovaného dokumentu len s dokumentom uvedeným v príslušnom riadku.

Krátené: Dokument má prekryv s veľkým počtom dokumentov. Zoznam dokumentov je krátený a usporiadaný podľa percenta zostupne. Celkový počet dokumentov je [**22**]. V prípade veľkého počtu je často príčinou zhoda v texte, ktorý je predpísaný pre daný typ práce (položky tabuliek, záhlavia, poďakovania). Vo výpise dokumentov sa preferujú dokumenty, ktoré do výsledku prinášajú nový odsek (teda dokumenty ktoré sú plne pokryté podobnosťami iných dokumentov sa v zozname nenachádzajú. Pri prekročení maxima počtu prezentovateľných dokumentov sa v zarážke zobrazuje znak ∞.

Univerzita Komenského v Bratislave
Fakulta matematiky, fyziky a informatiky

ZADANIE ZÁVEREČNEJ PRÁCE

Meno a priezvisko študenta: Mgr. Jozef Klimo
Študijný program: jadrová a subjadrová fyzika (Jednoodborové štúdium, doktorandské III. st., denná forma)
Študijný odbor: jadrová a subjadrová fyzika
Typ záverečnej práce: dizertačná
Jazyk záverečnej práce: anglický
Sekundárny jazyk: slovenský

Názov: Properties and production possibilities of exotic nuclei
Vlastnosti a možnosti produkcie exotických jadier

Anotácia: Cieľom práce je štúdium reakčných mechanizmov, vedúcich k produkcii ťažkých a superťažkých exotických jadier, pre štúdium ich vlastností pre potreby jadrovej fyziky, ale aj s ohľadom na využitie ako sekundárne zväzky alebo v transmutácii. V práci budú využité moderné modely jadrovo jadrových zrážok, vrátane mikroskopických transportných kódov a vhodných fenomenologických modelov.

Školiteľ: Mgr. Martin Veselský, PhD.
Katedra: FMFI.KJFB - Katedra jadrovej fyziky a biofyziky
Vedúci katedry: prof. RNDr. Stanislav Tokár, DrSc.

Dátum zadania: 06.08.2014

Dátum schválenia: 06.08.2014

RNDr. Štefan Olejník, DrSc.
garant študijného programu

.....
študent

.....
školiteľ

Comenius University in Bratislava
Faculty of Mathematics, Physics and Informatics

THESIS ASSIGNMENT

Name and Surname:	Mgr. Jozef Klimo
Study programme:	Nuclear and Subnuclear Physics (Single degree study, Ph.D. III. deg., full time form)
Field of Study:	Nuclear And Subnuclear Physics
Type of Thesis:	Dissertation thesis
Language of Thesis:	English
Secondary language:	Slovak

Title: Properties and production possibilities of exotic nuclei

Annotation: In the framework of this thesis reaction mechanisms leading to production of exotic nuclei and super-heavy elements will be in investigated, in order to better comprehend their physical properties, which are further applicable in fundamental nuclear physical research, in physics of secondary radioactive ion beams or in possible transmutation of nuclear fuel. The modern codes for simulation of nuclear reactions with heavy ions, both phenomenological models and microscopic transport models, are going to be used as the main tools of the thesis.

Tutor:	Mgr. Martin Veselský, PhD.
Department:	FMFI.KJFB - Department of Nuclear Physics and Biophysics
Head of department:	prof. RNDr. Stanislav Tokár, DrSc.
Assigned:	06.08.2014
Approved:	06.08.2014 RNDr. Štefan Olejník, DrSc. Guarantor of Study Programme

.....
Student

.....
Tutor

Acknowledgement

I express my great gratitude to my supervisor Dr. Martin Veselský for opportunity to work on very topical projects and for introducing me to the world of nuclear physics.

I thank to all teachers, professors and scientists who have influenced or inspired me in my scientific work in the last years, especially to Dr. Stanislav Antalic, Dr. Martin Venhart, Dr. João Pedro Ramos, Dr. Thierry Stora, Prof. Goergios Souliotis, Dr. Aldo Bonasera, Prof. Riccardo Raabe, Ing. Štefan Gmuca CSc, RNDr. Stanislav Hlaváč DrSc., Dr. Miroslav Ješkovský, RNDr. Ivan Sýkora, PhD, RNDr. Matej Florek, CSc, Doc. RNDr. Emil Běták, DrSc.

I would like to thank to my colleagues Robo, Matúš and Matúš from SAS in Bratislava, for team work and collective unity during all these years.

I want to thank to Ing. Jan Kliman, Dr.Sc. and Dr. Ľuboš Krupa for support and practical help during my stay in JINR Dubna.

I am very grateful to my friends, Vlado & Martinka, Janko & Ivanka, Robo & Drahomirka, Luki & Zuzka, Mišo & Kristínka, Martinka V., Peťo, Miňo, Roman and sisters Golis.

Special thank I address to my family, to my mother and sister Andrejka, and especially to my beloved wife Andrejka, for their big love and encouragement over the years.

The greatest thank goes to God, who makes things possible.

Abstrakt

Pomocou sofistikovaných mikroskopických modelov, akými sú Boltzmann-Uehling-Uhlenbeck model (BUU) a Constrained Molecular Dynamics (CoMD) boli študované potlačenia produkčných účinných prierezov super-ťažkých jadier vznikajúcich v reakciách horúcej a studenej fúzie. Tieto modely sú založených na dynamike Boltzmannovej rovnice a umožňujú simulovať jadro-jadrové zrážky s ohľadom na ich interakciu. Tá je reprezentovaná stredným jedno-časticovým poľom so závislosťou na jadrovej hustote a izotopickom spinovom momente. Tým je možné študovať stavovú rovnicu jadrovej hmoty v rôznych podmienkach. Implementovaný je tiež Pauliho princíp a elektrické odpudzovanie medzi protónmi. V práci je preukázaná závislosť dynamiky fúzie a kvázi štiepenia na voľbe stavovej rovnice, a to na voľbe parametra nestlačiteľnosti $K_{0,}$ a hustotnéj závislosti energie symetrie γ. Oba parametre riadia dynamiku vzniknutého dvoj jadrového systému, a rozhodujú o jeho (ne-) stabilite. Z experimentálne získaných pravdepodobnosti vytvorenia zloženého jadra, boli odvodené ohraničenia pre stavovú rovnicu jadrovej hmoty, $K_0 = 240 – 260$ MeV a $\gamma = 0.6 – 1.0$. Tento výsledok taktiež korešponduje so stavovou rovnicou odvodenou pre nedávno registrovanú zrážku dvoch neutrónových hviezd, tj. udalosť GW170817, potvrdzujúc náš výsledok o stavovej rovnici.

Okrem štúdia jadrovej hmoty, super-ťažkých exotických jadier, sú v práci prezentované výsledky jadrových reakcii, ktoré sa používajú alebo je možné použiť v produkcii exotických jadier vo fyzike rádioaktívnych zväzkov. Pomocou moderných kódov, ako je ABRABLA07, boli simulované kumulatívne účinné prierezy výťažkov spalačných reakcii. Kombinácia kódov DIT + SMM zas umožnila študovať hlboko nepružné zrážky a výťažky projektilu a terču podobných fragmentov. Oba reakčne mechanizmy boli podrobené štúdiu pri rôznych energiách zrážok, ako aj kombináciách projektil vs. terč. Vhodnou voľbou projektil vs. terč, a energiou zrážky, je možné dosiahnuť výrazne zlepšenie produkčných účinných prierezov, a to pre veľké množstvo exotických jadier. Následne vyššie toky rádioaktívnych zväzkov, tak môžu skvalitniť základný aj aplikovaný výskum, a tiež otvoriť nové možnosti v ich napredovaní.

Za účelom skvalitňovania teoretických modelov jadrových reakcií je ich konfrontácia s reálnymi dátami nevyhnutná. Len nedávno boli namerané dáta z fragmentačných reakcii experimentu SPALADiN, prostredníctvom ktorých boli analyzované výstupy modelov INCL++, kombinovaného so štatistickými modelmi pre popis de-excitačnej fázy, a to ABLA07, GEMINI++, SMM. Výsledky sú taktiež diskutované v práci.

Abstract

Fusion hindrance in reactions leading to super-heavy elements via cold and hot fusion is investigated using microscopic model of Boltzmann-Uehling-Uhlenbeck (BUU) and Constrained Molecular Dynamics model extended by quantum-mechanical fluctuations. Density dependent single-particle mean field with isospin dependence is considered. Pauli blocking for protons and neutrons is considered, and Coulomb interactions are introduced. Sensitivity of fusion vs. quasi-fission dynamics on the modulus of incompressibility K_0, governing competition of surface tension and Coulomb repulsion, and on the density dependence of symmetry energy γ, responsible for formation of neck region, is observed. Experimental fusion probabilities are used to derive constraint on the nuclear equation of state of nuclear matter, $K_0 = 240 – 260$ MeV and $\gamma = 0.6 – 1.0$. These results are in relatively good compliance with constraints derived based on the recently measured data of two neutron stars GW170817.

Along the study of properties of nuclear matter from the point of view of reaction dynamics, this thesis provides calculations for the most promising mechanism for production of exotic nuclei. Cumulative and isotopic cross sections are investigated in spallation and deep-inelastic transfer reactions, performed at wide energy range and various projectile-target combinations using ABRABLA07 model (spallation fragments), and model combination DIT + SMM (deep-inelastic fragments). Appropriate combination of projectile and target, and appropriate incident energy can rapidly improve production cross section of wide range of exotic nuclei and thus, can widely enhance yields of radioactive ion beams more and more frequently used in fundamental and applied research programs.

Prediction powers of theoretical models used for simulation of spallation/fragmentation reaction phase (INCL++) and describing statistical de-excitation (ABLA07, GEMINI++, SMM) are confronted with recently measured SPALADiN experimental data and results are discussed.

„… but those who hope in the Lord

will renew their strength.

They will soar on wings like eagles;

they will run and not grow weary,

they will walk and not be faint.“

Isaiah 40:31

Contents

Introduction

In the second half of the 20^{th} century a lot of efforts have been made towards heavy ion reactions, i.e. nucleus-nucleus collisions characteristic by wide range of transferred angular momenta between reaction participants. The term heavy ion usually points to nuclei with $A \geq 20$, which can be considered as approximately homogeneous objects, and many body approach can be applied. Over these decades a great progress was done on the field of nuclear theory and experiment using heavy ions collisions. The trends in experiments have been to go from inclusive ($a + b \rightarrow c +$ anything) to more exclusive measurements, when more exclusive measurements helped to discriminate one model from another. Thus theoretical models, previously designed as more phenomenological, and many of them provided relatively good agreement with inclusive measurements, were put under pressure by exclusive experiments. This was possible by advanced and sophisticated experimental techniques capable to collect many details on nuclear reactions. Next trend in theoretical models has emerged from phenomenological to more sophisticated models, microscopic models, which have been significantly improved till the present. The first model introducing the microscopic approach in calculations was intra-nuclear cascade model (INC).

One has to note that early experiments in nuclear physics reflected only nuclear properties at saturation density, when research was focused more on reaction processes. An important goal of heavy ion nuclear physics was achieved by extracting information about properties of nuclear matter at higher and lower densities than saturation density $\rho_0 \approx 0.16$ fm$^{-3} \approx 3.10^{14}$ g/cm^3 [Sie87]. Thus, many decades from very first nuclear experiments no information about the nuclear equation of state could be gathered. The first measurements were possible after the BEVELAC at the Lawrence Laboratory in Berkeley and the Synchrophasotron in Dubna started their operation at the beginning of the seventies of the 20^{th} century. These measurements provided relativistic heavy ion collisions, where nuclei were compressed in extremely short time, with typical time scale 30 fm/c = 10^{-22}s [Ber88]. In the nuclear matter experiments, one can usually measure final products created after decompression phase, and remonstration of history is performed by sophisticated analysis. After many decades of that research, this field still remains one of the most topical with many opened questions related with the explosion mechanisms of supernovae, the interior structure of neutron stars, and initial formation of universe depending on nuclear matter at wide range of densities and temperatures. Along with experimental data, the theoretical microscopic models represent the main tool in study of equation of state of nuclear matter. The most advanced models sensitive to equation of state of nuclear matter are based on molecular dynamics, incorporating density dependent nuclear mean field, and taking into account dissipation effects. The most successful models designed on those principles are the Improved Quantum-Molecular Dynamics model (ImQMD) or other approximations of Boltzmann equation, such as the Boltzmann-Uehling-Uhlenbeck model (BUU) or the Constrained Molecular Dynamics model (CoMD). Nonetheless, progress on the field of microscopic models is still required and the model parameters should be refined to describe reactions with various isospin asymmetries of interacting nuclei. The significant highlight of nuclear physics is to find universal model capable to describe any type of nuclear collision. Because we are still far from that goal, phenomenological

models remain as a first choice for many calculations of nuclear reaction, for experimental nuclear physics or other applications. This is given mainly by model simplicity. Probably the highest level of model universality one can find among models for relativistic collisions.

Nucleus-nucleus collisions along with nucleon-nucleus collisions at intermediate and high energies are presently at the forefront in production of unstable exotic nuclei and radioactive ion beams. These types of reactions allow spectroscopic measurements of nuclear matter with various isospin asymmetries, and provide answers to complex questions on behavior of atomic nuclei. On the other hand new physical questions are revealed as we go deeper in nuclear theory. It should be mentioned, that a great success on the field of radioactive ion beams came with development of the ISOL (Isotope Separation On-Line) method [Han51]. Use of that technique allows unstable nuclei, formed in the thick target after irradiation by proton beam, to be transported, ionized and subsequently re-accelerated as secondary low energy beams for decay spectroscopy. The worldwide leading facility of that kind is radioactive beam facility ISOLDE (CERN), where around 1000 isotopes of 75 different elements are possible to study by combination of spallation reactions (e.g. p + ^{238}U at 1.0 or 1.4 AGeV) and ISOL technique. Similar effect can be achieved by complementary method of in-flight fragmentation (IFF), usually performed with beryllium target in inverse kinematics. Very advantageous is to use of spallation source as neutron converter. This configuration enables production of approximately 15 neutrons in a single spallation, in average, where subsequently many of them can induce low energy fission with production of n-rich fragments. This leads to higher purity and higher intensity of some n-rich radioactive ion beams with option to study more n-rich nuclei comparing with classical spallation-fission. Not only wide range of isospin asymmetry, but also huge diversity of production species could be achieved using only one appropriate spallation or fragmentation reaction. This is for example not possible using compound nucleus reactions.

Nevertheless, the compound nucleus reactions around the Coulomb barrier represent the first choice for synthesis of super-heavy elements or for spectroscopy of n-deficient nuclei from the proton drip line region, up to lead isotopes. Many of very n-deficient exotic nuclei were synthesized using n-deficient ^{36}Ar and ^{58}Ni beams on various stable targets. This reaction mechanism is characteristic by relatively high cross sections dropping down from lead region, where nuclear fission starts to compete with evaporation channels. For the production of radioactive ion beams formed in compound nucleus reactions, the main obstacles related with limited target materials that can be used in experiments with secondary beams. All these considerations indicate that compound nucleus reactions will not be the forefront position in radioactive ion beam development in the near future.

Besides spallation and fragmentation reaction mechanism also deep-inelastic transfer reactions seem to be very perspective for future experiments with radioactive ion beams. This reaction mechanism is characterized by intense evolution of isospin degree of freedom, resulting to production of wide range of isotopes characteristic by high transfer of linear and angular momentum. For this mechanisms Fermi energy domain is typical, i.e. 15 - 50 AMeV. Especially, the region of very n-deficient isotopes, below Z = 30, can be prepared in reaction of ^{86}Kr, ^{82}Se + ^{64}Ni at 25 AMeV, where production cross sections exceeding those from spallation reaction of p + ^{238}U at 1 AGeV. Very promising are deep-inelastic reactions leading to production of n-rich nuclei from neutron closed shells N = 20 (^{40}Ar + ^{238}U at 16 AMeV), N = 50 (^{86}Kr + ^{90}Zr at 8.5 AMeV), N = 82 (^{136}Xe + ^{124}Sn at 7 AMeV) [Ves13]. Moreover, comparisons of simulations with existing

data at energies below 10 AMeV indicate that even higher production cross sections can be expected compared to Fermi energy domain [Ves11]. However, in order to join deep-inelastic transfer reactions in production of radioactive ion beams some improvements of experimental techniques are necessary.

Project of PhD Thesis

This thesis is connected with investigation of production possibilities of exotic nuclei and properties of very isospin asymmetric exotic nuclei, finite nuclear matter. The main tools of this thesis are heavy ion collisions from the Coulomb barrier up to relativistic energies. The subject of the presented PhD thesis can be divided into following parts:

- This thesis deals with investigation of reaction dynamics leading to production of super-heavy elements, which is governed by competition between fusion and quasi-fission. Fusion vs. quasi-fission dynamics is investigated in the context of nuclear equation of state. Many body approach of following microscopic models is used: the Boltzmann-Uehling-Uhlenbeck model (BUU) and Constrained Molecular Dynamics model (CoMD). It is the first time the experimental fusion probabilities are used to derive constraint on the nuclear equation of state, which still represent one of the most topical subjects of present fundamental research in nuclear physics.

- In order to expand the present possibilities of production of radioactive ion beams via spallation reactions, and to investigate a new possibilities using deep-inelastic transfer reactions, simulations using various transport models are presented here. More specifically, dependence of production cross section of spallation product on incident energy of protons is investigated for ISOLDE facility at CERN. In addition to standard spalatted uranium material ^{238}U, cross sections with alternative lighter materials of given isotopes ^{12}C, ^{28}Si, ^{40}Ca, ^{48}Tl were examined. Among others, deep-inelastic transfer reactions induced by n-rich exotic nuclei on uranium target ^{238}U are considered as option for production of a new n-rich nuclei from region of Z = 60 – 70. This goal is unattainable by present fragmentation technique but seem to be possible within HIE-ISOLDE post-accelerator facility.

- The results chapter is also dedicated to confrontation of theoretical models and recently measured data in fragmentation reactions ^{136}Xe + p and ^{136}Xe + ^{12}C at 1 AGeV in the SPALADiN experiment. The model of intra-nuclear cascade INCL++ combined with three different statistical models, i.e. ABLA07, GEMINI++ and SMM, are compared with experimental data.

Chapter 1

The nuclear equation of state

1.1 Nuclear matter at the saturation density

The liquid drop model allows to explain many properties of nuclei and phenomena in nuclear physics. The basic assumption of the liquid drop model relates with consideration of atomic nucleus as a liquid drop in thermo-dynamical equilibrium, consisting of extremely dense nucleonic content with density $\rho_0 \approx 3x10^{14}$ g/cm^3. That value is defined at zero thermo-dynamical temperature [Par88]. The nucleons are described as relativistic moving velocities of 20 % of the speed of light, performing so-called Fermi motion inside of a quantum fluid of the nucleus. The dominant interaction between nucleons is given by short-range nuclear force, as the residual interaction of strongly interacting quarks. From the character of the nuclear force, each participating nucleon can interact only with few neighboring nucleons. It`s attractive character is manifested at short distances up to 1 – 2 fm, and drops rapidly down to the zero value at larger distances. On the other side, the nuclear interaction between nucleons is becoming repulsive once the distance between nucleons is lower than 0.4 fm [Gle00]. Such a behavior of potential energy is depicted on the figure 1.1, and is characteristic for the finite range nuclear matter, as atomic nuclei at ground state. The maximum of the binding energy, the minimum of the potential energy, creates very stable system corresponding to the saturation density of nuclear matter. The saturation density and the binding energy per nucleon is varying as $\rho_0 = 0.15$ - 0.16 fm^{-3} (equivalent to ~ $3x10^{14}$ g/cm^3) and B = -16.3 - -16.0 MeV, respectively [Gle00], [Web99].The saturation of nuclear matter is also characteristic by zero nuclear force, and thus the pressure of the nuclear matter is vanished. For equilibrated nuclear matter the pressure is can be expressed as:

$$P = \rho^2 \frac{d}{d\rho}\frac{E}{\rho}. \tag{1.1}$$

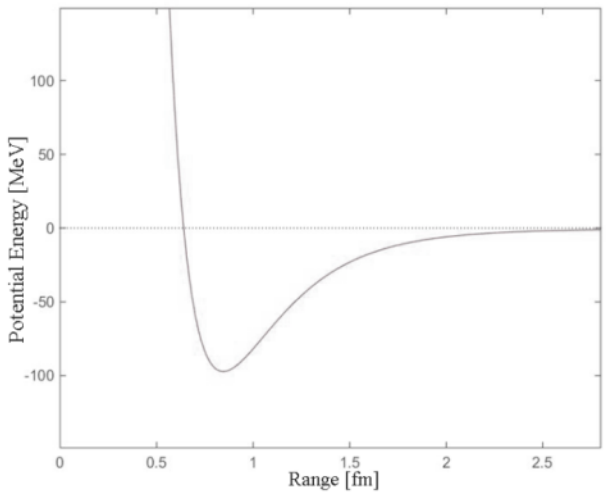

Fig. 1.1: Free space nucleon-nucleon potential for spin S = 0 and isospin T = 1 [Rei68].

Another parameter for probing of the nuclear matter stability represents the incompressibility parameter K_0, derived as the second derivation of the pressure at saturation density:

$$K_0 = 9\left[\rho^2 \frac{d^2}{d\rho^2}\frac{E}{\rho}\right]_{\rho=\rho_0} \tag{1.2}$$

where ρ is nucleon density, E / ρ is energy per particle. By incompressibility one can express the stiffness of nuclear matter and thus the stiffness of the equation of state by which the nuclear matter is defined. Hence, the stiffer the incompressibility, the more rapidly the pressure is changing with change of density. This is demonstrated on the figure 1.2. For the symmetric nuclear matter (Z≈N) many experiments have been performed to constrain the equation of state. From the giant monopole resonances investigated at the saturation density $\rho_0 = 0.16$ fm^{-3}, the incompressibility parameter was determined as $K_0 = 231 \pm 5$ MeV [You99], which can differ based upon various model assumptions. There are also results implying that the incompressibility should vary within $K_0 = 230 - 265$ MeV [Gle00], [Web99]. As for the high density measurements, the relativistic nucleus-nucleus collisions served as main tool in investigation of the incompressibility and the equation of state of nuclear matter at higher densities, i.e. $\rho_0 \in (2\rho_0, 5\rho_0)$, by measuring the collective flow. The main discrepancies result from the high sensitivity of the symmetry energy on the nuclear matter density.

The symmetry energy E_{sym} is proportional to parameter of asymmetry a_{sym}. This parameter is responsible for the slope of beta stability line in the nuclear chart. While light nuclei have approximately equal number of protons and neutron Z ≈ N, this is not the case of heavier systems. The heavier are nuclei, the energy of asymmetry tends to grow up with isospin asymmetry. This is because of an stabilizing effect of the nuclear system again the repulsive Coulomb interaction. Based on the definition the symmetry energy is expressed as the difference between the energy densities of neutron matter and symmetric nuclear matter, i.e. $E_{sym}(\rho) - E_{sym}(\rho_0)$. The measure of the symmetry energy is the parameter of symmetry contribution to the total energy of nucleus, to the total mass, defined as following:

$$a_{sym} = \frac{1}{2}\left[\frac{d^2}{dI^2}\frac{E}{\rho}\right]_{I=0}, \; I = \frac{\rho_N - \rho_P}{\rho} \tag{1.3}$$

The value of the a_{sym} parameter is estimated to be 33 – 33 MeV [Gle00], [Web99], [Lat07].

1.2 Nuclear matter away from the saturation density

In order to learn more about nuclear matter properties, it has to be studied away from saturation density, at super or supra-saturation density. Therefore, it is necessary to parameterize density and temperature of nuclear matter. As was mentioned the important degree of freedom is given by isospin asymmetry leading to symmetry energy. Thus the equation of nuclear matter is generally depending on energy density (pressure), temperature and isospin asymmetry via symmetry energy.

Let´s consider the nucleus-nucleus collision to qualitatively explain how the basics nuclear matter characteristics are changing during a collision. Suppose that the nuclear matter is heating due to the collision and pressing in the way its state is described by point A (super-heated phase) in the figure 1.3. The pressure is positive and the system is

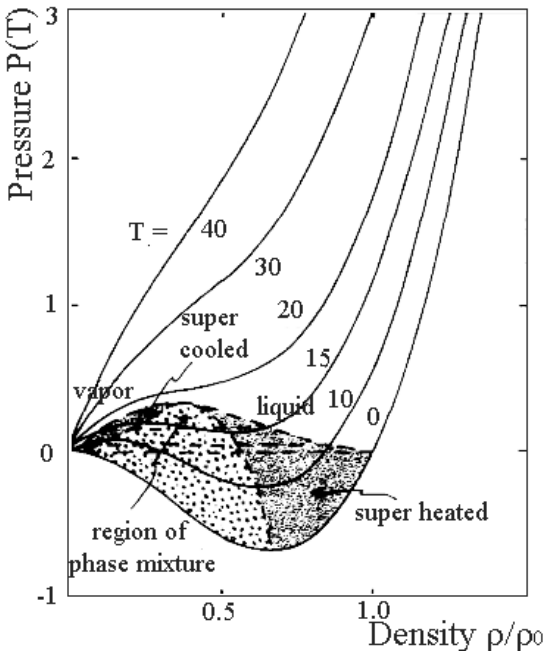

Fig. 1.2: Hypothetical pressure vs. density curve for nuclear matter at different temperatures [Bon94].

going to expand approximately along the isotherm. Because the total energy must be conserved, the matter will acquire a radial velocity outwards. Once the system is going back and reaches the point B, its density is optimal and the pressure is zero. However, the radial velocity of the system drives it beyond this stability. The outward expansion is going to slow down, but if its energy is large enough, the point C is going to be reached. The point C represents a point of instability. Now the pressure is not changing, i.e. dP /d $\rho = 0$, and the system is going to break up into an inhomogeneous phase (phase mixture region).

So, if the compression and entropy is too high the pressure is always positive and system expands till “freeze-out” configuration is reached and then creation of clusters starts. One can say, the higher the collision energy, the higher compression and change in temperature of the system with respect on the impact parameter. Also the entropy is increasing as the compression level is growing up. On the other side, if the compression is sufficiently low one can expect a harmonic motion and there is not enough energy to reach the point C. Very similar behavior is observed in a Van der Waals gas. The critical temperature is 15 MeV corresponding to collision energy in the lab frame of 50 - 100 AMeV. Then one can observe a phase transition from gas-liquid mix (phase mixture region) to gas of nuclides (n ,p, d, alpha, etc.).

1.3 Sources for nuclear matter investigation

There are three different ways, sources, to obtain information on the nuclear equation of state (EOS):

- Astrophysical measurements, i.e. the explosion of supernovae and the stability of neutron stars
- Giant monopole resonances or vibrations (GMR)
- High energy heavy ion collisions, i.e. deep-inelastic transfer reactions, multi-fragmentation

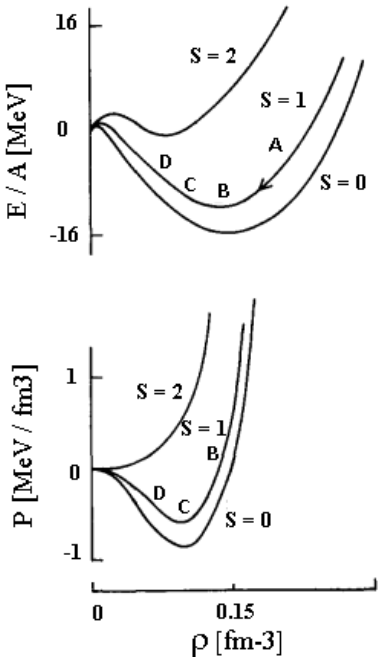

Fig. 1.3: Behavior of E / A against ρ and pressure P against ρ for Skyrme type interactions [Ber88].

All these approaches differ from each other in determination of physical quantities, e.g. as modulus of incompressibility by factor of two at maximum. In particular, models for description of supernovae need a soft equation of state with incompressibility of $K_0 \approx 140$ MeV, in order to reproduce supernovae explosion [Bar85]. A stiffer EOS, i.e. a larger value of K_0, does not allow sufficient energy to be stored during the collapse phase. Therefore, the subsequent explosion dies out on the way to the surface. As for the giant monopole resonances, early studies derived an incompressibility of $K_0 \approx 200$ MeV [Bla80] and a bit later the 4π data resulted to $K_0 \approx 380$ MeV [Sto86], [Kea88].

However, more astrophysical studies predict an incompressibility within the range $K_0 \approx 230 – 265$ MeV [Gle00], [Web90]. Among others, at the saturation density an incompressibility $K_0 \approx 231 \pm 5$ MeV was established from giant monopole resonances with relatively good precision [You99]. Moreover, based on the recent observation of the two neutron star merger event GW170817 and related calculations, it results that the incompressibility should be K = 245 MeV to form neutron star and not a black hole [Abb17], [Per19], [Put19].

All these approaches differ in assumptions made in the calculations of heavy ion reactions and astrophysical phenomena, i.e. different time scale, momentum distributions, and thus it consequently leads to discrepancy between them. Whereas the nuclear matter density in giant monopole resonances is less than tenth of a percent, in heavy ion collisions we expect more than twice nuclear matter density.

Chapter 2

Transport equations

2.1 Boltzmann-Uehling-Uhlenbeck equation (BUU)

The Boltzmann-Uehling-Uhlenbeck equation is one of the approximations for finding solution of Boltzmann equation for nuclear matter. Another models handling heavy ion collisions in similar way as BUU are Vlasov-Uehling-Uhlenbeck equation, the Boltzmann-Nordheim equation or the Landau-Vlasov equation. In contrary to cascade model, besides hard nucleon-nucleon collisions BUU model includes nuclear mean field and quantum effects. Thus it can serve as tool for investigation of equation of nuclear matter. The Pauli blocking in nucleon-nucleon collisions is strictly preserved, separately for protons and neutrons. The physical quantity from which all relevant observables are evaluated is distribution function $fi(\vec{r},\vec{p},t)$ defined over the phase space $(\vec{r},\vec{p})$ for i-th nucleon. For N-body system the distribution function is the sum over the single particle distribution functions $fi(\vec{r},\vec{p},t)$

$$f = \sum_i^N f_i \tag{2.1}$$

, where N is a number of nucleons inside of the available phase space, bounded by radius of static nucleus R. So $f(\vec{r},\vec{p},t)$ has to fulfill the equation 2.2 and is solved by test particle method of Wong [Won82]

$$\frac{\partial f}{\partial t} + \vec{v}.\nabla_r f - \nabla_r U.\nabla_P f = \left(\frac{\partial f}{\partial t}\right)_{coll} \tag{2.2}$$

$$U = U(skyrme) = a\rho + b\rho^{\kappa} + 2a_s\left(\frac{\rho}{\rho_0}\right)^{\gamma}\tau_z I \tag{2.3}$$

$$I = \frac{(\rho_n - \rho_p)}{\rho} \tag{2.4}$$

$\vec{v}$ is the velocity of particle, U(ρ) is the sum of single particle mean field potential with isospin-dependent symmetry energy term. Thus the Hamiltonian consists of kinetic energy and the two-body mean field potential as Skyrme-like effective nucleon-nucleon potential, i.e. H = T + U_{Skyrme}. The coefficients a, b, κ in potential energy relate with properties of symmetric matter, the parameter a_s is the symmetry energy at saturation density and γ is the density dependence of symmetry energy. The coefficient τ_z equals 1 for neutron and -1 for protons. In general, the third term in the equation 2.3 describes contribution of symmetry energy. Because, nucleon position in the phase space will imply a certain density, the mean field could be defined as dependent on it. Thus ρ, ρ_n, ρ_p represent nucleon, neutron and proton density, respectively.

The left-hand side is the total differential $df(\vec{r},\vec{p},t)/dt$, which is equal to zero for non-collision scenario characteristic for equilibrium state, where the total amount of particles in the phase space is conserved. Due to the fact the phase space volume is constant, following Liouville´s theorem, for non-collision case one can write $f(\vec{r},\vec{p},t)$ =

$f(\vec{r} + \Delta\vec{r}, \vec{p} + \Delta\vec{p}, t + dt)$. However, once the nucleus-nucleus collisions take place the collision term has to be considered and in the BUU it is implemented as following

$$I_{coll} = \left(\frac{\partial f}{\partial t}\right)_{coll} = \frac{4}{(2\pi)^3}\int d^3p_2 d^3p_3 \int d\Omega \frac{\mathrm{d}\sigma_{NN}}{\mathrm{d}\Omega} |v_{12}| P \delta^3(\vec{p}_1 + \vec{p}_2 - \vec{p}_3 - \vec{p}_4) \quad (2.5)$$

, where probability including Pauli blocking of fermions P is given by the equation

$$P = f_3 f_4 (1 - f_1)(1 - f_2) - f_1 f_2 (1 - f_3)(1 - f_4) \quad (2.6)$$

$$\begin{aligned} f_1 &= f(\vec{r}, \vec{p}_1, t) \\ f_2 &= f(\vec{r}, \vec{p}_2, t) \\ f_3 &= f(\vec{r}, \vec{p}_3, t) \\ f_4 &= f(\vec{r}, \vec{p}_4, t) \end{aligned} \quad (2.7)$$

The differential in-medium cross section for nucleon-nucleon scattering $d\sigma_{NN}/d\Omega$ relates with particular change of the momentum $(\vec{p}_1 - \vec{p}_3)$, and $(\vec{p}_2 - \vec{p}_4)$, at collision with relative velocity of the two colliding nucleons $v_{12} = \hbar|\vec{p}_1 - \vec{p}_2|/m$. Its value is approximated using the experimental cross sections of free nucleons, i.e. using parameterization of Cugnon [Cug81]. Other possibility to determine in-medium cross section is from equation of state [Li93], [Li94].

The P factor is zero for equilibrium system, where no collisions are considered. In general, for fermions the P factor is expressed via the first and the second term in the equation 2.6, as a sum of gain and loss factor, respectively. Such an expression is consistent with the figure 2.1, where the initial states have to be occupied and final states unoccupied preserving the Pauli blocking for fermions. This preservation principle is fulfilled via terms $(1 - f_i)(1 - f_{i+1})$. The *fi* parameters are transition matrices connecting the initial and the final momentum states for two body collisions.

The delta function expresses conservation of linear momentum in each collision. Once a nucleon-nucleon collision is evaluated as elastic, the similar term is valid between input and output energies.

All nucleons between collisions move classically according to Hamilton`s equations 2.8 and protons are interacting by their charges via Coulomb interaction.

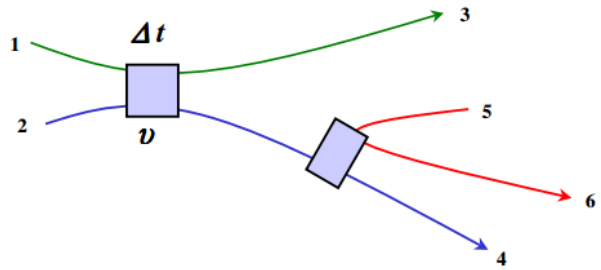

Fig. 2.1: Two body collisions, or interactions. Scattering of two states from 1, 2 to 3,4 (1+2 → 3+4). If the phase space around $(\vec{r}_3, \vec{p}_3, t)$ and $(\vec{r}_4, \vec{p}_4, t)$ is empty then the scattering is allowed, otherwise the scattering is suppressed.

The mean position and linear momentum for individual nucleons in the phase space is driven by classical Hamiltonian equations of motion as nucleons between collisions behave by lows of classical mechanics:

$$\langle \dot{r}_i \rangle = \frac{\partial H}{\partial \langle p_i \rangle} \quad \langle \dot{p}_\iota \rangle = -\frac{\partial H}{\partial \langle r_i \rangle}. \tag{2.8}$$

2.2 Constrained Molecular Dynamics (CoMD)

The Constrained Molecular Dynamics or CoMD model represents another approximation of Boltzmann transport equation. The model was originally designed for simulations for intermediate and high energy heavy ion collisions following the quantum molecular dynamics model QMD [Aic91]. The QMD itself was designed as a semi-classical microscopic dynamics model based on the demand for microscopic simulations of heavy ion collisions. The CoMD model [Pap01], [Mar02] along with IQMD [Bas93], [Zha99] and ImQMD, UrQMD [Ble99] are derived from the original QMD as different extension versions.

The competition of fusion and quasi-fission was recently addressed using the quantum molecular dynamic known as ImQMD [Wan02], [Zha08], [Wan13], [Cho14] and using the time dependent Hartree-Fock theory [Gol09], [Wah14], [Obe14], [Sek16], [God19]. It is expected that surface properties of nuclei play significant role on competition of these processes, via the equation of state. In particular, these processes are governed by interplay of the Coulomb and surface energy, with strong dependence on the symmetry energy. Only recently, the CoMD model was employed to study of proton induced fission from low to high energies, and fission dynamics was reproduced reliably [Von15]. Hence, there is an assumption that fusion vs. quasi-fission dynamics can be described using the CoMD model as well.

Compared to the BUU model the nucleons in the CoMD model are considered as wave packets, and thus the quantum mechanical fluctuations, fluctuations of density are not removed by taking an average value over the large set of test particles. Contrary to the ImQMD, the CoMD itself contains the Pauli blocking for nucleon-nucleon scattering, separately for protons and neutrons. However, it is also expected that for low energy reactions the collision integral has less important as the mean field.

In the CoMD model each nucleon represents localized wave packet preserving the Heisenberg principle of uncertainty. The nucleonic wave function $\Phi_i(\boldsymbol{r})$ in coordinate space is expressed as Gaussian function distributed around centers of position $\langle \boldsymbol{r_i} \rangle$ and momentum $\langle \boldsymbol{p_i} \rangle$ with uncertainty in position denotes as σ_r . So we can write:

$$\Phi_i(\boldsymbol{r}) = \frac{1}{\left(2\pi\sigma_r^2\right)^{3/4}} exp\left[-\frac{(\boldsymbol{r}-\langle \boldsymbol{r_i} \rangle)^2}{2\sigma_r^2} + \frac{i}{\hbar}\boldsymbol{r}.\langle \boldsymbol{p_i} \rangle\right], \tag{2.9}$$

where the total wave function is assumed to be a direct product of the single particle wave functions, neglecting antisymmetrization:

$$\Phi = \prod_i \Phi_i(\boldsymbol{r}) \tag{2.10}$$

The phase space distribution function $f_i(\boldsymbol{r})$ is then obtained by the Wigner transformation of the nucleon wave function $\Phi_i(\boldsymbol{r})$:

$$f_i(\boldsymbol{r},\boldsymbol{p}) = \int d^3s\, \Phi_i^*(\boldsymbol{r}-\boldsymbol{s/2})\Phi_i(\boldsymbol{r}+\boldsymbol{s/2})\exp(i\boldsymbol{p}.\boldsymbol{s}), \tag{2.11}$$

leading to Gaussian distribution function

$$f_i(\boldsymbol{r},\boldsymbol{p}) = \frac{1}{(\pi\hbar)^3} exp\left[-\frac{(\boldsymbol{r}-\langle \boldsymbol{r_i}\rangle)^2}{2\sigma_r^2} - \frac{2\sigma_r^2(\boldsymbol{p}-\langle \boldsymbol{p_i}\rangle)^2}{\hbar^2}\right], \tag{2.12}$$

and preserving the minimum uncertainty relation $\sigma_r\sigma_p = \hbar/2$ in one-body phase space we get

$$f_i(\boldsymbol{r},\boldsymbol{p}) = \frac{1}{\left(2\pi\sigma_r\sigma_p\right)^3} exp\left[-\frac{(\boldsymbol{r}-\langle \boldsymbol{r_i}\rangle)^2}{2\sigma_r^2} - \frac{(\boldsymbol{p}-\langle \boldsymbol{p_i}\rangle)^2}{2\sigma_p^2}\right]. \tag{2.13}$$

After summing over the single-particle distribution functions $f_i(\boldsymbol{r})$, N-body phase space distribution function is expressed in following way:

$$f(\boldsymbol{r},\boldsymbol{p}) = \sum_i f_i(\boldsymbol{r},\boldsymbol{p}). \tag{2.14}$$

The equation 2.13 is thus generalization of the classical distribution function for point-like particles:

$$f_i(\boldsymbol{r},\boldsymbol{p}) = \delta(\boldsymbol{r} - \langle \boldsymbol{r_i}\rangle)\delta(\boldsymbol{p} - \langle \boldsymbol{p_i}\rangle). \tag{2.15}$$

The mean coordinates and momentum in the phase space are determined from the Hamiltonian equation of motion of centroids, the equations 2.8. The Hamilton operator for *A* particles with mass *m* is given by the kinetic energy and effective potential interaction V_{eff}:

$$H = \sum_i \frac{\langle \boldsymbol{p_i}\rangle^2}{2m} + A\frac{3\sigma_P^3}{2m} + V_{eff}. \tag{2.16}$$

The second term is the Gaussian width in the momentum phase space. As it is set to constant it is skipped in the CoMD simulations. The third term is Skyrme-like effective potential for nucleon-nucleon interaction given by the volume term V_{vol}, three-body term $V_{(3)}$, the part resulting from symmetry energy V_{sym}, the surface energy term V_{surf}, and the Coulomb repulsion V_{Coul}:

$$V_{eff} = V_{vol} + V_{(3)} + V_{sym} + V_{surf} + V_{Coul}. \tag{2.17}$$

Particular terms in the effective potential contribute to total potential energy via interaction density ρ_{ij} like following:

$$V_{vol} = \frac{t_0}{2\rho_0}\sum_{i,j\neq i}\ \rho_{ij}\ , \tag{2.18}$$

$$V_{(3)} = \frac{t_3}{(\mu+1)(\rho_0)^\mu}\sum_{i,j\neq i}\ \rho_{ij}^\mu\ , \tag{2.19}$$

$$V_{sym} = \frac{a_{sym}}{2\rho_0}\sum_{i,j\neq i}\ \left[2\delta_{\tau i,\tau j} - 1\right]\rho_{ij}\ , \tag{2.20}$$

$$V_{surf} = \frac{C_s}{2\rho_0}\sum_{i,j\neq i}\ \nabla^2_{\langle \boldsymbol{r_i}\rangle}\left(\rho_{ij}\right)\ , \tag{2.21}$$

$$V_{Coul} = \frac{1}{2}\sum_{\substack{i,j\neq i \\ i,j\in prot}} \frac{e^2}{|\langle \boldsymbol{r_i}\rangle - \langle \boldsymbol{r_j}\rangle|} erf\left(\frac{|\langle \boldsymbol{r_i}\rangle - \langle \boldsymbol{r_j}\rangle|}{2\sigma_r^2}\right). \quad (2.22)$$

The parameter with τ_i is the *z* component of the nucleon isospin degree of freedom. The position of nucleons in the phase space implies nucleon-nucleon interaction density ρ_{ij}, which is the main quantity in the representation of effective potential energy, as one can see from the above equations 2.18 - 2.22. From the definition, for ρ_{ij} one can write:

$$\rho_{ij} \equiv \int d^3r_i\, d^3r_j \rho_i(\boldsymbol{r_i})\rho_j(\boldsymbol{r_j})\delta(\boldsymbol{r_i} - \boldsymbol{r_j}), \quad (2.23)$$

and the single particle nucleon density is given by the term:

$$\rho_i \equiv \int d^3p f_i(\boldsymbol{r}, \boldsymbol{p}) \quad (2.24)$$

Similar to the BUU simulations, the Pauli principle at each time step during an evolution of the system is restored. The following condition should be fulfilled to preserve the Pauli principle:

$$\overline{f_i} \leq 1 \text{ , (for all i)} \quad (2.25)$$

$$\overline{f_i} \equiv \sum_j \delta_{\tau i,\tau j}\delta_{si,sj} \int_{h^3} f_i(\boldsymbol{r}, \boldsymbol{p}) d^3r d^3p \quad (2.26)$$

and s_i is the projection of spin to axis *z* of the nucleon *i*. The integration in the equation 2.26 takes place over the phase space volume of size $\hbar^3$ with centroid around the point $(\langle r_i\rangle, \langle p_i\rangle)$ with width:

(2.27)

$$\sqrt{\frac{2\pi\hbar}{\sigma_r\sigma_p}}\sigma_r, \qquad \sqrt{\frac{2\pi\hbar}{\sigma_r\sigma_p}}\sigma_{p.}$$

For each particle the occupation probability $\overline{f_i}$ is checked at each time step to ensure the condition from the equation 2.25 is preserved. If not, and $\overline{f_i} > 1$, then an ensemble of the nearest particles is determined within the distances $3\sigma_r$ and $3\sigma_p$ within the phase space. The momenta of the nearest particles in ensemble are then changed for new generated sample as well in order the total momentum and the total kinetic energy is conserved. Eventually, the new sample is accepted if it reduces the phase space function $\overline{f_i}$. The preservation of the angular momentum in heavy ion collisions is very critical to get accurate description of reactions and fission or quasi-fission. This condition is preserved in the present version of CoMD.

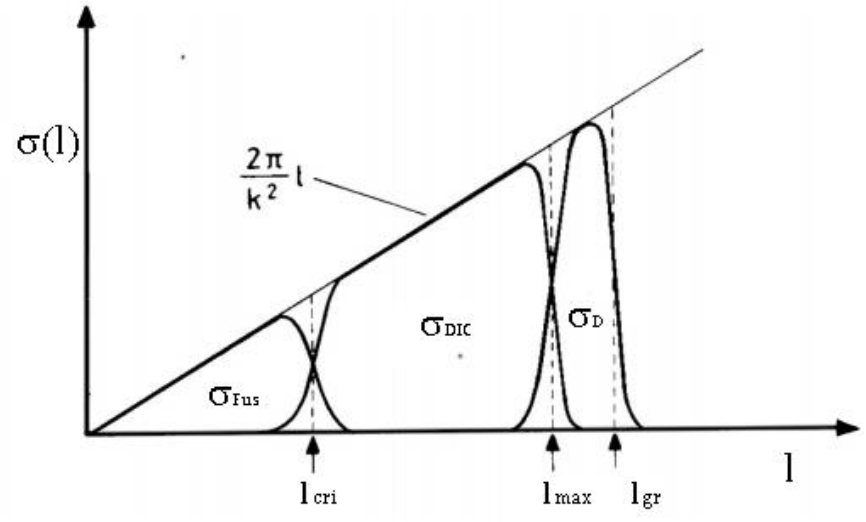

Fig. 2.2: Distribution of low energy nuclear reactions of heavy ions based upon an angular momentum at a certain incident energy. Fusion: $l < l_{cri}$ (σ_{Fus}), deep-inelastic transfer reactions: $l_{cri} < l < l_{max}$ (σ_{DIC}), and direct reactions: $l_{max} < l < l_{gr}$ (σ_D).

2.3 Deep-Inelastic Transfer model (DIT)

The model of deep-inelastic transfer reactions was initially developed by Randrup [Ran78], [Ran79], and later it was implemented by Tassan-Got [Tas91] into the Monte Carlo code DIT, which is based on the solution of the Focker-Planck equation. The Focker-Planck transport equation itself represents a special case of Boltzmann equation. The DIT model is a phenomenological approach to describe (mid-) peripheral reactions at Fermi energy domain 15 - 50 AMeV and also at low energies, below 10 AMeV, if some adjustment on the nuclear mean field parameterization are applied. Very good reproduction of experimental data was obtained by combination of the DIT model, as first stage model, with the simultaneous multi-fragmentation model SMM for description of the de-excitation phase of reaction. Moreover, for the Fermi energy domain the DIT model has to be combined with pre-equilibrium model, and also the incomplete fusion has to be taken into account, as it is becoming dominant at more central collisions. More on the theoretical background of the deep-inelastic reaction is explained below.

Trajectories of nuclei in deep-inelastic transfer reactions

Collisions of heavy nuclei at several MeV per nucleon leading to deep-inelastic transfer reactions are characteristic by the angular momentum ranging from l_{crit} as the limit for compound nucleus reactions to l_{max} restricted direct reactions from below, the figure 2.2. As long as nuclei interact, their collective properties are changing from the initially non-equilibrium state into equilibrium one. Before dissipation process, two approaching nuclei are moving along their trajectories. These trajectories of two nuclei can be described by the classical Newtonian equations, as the following:

$$\frac{d}{dt}(\mu\dot{r}) - \mu r\dot{\varphi}^2 + \frac{dV}{dr} + K_r\dot{r} = 0\,, \qquad (2.28)$$

$$\frac{d}{dt}(\mu r^2\dot{\varphi}) + K_\varphi r^2\dot{\varphi} = 0\,,$$

here (r, φ) are polar coordinates of relative position of two interacting nuclei. μ is their

reduced mass, V is the total interaction potential (Coulomb + nuclear part), and K_r, K_φ are friction coefficients arising from mutual friction between projectile and target nucleus governed by nuclear interaction:

$$K_r = K_r^0(\nabla V_N)^2 \,, \qquad (2.29)$$
$$K_\varphi = K_\varphi^0(\nabla V_N)^2 \,,$$

V_N is the nuclear part of interaction potential, and K_r^0, K_φ^0 are constants established as 12 fm/(MeV.c) = 4.10^{-23} s/MeV and 0.03 fm/(MeV.c) = 10^{-25} s/MeV. The equations 2.29 are valid in the case of proximity potential, suggested by Gross and Kalinowski [Gro75]. It is obvious that in the minimum of the potential valley the friction vanishes, and the coefficients equals zero. However, the friction can also gradually vanish before the potential minimum is reached. This can happen once the projectile is "sticked" to target nucleus, and so-called sticking configuration is reached. From that moment the momentum dissipation is stopped, and the di-nuclear system can only rotate as one system. For the angular momentum conservation one can write:

$$l_{st} = \frac{I_{rel}}{I_1+I_2+I_{rel}} l \,, \qquad (2.30)$$

where l_{st} is angular momentum at the sticking configuration, l is initial angular momentum, and I_1, I_2, I_{rel} are moments of inertia of both interacting nuclei and their mutual moment of inertia at sticking configuration, respectively. If the interacting nuclei have spherical symmetric shape then $l_{st} \leq \frac{5}{7} l$. Eventually, based upon these equations one can construct the well-known Wilczyński graphs once we know the differential cross-sections.

Focker-Planck equation

Based on the Randrup theory [Ran78] it is possible to assume that dissipation in deep-inelastic transfer reactions proceeds mainly through stochastic transfer of nucleons, which are decoupled in time. When two approaching nuclei described by classical their trajectories are close enough to each other a window defined by potential barriers can open, and stochastic transfers may occur. Such transfers trigger dissipations and fluctuations modeled by a Monte Carlo method on an event-by-event basis.

Because of the system preserve its binary character, the mass asymmetry η was suggested to be introduced as a degree of freedom evolving during dissipation process. As the transfers itself are stochastic, the mass asymmetry exhibits stochastic time evolution as well. It has been shown by Nörenberg [Nör74], [Nör75], that the dynamical evolution of the nuclear mass asymmetry can be approximated by the transport equation of Focker-Planck. Such an approach can be also applied to other macroscopic variables (x). So, for a general variable x one can write the Focker-Planck equation in the following form:

$$\frac{\partial P(x,t)}{\partial x} = -v_x \frac{\partial P(x,t)}{\partial x} + D_x \frac{\partial^2 P(x,t)}{\partial x^2}. \qquad (2.31)$$

$P(x,t)$ is the probability to find macroscopic variable within the interval $(x, x+dx)$ at the time t. v_x is the drift velocity of observed variable, and D_x represents the diffusion coefficient. Both of them are so-called transport coefficients. If the variable is

investigated at infinitesimal time steps, and the diffusion coefficient is constant as well, the equation 2.31 is complete. Otherwise, derivatives of higher level have to be taken into account. The solution of the Focker-Planck equation 2.31 can be founded at the initial condition $P(x,0) = \delta(x - x_0)$ as the Gaussian:

$$P(x,t) = \frac{1}{\sqrt{2\pi D_x T}} exp\left[-\frac{(x-v.t)^2}{4D_x t}\right]. \tag{2.32}$$

This Gaussian peak is evolving with time, and its mean position is changing as

$$\langle x \rangle = v.t \tag{2.33}$$

and the width is increasing as

$$\Gamma = 4\sqrt{log2D_x t} \tag{3.34}$$

As one can see, the Gaussian maximum is moving linearly with the time and the Gaussian width is growing. In spite of that, the total integral under the curve is constant all the time, and we write

$$\int P(x,t)dx = 1. \tag{2.35}$$

Based upon the Focker-Planck equation it is possible to express various forms of cross-sections. The expression 2.32 thus results to differential cross section:

$$\frac{d\sigma}{d\vartheta} = 2\pi \int_0^\infty db\ b\ P(\vartheta, b, t \to \infty). \tag{2.36}$$

This equation is formal as the integration is going over all impact parameters for asymptotic solutions, i.e. a long time after the collision, formally expressed as $t \to \infty$. Taking into account only deep-inelastic transfer reactions with the solution $P(x = \vartheta, t \to \infty)$ from the equation 2.32 one can write:

$$\frac{d\sigma}{d\vartheta} = 2\pi \int \frac{db\ b}{\sqrt{4\pi\chi^{\vartheta\vartheta}}} exp\left[-\frac{(\vartheta-\vartheta^c)^2}{4\chi^{\vartheta\vartheta}}\right], \tag{2.37}$$

by the index *c* asymptotic values ($t \to \infty$) are marked, and $\chi^{\vartheta\vartheta}$ is the second moment of angular distribution, defined as:

$$\chi^{\vartheta\vartheta} = \frac{1}{2}\langle(\vartheta - \vartheta^c)^2\rangle. \tag{2.38}$$

Analogically it is possible to write:

$$\frac{d\sigma}{d\varepsilon d\vartheta} = 2\pi\sqrt{\frac{\mu}{2\varepsilon}} \int db\ b\ P\big(\vartheta, p_r, b, t \to \infty\big) \tag{2.39}$$

$$= 2\pi\sqrt{\frac{\mu}{2\varepsilon\Delta}} \int db\ b\ exp\left[-\frac{\omega_{rr}(\vartheta-\vartheta^c)^2}{4\Delta} - \frac{2\psi_r^\vartheta(\vartheta-\vartheta^c)(p_r-p_r^c)}{4\Delta} + \frac{\chi^{\vartheta\vartheta}(p_r-p_r^c)^2}{4\Delta}\right],$$

and

$$\Delta = \omega_{rr}\chi^{\vartheta\vartheta} - \left(\psi_r^{\vartheta}\right)^2, \ \omega_{rr} = \frac{1}{2}\langle(p_r - p_r^c)^2\rangle \tag{2.40}$$

$$\psi_r^c = \frac{1}{2}\langle(p_r - p_r^c)(\vartheta - \vartheta^c)\rangle. \tag{2.41}$$

The factor $\sqrt{\mu/2\varepsilon}$ in the equation 2.39 results from exchange of collective variable p_r, the radial component of momentum, μ represents the reduced mass.

The equations for trajectory calculation, 2.28 and 2.29, together with the equations for the second moments, 2.38 and 2.41, can be used to derive the theoretical Wilczyński graphs.

Transport coefficients

The variable *x* from the above Focker-Planck equation can be substituted by the mass asymmetry parameter $\eta = (A_1 - A_2)/(A_1 + A_2)$, or by the or other macroscopic variables such as mass of the projectile nucleus A_1. The transport coefficients then relate with the change in the average mass asymmetry η and its dispersion, or with change in the average mass number A_1, and its dispersion. In general, for any macroscopic variable one can write the following set of equations for time dependent transport coefficients:

$$\frac{d}{dt}\bar{x} = \overline{v_x} \approx v_x(\bar{x}) \tag{2.42}$$

$$\frac{d}{dt}\sigma_x^2 = 2\overline{D_x} \approx 2D_x(\bar{x})$$

Particularly, if we are talking about the mass transport coefficients v_A, D_A, their time dependence arising from the coupling of the nuclear mass asymmetry η to other collective degrees of freedom, such as the separation distance between two interacting nuclei. One way how to calculate those transport coefficients is based on the nuclear mean field approximations, applicable for strongly damped nuclear collisions and low temperature nuclear matter. Then the motion of nucleons is governed by the one-body Hamiltonian, and the transport coefficients are considered as microscopic currents flowing between two interacting nuclei. Appropriate method to derive these transport coefficients from the nuclear mean field approximation for peripheral collisions is based upon the proximity method, using a proximity potential. More on the proximity method is possible to find in the paper of Randrup [Ran87], [Ran89].

2.4 Abrasion-Ablation model

Nuclear reactions at relativistic energies, typically above 100 AMeV, differ from low and intermediate energies in few aspects. Collisions in that region of energies are faster and relativistic effects have to be considered. The simple geometric picture of Glauber is usually applied to describe the nucleus-nucleus collisions, based upon the straight line trajectories of reaction participants. This approach is widely utilizing the multiple scattering theory. As the threshold of particle production is easily achieved in relativistic collisions, the degree of freedom related with hadronization plays an important role.

The abrasion-ablation model was firstly introduced by Bowman, Swiatecki and Tsang to describe the relativistic heavy ion collisions. Its idea can be explained briefly like following: When two heavy mass ions are approaching with relativistic velocity close enough so their volumes are overlapping, this overlapping parts, participant zone, is sheared away, see the figure 2.3. This is a first phase of reaction also called abrasion

phase. The rest of projectile and target nuclei, spectators, formed right after abrasion represents cold projectile-like and target-like fragments. Both are continuing in their motion almost undisturbed. Thus velocity of spectators is almost unchanged. Because they carry out excitation energy and angular momentum, they emit charged and uncharged particles, what is described within ablation phase. Nonetheless, if spectators are warmed enough they can undergo multi-fragmentation, especially in very central collisions. If fragments of our interest is projectile-like fragments it is traditionally used the term fragmentation, and if we interesting in the target-like fragment then we talk about spallation.

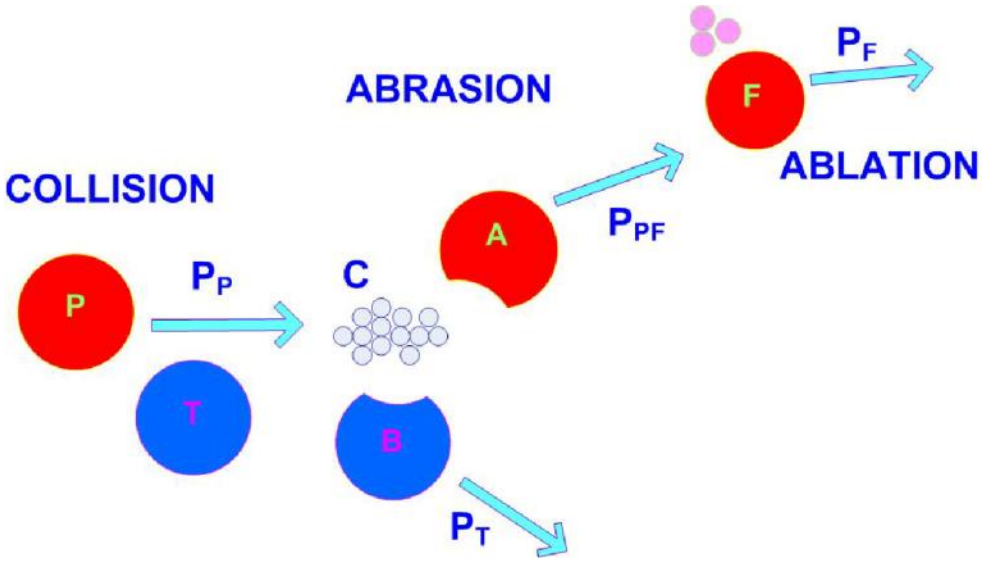

Fig. 2.3: The schematic picture of abrasion-ablation model. In the abrasion phase, two spectators, marked by A and B latters, and one participant zone C are created. The next step is modeled as the ablation, characteristic by energy and angular momenta dissipation, adopted from [Gia69].

The abrasion of *n* nucleons from projectile nucleus is described by binomial distribution derived from multiple scattering theory of Glauber.:

$$\sigma_{n'}(\vec{b}) = \binom{A}{n'}\left[1 - P(\vec{b})\right]^{n'} P(\vec{b})^{A-n'}, \tag{2.43}$$

where $P(\vec{b})$ is the probability that n' nucleons stay in the projectile-like spectator at the impact parameter $\vec{b}$, in the plane perpendicular to projectile direction oriented to *z*-axis, and $1 - P(\vec{b})$ denotes the probability that n' nucleons are ejected from the projectile nucleus. Following this equation, the abrasion of n of N neutrons and z of Z protons from the projectile nucleus could be expressed in a similar way:

$$\sigma_{nz}(\vec{b}) = \binom{N}{n}\binom{Z}{z}\left[1 - P(\vec{b})\right]^{n+z} P(\vec{b})^{A-n-z}. \tag{2.44}$$

The probability $P(\vec{b})$ depends only on the single particle density $\rho_p(\vec{x})$ of the projectile and on the nucleon-nucleon optical potential:

$$P(\vec{b}) = \int d^2s\, dz\, \rho_p(\vec{s}, z) \left| e^{i\chi^{opt}(\vec{s}+\vec{b})} \right|^2 . \quad (2.45)$$

The optical potential is usually taken from nucleon-nucleus scattering data or based upon the calculation from multiple scattering theory, which is rather reliable as well. When one neglects all correlations related with calculation of optical potential parameter χ^{opt}, related with scattering amplitude, then one can rewrite the above term as following:

$$P(\vec{b}) \approx 1 - A_T \sigma_{tot}^{NN} \int d^2s\, dz\, \rho_P(\vec{s}, z) \rho_T(\vec{s} + \vec{b}, z')dz' . \quad (2.46)$$

This integral represents the overlapping of densities of the projectile and target at a distance $\vec{b}$ from mass centers. The position vector of *j*-th nucleon in the projectile nucleus is given as $\overrightarrow{x_j} = (\overrightarrow{s_j}, z_j)$, where the first component refer to projectile center of mass, and is the projection of its position to impact parameter plane, and the later one represents projection of nucleons to direction of the projectile. In similar way, one can write the *i*-th nucleon position in the target nucleus as $\overrightarrow{x_i} = (\overrightarrow{s_i}, z_i)$.The parameter σ_{tot}^{NN} represents total nucleon-nucleon scattering cross section. The term $P(\vec{b}) - 1$ is proportional to the sheared off volume in the abrasion phase.

Some of geometrical models supposed straight trajectories, which can be determined based upon the impact parameter [Gos77], [Day86]. Other approaches assumed Coulomb trajectories and only after reaching closest contact point the trajectories are considered as straight lines [Abu80], [Har83].

These spectators are characteristic by much lower excitation energy as participant zone. However, some energy of the relative motion is dissipating due to nucleon-nucleon collisions. More about the excitation energy of projectile or target spectator can be found [Gai91], where it is considered proportional to amount of nucleons abraded in the first stage of the reaction.

The model of abrasion-ablation is implemented in the ABRABLA code [Gai91], [Jun98], [Ben98], [Jur03]. That model is used to for prediction of production cross section and yields of the products of spallation and fragmentation reactions. The geometric abrasion-ablation model can be found also in EPAX [Sum00] and COFRA [Hel03] models. The main advantage of abrasion-ablation models is possibility of fast and reliable calculation of production cross sections. This is very valuable property for several fields of physics, e.g. physics of rare ion beams, or development of devices for the future nuclear waste transmutation (ADS). On the other hand, there is intra-nuclear cascade (INC) model characteristic by much longer computational time. Contrary to abrasion model the INC model allows to predict all kinds of particle production, i.e. neutron, protons, pions etc.

2.5 Intra-nuclear cascade model (INC)

Similar to abrasion-ablation models, considering geometric picture of spectator and participant zone, models of intra-nuclear cascade (INC) can be justified at relativistic energies too, in order to describe some characteristics of high energy collisions. In this context, the threshold energy for relativistic collisions corresponds to about 20% of nucleon mass, which is approximately incident energy of 200 - 250 AMeV. This statement corresponds to assumption that de Broglie wave length of nucleons is shorter than the range of interaction, and collisions are well separated in the space and time. Such an energy limit can be understood as sufficient but not necessary in general. The

most extensively utilized INC model, the Liège intra-nuclear cascade model (the code INCL++) gives surprisingly good results also at lower incident energies, based upon available data between 40 to 250 AMeV [Cug03]. In spite this fact, predictions seem to be better at higher incident energies, also when a target mass increases, and for intermediate angles measurements.

The main idea of the INC model lies in consideration that each reaction can be described as sequence of independent nucleon-nucleon collisions. For now, let´s consider the simple scenario, where a single nucleon of a projectile, i.e. proton or neutron, enters the target nucleus. Once it enters inside a nucleus, it subsequently triggers the intra-nuclear cascade, the figure 2.4. The cascade itself is typically accompanied by an emission of particles, such as light charged particles, nucleons and by production of sub-nuclear particles. As long as nucleon-nucleon collisions take place there is dissipation of the kinetic energy of relative motion into internal degrees of freedom. The excited pre-fragment is formed at the end of the cascade, so-called hot nucleus, Consistently with abrasion-ablation approach modeling spectator and participant zones, the hot and cold zones are created during the collision.

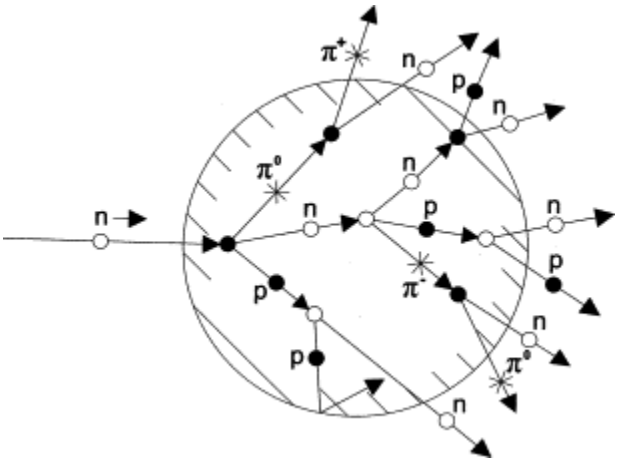

Fig. 2.4: Picture of an intra-nuclear cascade induced by relativistic neutron [Yas10]. In the first collision the neutron is hitting a proton and the pion π^0 is produced, i.e. $n + p \rightarrow n + p + \pi^0$. Such kind of collision is deep non-elastic as massive pion is produced. However, an elastic scattering is also taken place at very low collision energy.

To better understand the INC model, one can explain it on the example of the most extensively used model, the Liège intra-nuclear cascade model. The following assumptions are crucial:

- Each collision is initialized at the time t = 0, when the incident nucleon is hitting the target nucleus surface. At the same time, the target nucleons are randomly occupied inside the target nucleus bounded by the sphere with radius of $R = 1.12A^{1/3}$. The linear momentum of each nucleon is generated stochastically as well within a Fermi sphere defined by maximum radius p_F = 270 AMeV. Thus the phase space is defined.
- All nucleons inside of the target nucleus feel a constant potential, with potential depth of 40 MeV.
- The target nucleons are well separated by the space and time and are moving

along straight line trajectories. Once they reach the minimum relative distance $d_{min} \leq \sqrt{\sigma_{tot}/\pi}$, they scatter each other in elastic or inelastic scattering, so momentum and energy is conserved. The parameter σ_{tot} represents the total cross section, established from the experimental differential cross section.

- Relativistic kinematics is used.
- Each nucleon-nucleon collision obeys the Pauli principle. When the final state of nucleon is already occupied the collision is forbidden. This is preserved within the model by the Pauli blocking factor:

$$P_{12} = (1 - f_1)(1 - f_2) \tag{2.47}$$

, where $(1 - f_1)$ and $(1 - f_2)$are probabilities to change the phase space of the particle 1 and the particle 2. The collision is blocked if P_{12} factor is out of the interval (0, 1). Each nucleon has position (r_i, p_i) with defined phase space volume, with r-space radius of 2 fm, and p-space radius of 200 MeV/c.

- Spectator nucleons are not allowed to collide.
- When a nucleon hits the potential wall, it either reflected if its total energy is lower the threshold, otherwise it reaches nuclear surface. In the latter case, the nucleon can be reflected from the surface or leaves the nucleus. The probability of transmission through the surface is then expressed by a transmission probability P_{tr} as a function of the nucleon kinetic energy T, potential depth V_0 and Gamow factor G:

$$P_{tr} = \frac{4\sqrt{T(T-V_0)}}{2T-V_0+2\sqrt{T(T-V_0)}} e^{-2G} , \tag{2.48}$$

and for the Gamow factor one can write

$$G = \frac{Z_T z e^2}{\hbar c} \sqrt{\frac{2M}{T-V_0}} (\arccos x - x\sqrt{1-x^2}), \tag{2.49}$$

$$x = \frac{T-V_0}{B}, B = \frac{Z_T z e^2}{R} , \tag{2.50}$$

z and Z_T are charges of the incident particle and of the target nucleus. M is the mass of the particle. When the particle leaves the target nucleus the total energy is conserved.

- Besides nucleons also Δ particles and pions production are considered [Cug97].
- Isospin degrees of freedom are introduced.
- The cascade stage is running till the stopping time t_{stop}.
- The excitation energy after each nucleon-nucleon collision is checked, and if it equals zero, than the cascade is going to be stopped.

Everything what is going to happen after the stopping time relates with a subsequent de-excitation of hot pre-fragments. Thus the parameters such as excitation energy, charge and mass number of the pre-fragment can be transmitted to de-excitation phase, well described by appropriate de-excitation models such as SMM, Gemini or ABLA07 etc.

The above assumptions are related to standard Liège intra-nuclear cascade model. The new version of model incorporates some new ingredients:

i) The introduction of a diffuse nuclear surface related with a Woods-Saxon density distribution
ii) Consistent dynamical Pauli blocking
iii) Division into participants and spectators
iv) Improvement of pion dynamics
v) Extension to incident light clusters

The latest version of INC model has been successfully implemented in the code INCL++ [Cug81], [Bou02], [Cug11], [Bou13], [Ler13], [Man14]. Also, the reliable results are provides by the code ISABEL [Yar81], or other alternative models based on the INC physics such as MCNP [MCNP], MARS [MARS] or Geant4 [Ago03] providing a hybrid set of models describing the particular stages of given type reactions. Namely, they allow simulating of a hadronic cascade, primary and secondary fragmentation, and particle transport.

The applicability of the INC based models is really extensive on different fields of research and industry at the present. It represents a very useful tool in designing of nuclear radiation detectors, utilized also in nuclear energy for waste recyclation, and in space research.

From the point of mass distribution of pre-fragments the abrasion-ablation models appear much faster compared to the INC model, with significantly better computational time. However, when one put emphasis on prediction of all particles and products, then the model based upon the intra-nuclear cascade is definitely more applicable. Besides nucleons and light charged particles, non-elastic nucleon-nucleon scattering products such as pions can be predicted by the INC model.

Chapter 3

De-excitation models for heavy nuclei collisions

3.1 Statistical models ABLA, GEMINI, SMM

Many statistical models have been developed till the present in order to reproduce a de-excitation phase of low, intermediate and high energy nuclear reactions. Within this chapter only those models which were utilized in thesis are discussed. This chapter is dedicated to brief description of model framework of the very extensive used statistical models, i.e. ABLA, GEMINI and SMM, in description of the de-excitation phase in fragmentation, spallation or deep-inelastic transfer reactions.

While at low energies, well below 1 AMeV, the excited system gets rid of its energy excess mainly via evaporation of nucleons and alpha particles, in competition with nuclear fission at higher angular momentum and energies, at high excitation states also heavier fragments can be emitted. These fragments are marked as intermediate mass fragments or shortly IMF ($Z \geq 3$). Such a process is called fragmentation and can be observed if the excitation energy exceeds the threshold value ~ 1 AMeV. Once the excitation energy per nucleon is high enough a sequence of IMF-IMF emission is possible too. When the excitation energy overcomes the limit 2 AMeV, then the simultaneous multi-fragmentation, or break-up of a nucleus starts to play a role in the output channel. This is managed by different models in little bit different way. In the last decades the models such as ABLA, GEMINI or SMM have been improved in order to cover de-excitation phase of nuclear reactions with relative low excitation energy, and low angular momentum, up to region of high energies and compression of nuclear matter. A very good option for such an observation comes with spallation and fragmentation reactions. In order to describe fragmentation and multi-fragmentation, the classical model of compound nucleus suggested by Hauser-Feschbach [Hau52] was extended by emission of IMF fragments, developed by Moretto [Mor75]. Moretto suggested that the IMF emission can be described as a binary fission-like split, where production of the IMF is accompanied by heavier residual fragments. Thus the Sequential Binary Decay model (SBD) has been developed and is implemented in GEMINI code. The IMF probability is described by fission barrier properties of asymmetric nuclear fission, and it is determined statistically. Using this attempt many data have been reproduced up to the present. However, the SBD model cannot explain IMF emission in simultaneous multi-fragmentation (break-up) in reliable way. The most significant discrepancies are usually observed at zero-angle measurements. Besides this also some fragments correlations are not described in agreement with experimental data [Kre93].

The statistical phase space model of multi-fragmentation provides much better description comparing with the SBD model. The properties of pre-fragments are characterized in so-called “freeze-out” configuration. At this configuration distances between IMF pre-fragments are assumed to be larger as short range nuclear interaction, due to the thermal expansion of the system. The system undergoes change in the nucleon density as its volume expands. Within the statistical phase space model an

evaporated residue probability is given by the available phase space to populate this state. As for the fission probability, it is evaluated based on the available phase space at the saddle point configuration above the fission barrier. For the break-up channel, the probability of decay to certain IMF fragments combination is given by available phase space for a given multi-fragment configuration at freeze-out state where short range interactions between fragments vanishes. At the freeze-out state the all IMF fragments are expected to be pre-formed and well defined. In order to evaluate the probabilities of each multi-fragment configuration micro-canonical [Gro97], canonical or grand-canonical approximations can be applied [Bon95]. The model capable to describe simultaneous multi-fragmentation is the mentioned Statistical Model of Multi-fragmentation or briefly SMM. The SMM model can provide calculation where IMF fragments are excited (hot fragments) or their excitation energy is zero (cold fragments). In the SMM calculations the freeze-out volume depends on fragment multiplicity. Along with SMM and GEMINI code also ABLA de-excitation code can be used as statistical de-excitation code for nucleon-nucleus or in nucleus-nucleus collisions.

ABLA07 code

In the recent years, development of statistical de-excitation model ABLA has been guided by the empirical way based on the experimental data on the nuclide distribution measured at GSI in Darmstadt. Consequently, some new processes have been implemented to the version ABLA07, such as very asymmetric binary splits, multi-fragmentation and microscopic structure on the fission process. These processes thus extend de-excitation channels of thermal nucleus, where at lower excitation energies evaporation and fission channels dominate, to channels as (multi-) fragmentation, becoming more dominant as excitation energy is increasing. Once the excitation energy is over the threshold value a multi-fragmentation module is triggered. The default value of the threshold is set to $E^* / A = 4.2$ AMeV, but can also be set depending on the mass of the excited system following the systematics of Natowitz et al. [Nat02]. ABLA07 works with one set of the model parameters fixed for all system and energies. Similar to others statistical codes, the starting point is given by thermal equilibration of nuclear system. Within ABLA07, the simultaneous break-up is considered as the cracking of the hot nucleus into several fragments, as a consequence of thermal instabilities. The particle evaporation is based on the Weisskopf-Ewing formalism [Wei40], and the fission decay width is calculated taking into account dynamical effects [Jur03]. The basic components of the model one can find in [Ric06].

GEMINI code

In the framework of GEMINI code, developed by Charity et al. [Cha88], [Cha10], de-excitation phase is described as a series of binary decays. The particle emission $Z \leq 3$ are managed by Hauser-Feshbach evaporation formalism [Hau52]. In case of fission, the formalisms of Moretto [Mor75] is applied in order to described emission of fragments with $Z > 3$. The Sierk´s finite-range fission barriers [Sie85] are considered in fission and (multi-)fragmentation channel. As for the fission width of heavy nuclei, values from Bohr-Wheeler model are accepted [Boh39].

SMM code

The simultaneous statistical model SMM, developed by Bondorf et al. [Bon95], is the most appropriate for de-excitation of equilibrated nuclear systems and residues

produced in nucleon-nucleus collisions or for description of spectator parts of nuclei from peripheral heavy nuclei collisions. The characteristic for such collisions is that collective degrees of freedom do not play an important role. Similar to the above statistical models, the formation of fragments in head-on collisions cannot be explained via pure statistical model as it is governed by the dynamical effects associated with large collective flow of matter. In comparison with the GEMINI model, the SMM model operates with expansion of nuclear matter leading to simultaneous IMF emission, so-called break-up of a thermalized system. Within the SMM model finite size effects, the Coulomb interaction between fragments, and their internal excitation energies are considered. Break-up channels are described via grand-canonical ensembles. Hot primary pre-fragments, or IMF pre-fragments, are described via the liquid drop model approximations.

3.2 Beyond the statistical model description

The statistical models rely on two-step mechanisms of nuclear reactions, an initial phase or collision phase, and the second phase described as de-excitation starting at the moment of thermal equilibrium of a given system is reached. Usually, any statistical model calculation starts with set of following parameters (E*, J, A, Z), i.e. excitation energy, angular momentum, mass and atomic number of pre-fragment. However, there are some processes with strongly depend of the output channel on the initial conditions of collision. Such a behavior of nuclear reactions can be observed in reactions of synthesis of super-heavy element, i.e. competition between fusion vs. quasi-fission, or in high energy collision with significant compression of nuclear matter. These processes are usually simulated using dynamical models with explicit time dependence. Such models are represented by the time dependent Hartree-Fock model or approaches based on the Boltzmann transport equation incorporating not only nuclear mean field, and its time evolution, but also collisions of nucleons. The latter property is especially important for two body dissipation. Here are the most reliable implementation of Boltzmann transport equations, or its approximations: Boltzmann-Uehling-Uhlenbeck (BUU), Vlasov-Uehling-Uhlenbeck (VUU), Boltzmann-Nordheim-Vlasov (BNV), Landau-Vlasov (LV), Quantum Molecular Dynamics (QMD), Constrained Molecular Dynamics (CoMD) and others.

Chapter 4

Results and Discussions

4.1 Investigation of fusion hindrance in reactions leading to production of super heavy elements

The contemporary research of super-heavy elements has relied on nucleus-nucleus collisions around the Coulomb barrier leading to formation of compound nucleus system, which can results to complete fusion reaction. At the end of this multi-step process a cold evaporated residue (ER) can be produced, what we note as super-heavy elements or briefly SHE, see the figure 4.1. Such scenario is valid only for the most central collisions with small impact parameter, when the reaction is going via so-called adiabatic way. Otherwise heavy-ion collisions are peripheral leading to deep-inelastic reactions, where typically projectile and target like fragments are observed in the output channel.

The heaviest elements were synthesized in cold fusion reactions with Pb or Bi targets, up to Z = 112, accompanied by emission of one neutron [Hof98]. However, a rapid decrease in production cross sections of SHE to the level of few pb, caused by competition with quasi-fission, eliminates cold fusion reaction for investigation of SHE elements heavier than Z = 112. Therefore, hot fusion has become preferable on the way to the heaviest SHE systems. The hot fusion mechanism has opened up a possibility to synthesize the elements with atomic numbers 113 – 118, first time applied in FLNR, in Dubna. Use of heavy actinide targets made of uranium up to californium, bombarded by double magic ^{48}Ca nucleus, has allowed to reach this goal [Oga04-13]. Despite the fact that fusion hindrance is not as strong in hot fusion compared to cold fusion reaction, quasi-fission is still present and remains dominant for Z > 112. Today it is clear that understanding of quasi fission plays a crucial role on the field of synthesis of new SHE. Therefore comprehension of quasi-fission can allow finding appropriate target vs. projectile combination and set the most appropriate beam energy. Besides synthesis of SHE in laboratory conditions, the main factory for their production in the Universe are still astrophysical objects such as neutron stars. These natural factories use r-process nucleo-synthesis for production of SHE, which starts after collision of two neutron stars, i.e. two neutron star mergers. After many years of research, the quasi fission process still remains a topic of fundamental research. The systematic measurements on quasi fission were performed by experimental groups from Dubna [Itk03], Tokai [Nis10] and Canberra [Rie13]. Similar to complete fusion and nuclear fission, quasi fission was theoretically investigated by the model of di-nuclear system [Ada97], [Ada98], [Gia13], and by the Langevin equation [Zag05-07], [Ari12]. Beside others, models based on the Boltzmann equation, such as ImQMD [Wan02], [Wan13], [Zha08], [Cho14] (approximations of Boltzmann equation) or models based on the time dependent Hartree-Fock theory [Gol09], [Wak14], [Obe14], [Sek16] are frequently used as well.

Within this chapter the studies on fusion hindrance by utilizing two approximation of Boltzmann equation are presented. The first model is based on the Boltzmann-Uehling-

Uhlenbeck (BUU) [Ber88] equation whose results are compared with Constrained Molecular Dynamics (CoMD) [Bon94]. Both of these approaches respect Pauli principle, implemented separately for protons and neutrons, and the Coulomb interaction between protons is included too. Both of models describe the reaction dynamics applying similar physics. However, each of them describes nucleon density (quantum mechanical fluctuations) in a different way and collision integral is established differently as well. The given results in the following sub-chapters show the influence of different parameters of the equation of state of nuclear matter (EOS) on the competition of fusion vs. quasi-fission. We have performed a systematic study on the competition of fusion and quasi fission leading to the production of SHE, and BUU and CoMD simulations were compared with experimental data. The high quality data measured in Dubna, Tokai and Canberra allowed us to find more stringent parameterization for the equation of state of nuclear matter nearby scission point of quasi-fission. The constraint relates with the stiffness of the nuclear equation of state and the density dependence of the symmetry energy. For selected investigated reactions around Coulomb barrier, the effect of EOS parameterization should play a role in the region where density gradually drops down from saturation density ρ_0 to zero. Such behavior is typical for surface of the di-nuclear system (DNS) and in the neck region where nucleon density differs from those in the bulk of DNS.

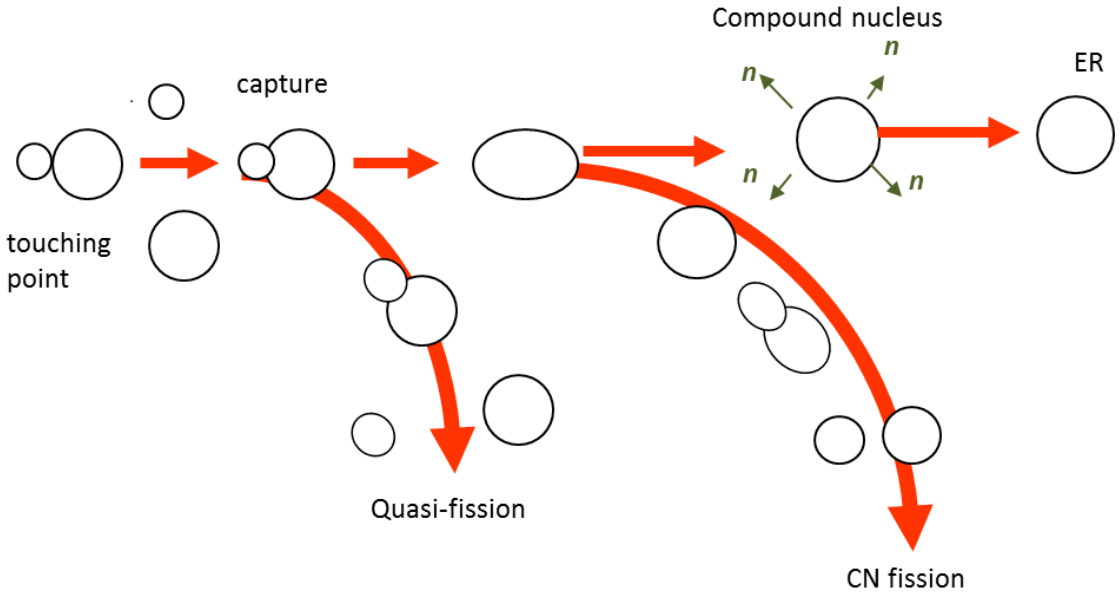

Fig. 4.1: Central nucleus-nucleus collision: In the first step di-nuclear system is created by capturing projectile nucleus on the target. The created DNS system can evolve to the so-called scission configuration and undergoes quasi-fission. In the case of synthesis of the heaviest SHE the DNS can evolve towards the saddle point of fusion barrier and subsequently fusion – fission or complete fusion can take place. In the latter one scenario, evaporated residue ER is created after hot nucleus gets rid of excitation energy by emission of 1 – 2 neutrons (cold fusion) or 3 – 4 neutrons (hot fusion). The rest of the exceeding energy and angular momentum is typically carried out by gammas as yrast cascade Cold fragment ER is finally created.

4.1.1 Boltzmann-Uehling-Uhlenbeck simulations (BUU)

Boltzmann-Uehling-Uhlenbeck (BUU) equation is very extensively used approximation of Boltzmann equation for describing dynamics of nucleus-nucleus collisions at intermediate and high energies. As the nucleon density of the system is evolving during a collision, its equation of state of nuclear matter should differ from that at saturation density ρ_0. The BUU model allows thus studying the equation of state of the nuclear matter out of the saturation density via heavy ion collisions, where nuclear matter is evolving to super- or to supra-saturated density ($\rho > \rho_0$, $\rho < \rho_0$). However, nucleon density is not evolving only in nucleus-nucleus collisions right up from the intermediate energies or far away from super-saturated density, but also at the lower energies as well. The proof of relevance of the equation of state at low energies reactions is provided by Isoscalar Gigantic Monopole Resonances (ISGMR). At the present, the ISGMR resonances measured for light nuclei shown as the method for investigation of incompressibility parameter for ground state, with excitation energies varies from ~ 12 up to ~ 25 MeV for heavy and light nuclei, respectively. Hence, it is demanded to investigate a possible effect of equation of state on dynamics of fusion and quasi-fission in synthesis of SHE. Similar to ISGMR, the reactions close to the Coulomb barrier lead to relatively low excitation energies and densities around saturated density.

In order to get realistic theoretical description of nucleus-nucleus collisions for dense fermionic system or nuclear matter, some approximations of the Boltzmann equation are needed. In the framework of BUU model the potential energy is described by the single particle mean field evolving as the nucleonic content, shape and size of di-nuclear system is changing with elapsing time. For realistic description of nucleonic distribution function in phase space *f(r, p, t)*, the equation 2.2 as the solution of the Boltzmann equation respects the Pauli principle is taken into account, separately for protons and neutrons. The Coulomb interactions between protons are considered in order of proper description of the nuclear mean field and collision integral. Implementing the nuclear mean field and collision integral to BUU ensures the attractive and repulsive forces between nucleons, respectively. The solution of BUU distribution function *f(r, p, t)* is eventually reached by test particle method of Wong [Won82], where the collision term on the right side of equation 2.5 is calculated as in Cugnon et al. [Cug81]. Such a collision integral is dependent on the particular parameterization of EOS.

Assumptions & settings of BUU simulations

In the framework of our simulations we have tested sensitivity of fusion and quasi-fission on various sets of parameters of the equation of state EOS in appropriate set of nuclear reactions leading to formation of SHE. This sensitivity originates from nuclear mean field, which also depends on the energy of symmetry, and is sensitive on $\kappa(K_0)$ and γ parameters, see the equation 2.3. However, these values are still not exactly known for asymmetric nuclear matter. There are only constraints of these values to certain interval derived from nucleus-nucleus collisions, collective excitations or from neutron star observation. Therefore, various assumptions on the stiffness of EOS of nuclear matter and assumptions on properties of studied reactions are needed:

- We considered parameter of incompressibility from sufficiently wide range of values, i.e. K_0 = 200 – 380 MeV, also consistent with ISGMR measurements. This corresponds to the parameter κ from the range 1.16 – 2.0, see the equation 2.3. Also one can assume that the density dependence of symmetry energy should vary within γ = 0.5 – 1.5.

- As for the reactions we selected representative set of reactions leading to production of SHE, where the quality data exist, see the table 4.1. The collision energy 5 AMeV for each collision in our simulations correspondence to the available data measured experimentally, within few MeV per total beam energy.
- We expected that quasi-fission is dominant at most central collisions with very similar impact parameter, similar as we observe in fusion.
- Due to lack of information on angular momentum of quasi-fission fragments, and in order to eliminate peripheral collisions, we considered only central collisions with impact parameter up to 0.5 fm. The dominant peripheral nuclear reactions are deep-inelastic transfers, typically spreading over the impact parameter range from 4 to 16 fm.
- Time window for observation of each collision was set to t = 3 000 fm/c. This is long enough to observe fusion or quasi-fission products.
- Each reaction stated in the table 4.1 were simulated 20 times at a given parameter set [K_0, γ], using 600 test particles.

Projectile & Target	P_{CN} (exp.)	References
$^{48}Ca + ^{208}Pb$	~ 1	[Boc82], [Pro08]
$^{48}Ca + ^{238}U$	~ 0.2 – 0.5	[Itk07]
$^{48}Ca + ^{249}Cf$	10^{-3} <	[Oga12]
$^{64}Ni + ^{186}W$	~ 0.4 – 0.8	[Kny08]
$^{64}Ni + ^{208}Pb$	10^{-3} <	[Boc82]
$^{64}Ni + ^{238}U$	10^{-3} <	[Koz10]

Tab. 4.1: Reactions leading to production of SHE, where fusion and quasi-fission was experimentally observed. The set of given reactions we used for testing the sensitivity of DNS system on different EOS.

By using four Xeon Phi coprocessor cards it was possible to perform many parallel simulations as each of the card is equipped by 61 cores allowing to run up to ~ 1 000 calculations at once.

Experimentally deduced fusion probabilities P_{CN}

The reactions were selected in order to study fusion vs. quasi-fission in synthesis of SHE in both of hot and cold fusion, given by projectile or target nucleus of ^{48}Ca and ^{64}Ni, investigated in the direct or in inverse kinematics. As for targets, spherical and deformed nuclei were combined with given projectiles. The selection of reactions cover SHE region with atomic numbers of compound system Z_{CN} = [102, 112, 118], in reactions with ^{48}Ca, and Z_{CN} = [102, 110, 120] in collisions with ^{64}Ni. In general, the higher $Z_{CN,}$ the lower fusion probability one can expect in output channel, with respect on other macroscopic parameters of the given DNS. One of the most decisive parameters is mass asymmetry between target and projectile nucleus, where the higher

mass asymmetry leads to hot fusion. In contrast to cold fusion, hot fusion is characteristic by stabilization effect on production of SHE heavier than Z = 112.

Based on the experimental measurements, ^{48}Ca + ^{208}Pb reaction leads to production of one of the heaviest system ^{256}No, where fusion channel is still dominant over quasi-fission [Boc82], [Pro08]. This statement results from the dominance of fusion and fusion-fission peak observed in mass spectra. The symmetric fusion-fission was experimentally distinguished from quasi-fission by analyzing differential cross section depicted as Mass vs. TKE of fragments. So the total fusion probability for the hot fusion reaction ^{48}Ca + ^{208}Pb was evaluated to almost 100 [%] [Boc82], [Pro08]. The reaction where quasi-fission starts to contribute is ^{64}Ni + ^{186}W, with compound system ^{250}No [Kny08]. Although both of these reactions lead to similar compound system, the latter reaction is cold fusion a thus the fusion hindrance was more significant. The upper limit for fusion probability in case of ^{64}Ni + ^{186}W was evaluated as 40 - 80 [%]. The evaluation is based on the comparison with the measured data of ^{48}Ca + ^{238}U [Itk07], were quasi-fission occurs even more frequently, and upper limit for the total fusion is established to 20 - 50 [%]. Comparing ^{64}Ni + ^{186}W with ^{48}Ca + ^{238}U data one can conclude that in tungsten reaction, fusion probability is almost two times higher as in the reaction with uranium. The strongest hindrance of fusion was observed in reactions ^{48}Ca + ^{249}Cf, ^{64}Ni + ^{208}Pb and ^{64}Ni + ^{238}U. Such a strong suppression of fusion results to very small probabilities, ranging from 10^{-3} to 10^{-5}. Evidently, the given reactions fusion probability spreads over a wide range, i.e. from 0 [%] up to 100 [%], what consequently, enables to test the limit for soft and stiff EOS.

Simulations of nucleonic density

Once we have a clue about experimentally measured fusion probabilities P_{CN}, it is possible to test sensitivity of selected set of reactions on various parameterization of EOS. In our simulations we focused on evolution of nucleonic density within the time window 3 000 fm/c, where each reaction was tested for few parameter sets [K_0, γ]. Based on the evaluated fusion vs. quasi-fission statistics resulting from our simulations, and taking into account the level of compliance with the experimental data, some of parameter sets [K_0, γ] could be eliminated. Obvious example of interplay between parameter of incompressibility and density dependence of symmetry energy is demonstrated on the figure 4.2. From all analyzed reactions, reaction ^{64}Ni + ^{186}W shows up as the most sensitive on stiffness or softness of EOS. This is consequence of approximately equal probabilities for fusion and quasi-fission.

One can see, that the choice of soft-soft parameter set [K_0, γ] = [202 MeV, 0.5], caused the system undergoes quasi-fission in all 20 simulated collisions. A splitting of DNS system to two fragments takes place at scission time, typically around 1 200 fm/c. The same scenario was observed in all 20 simulated collisions. However, we know that it does not correspond to the observed reality. Hence, we can conclude that this parameter set cannot be appropriate, even though our analysis is limited to 20 events. And although our analysis has limitations, mainly related with computational time of used super-computer, it still enables to make constraint on EOS parameterization. In this case, all 20 events lead to quasi-fission and imply total disagreement with data.

Since quasi-fission is controlled by counterbalance of surface energy and Coulomb repulsion force, their interplay is deciding. Obviously, the Coulomb repulsion is dominant on the Fig. 4.2. In the terminology of EOS, one can say that weak surface tension influences the fusion probability and eventually prevents fusion again quasi-fission. However, to prevent quasi-fission is possible by controlling the nuclear matter asymmetry in the neck region of DNS. The stiffer the density dependence of symmetry

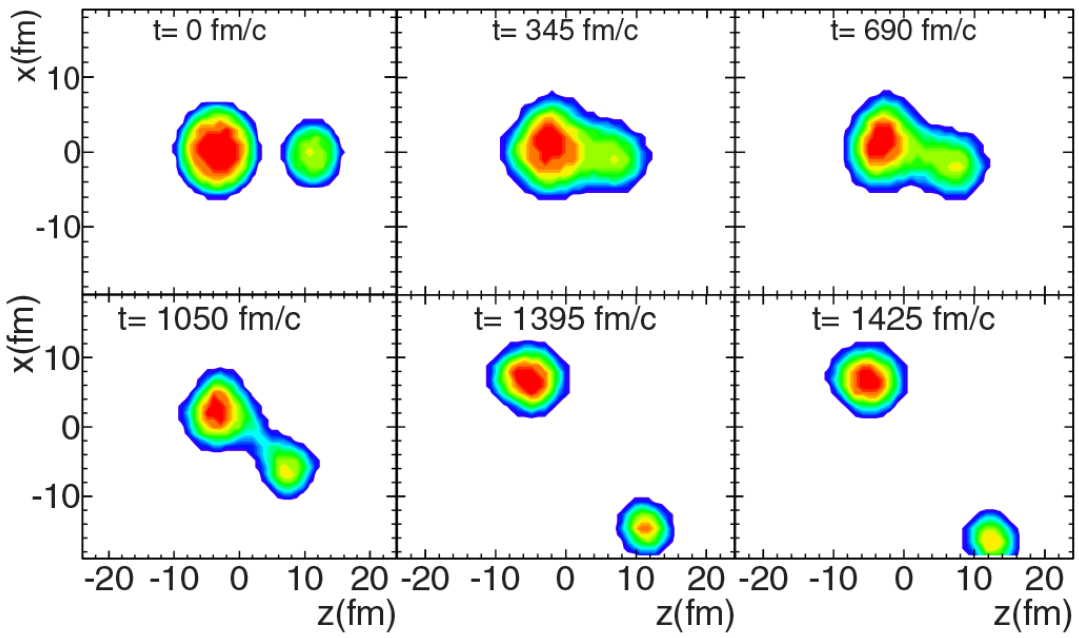

Fig. 4.2: Evolution of nucleonic density for the most central collisions ^{64}Ni + ^{186}W at 5 AMeV. Soft-soft parameter set [K_0, γ] = [202 MeV, 0.5] was used.

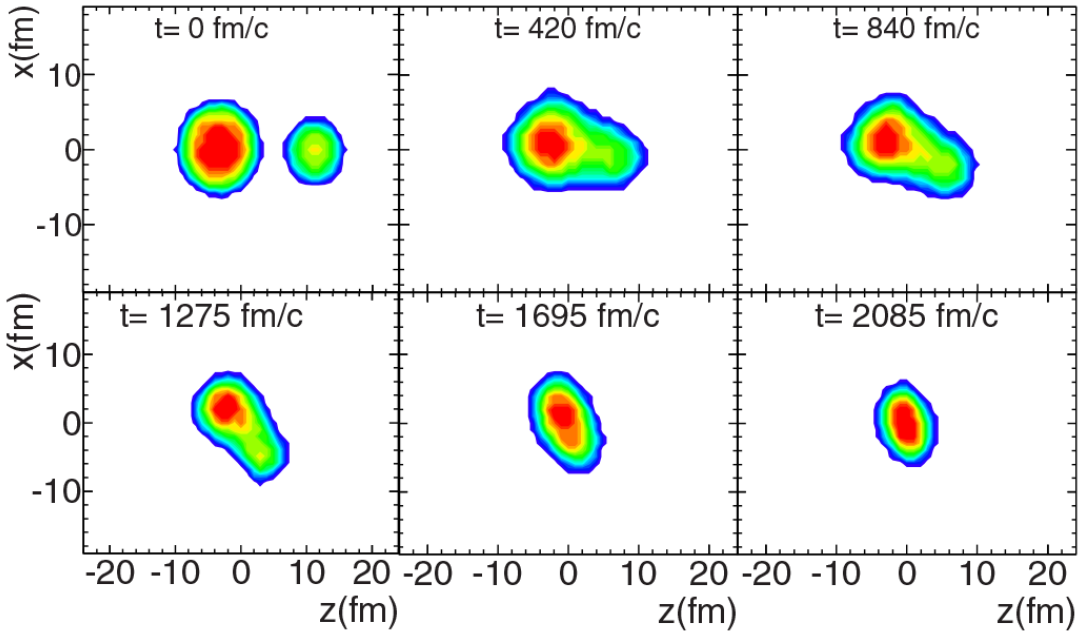

Fig. 4.3: Evolution of nucleonic density for the most central collisions ^{64}Ni + ^{186}W at 5 AMeV. Stiff -soft parameter set [K_0, γ] = [300 MeV, 0.5] was used.

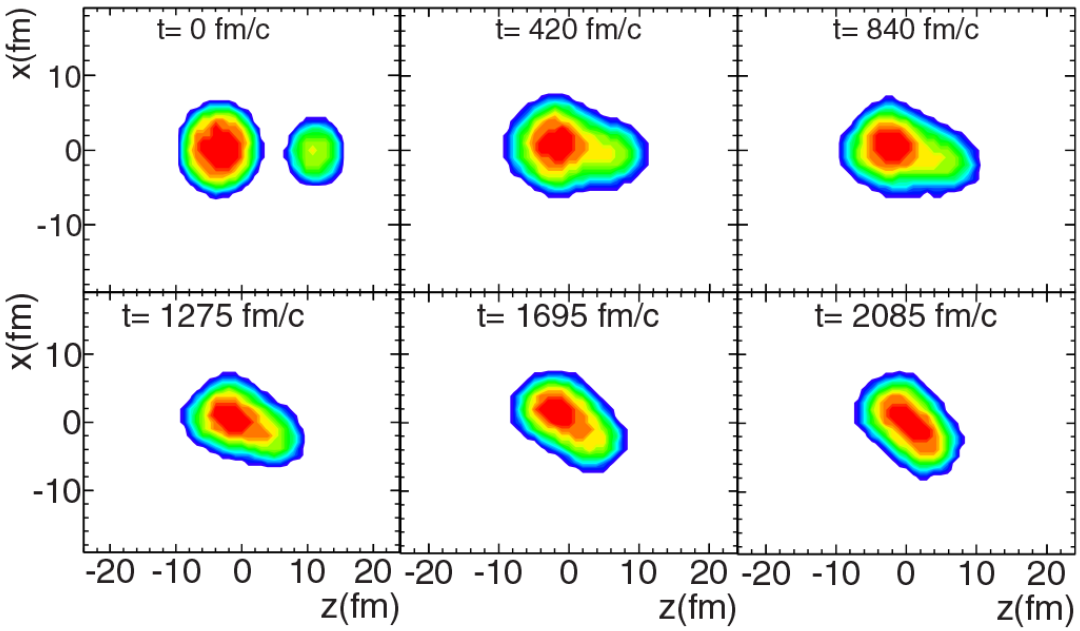

Fig. 4.4: Evolution of nucleonic density for the most central collisions ^{64}Ni + ^{186}W at 5 AMeV. Soft-stiff parameter set [K_0, γ] = [202 MeV, 1.5] was used.

energy the more symmetric content in the neck region one can expect. These statements are demonstrated on the figures 4.3 and 4.4, with parameter sets [K_0, γ] = [300 MeV, 0.5] and [K_0, γ] = [202 MeV, 1.5], respectively. The figure 4.3 thus points out on strong stabilization effect of stiff incompressibility as the nucleonic density of DNS is evolving. Even though the density dependence of symmetry energy remains soft, i.e. γ = 0.5, the surface tension is sufficient to overcame coulomb repulsion as DNS evolves in time and fusion finally happened. The similar effect can be reached using stiff density dependence of symmetry energy and soft incompressibility parameter, i.e. [K_0, γ] = [202 MeV, 1.5], see the figure 4.4. In this case, despite the weak surface tension the DNS has more elongated shape, the stabilization is reached, and the system prevents quasi-fission. Hence, softer incompressibility can be compensated by stiffer density dependence of symmetry energy to prolong life time of DNS and fusion is more probable. Eventually, the compound system or mono-nucleus can be formed. This approach of testing EOS parameterization was applied for the rest of reactions. All the results on the constraint of nuclear matter are discussed in the following sub-chapter.

4.1.2 Constraining the equation of state of nuclear matter, BUU model

The given set of nuclear reactions can help us to find more stringent constraint of K_0 and γ parameters of EOS. Both of the parameters have impact on nucleonic density evolution as DNS is evolving in time and control competition between quasi-fission and fusion.

^{48}Ca + ^{208}Pb, ^{48}Ca + ^{249}Cf, ^{64}Ni + ^{208}Pb, ^{64}Ni + ^{238}U at 5 AMeV

("pure" fusion and "pure" quasi-fission reactions)

Whereas in ^{48}Ca + ^{208}Pb reaction fusion is still dominant over quasi-fission, with probability close to P_{FUS} ~ 100 [%], in collisions ^{48}Ca + ^{249}Cf, ^{64}Ni + ^{208}Pb, ^{64}Ni + ^{238}U the fusion probability is strongly hindered. In other words, the probability for the latter

set of reactions at the most central collisions can be written as $P_{FUS} = N_{FUS} / N_{TOT} = N_{FUS} / N_{QF} \sim 0$ [%].

Based on our analysis we conclude that any parameterization out of the area [K_0, γ] = [202 - 230, 0.5 – 1.0] results to fusion of the DNS formed in ^{48}Ca + ^{208}Pb reaction. However, within that interval quasi-fission became dominant, what is actually in disagreement with the experimental observation, and it incorrectly implies that quasi-fission takes place at mb scale. Therefore, such a soft-soft parameter set can be excluded. The upper constraint we can get from the other three reactions, i.e. predominantly undergo quasi-fission. By investigation of EOS for stiff-soft parameter set [K_0, γ] = [272 - 300, 0.5 – 1.0] we observed too strong stabilization effect on DNS, and fusion became solely dominant channel. Hence, such parameter set does not reproduce the observed reality, and cannot be accepted as well. Also soft-stiff parameterization [K_0, γ] = [202-255, 1.5] leads to dominance of fusion and has to be rejected. In contrast, quasi-fission was observed for [K_0, γ] = [205 - 255, 0.5 – 1.0]. Finally, the presented analysis of almost pure fusion or quasi-fission reactions leads us to constraint of EOS to parameterization [K_0, γ] = [240 – 255, 0.5 – 1.0]. This result is not in contradiction with experimental data for a given set of reactions.

^{48}Ca + ^{238}U, ^{64}Ni + ^{186}W at 5AMeV

(fusion and quasi-fission are comparable)

Based on the previous set of reactions, where fusion or quasi-fission is exclusively dominant, we got constraint on EOS parameters. The given result is reproducing the experimental data well within the sensitivity of method. From the previous simulations we are able to evaluate rough boundaries of K_0, γ region within taken account the sensitivity of that method. Based on the simulation of ^{48}Ca + ^{238}U and ^{64}Ni + ^{186}W reactions we tried to verified constraint on K_0, γ deduced from the pure fusion or quasi-fission data. The results from both of reactions ^{48}Ca + ^{238}U and ^{64}Ni + ^{186}W give consistent results with those derived from the reactions where fusion is close to 0 % or 100 %. The constraint on parameterization of EOS was derived from BUU simulations and experimental data to more stringent interval given as [K_0, γ] = [240 – 260, 0.5 – 1.0], and the 2D plot of possible γ vs. K_0 values is depicted on the figure 4.5.

4.1.3 Discussion

The main aim of BUU simulations in this chapter related with description of DNS dynamics close to the scission point. The presented study is based on the assumption that the system is becoming sensitive to density dependence of symmetry energy and stiffness parameter of the equation of state of nuclear matter, as was previously proved in the giant monopole resonances. The BUU simulations were compared with experimental data and more strict constraint on EOS parameterization was established. In the framework of available data and restrictive computational time, the EOS parameters are expected to vary within the interval K_0 = 240 – 260 MeV with γ = 0.6 – 1.0, also published in [Ves16]. This implies that DNS system should be driven by stiffer EOS, where maximum density 1.4 – 1.5 of the saturation density was reached in the given reactions.

We observed that DNS system typically splits to two fragments at scission time around ~ 1 300 fm/c, what seems to be consistent with previous studies with TDHF [Sek16] and ImQMD models [Cho14]. Also the measured kinetic energy of fragments in ^{64}Ni + ^{208}Pb and ^{48}Ca + ^{238}U reactions is in good agreement with Coulomb potential

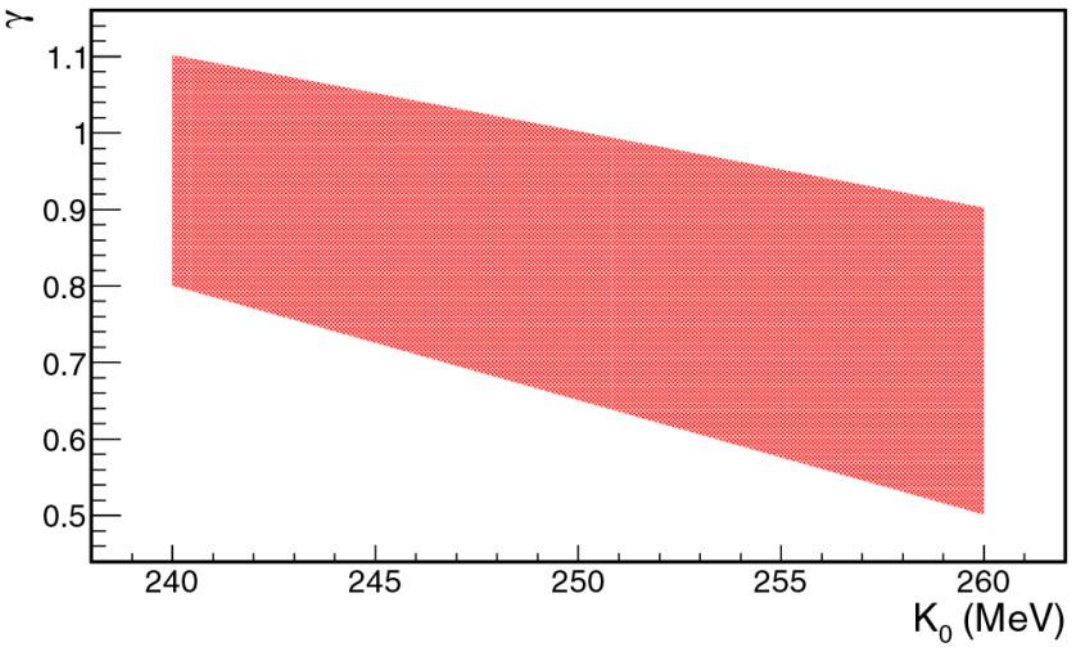

Fig. 4.5: Constraint on the modulus of incompressibility K_0 describing stiffness of symmetric nuclear matter and on density dependence of the symmetry energy γ. Any parameter set [K_0, γ] used in our simulations from inside of the purple area was in agreement or was not excluded based on the comparison with experimental data.

energy at scission point. As the shell effects are not included in BUU model, fission fragments have symmetric fragment mass distribution. The effect of shell structure is still open question on the field of quasi-fission. Besides shell effects also deformation of target nucleus can impact fusion cross section of SHE. Whereas deformation can really improve fusion cross section at sub-barrier reactions, its impact on reactions above the Coulomb barrier is still not clear. Hence, its influence on the investigated reactions cannot be totally excluded. Among others, the recent study on quasi-fission with deformed target nucleus ^{238}U with ^{40}Ca above the Coulomb barrier indicates that quasi-fission mass distribution is sensitive on beam energy, and its cross section can be improved with the beam energy [Wak14]. Because the presented constrain on EOS parameterization is relatively narrow, it can imply that if some influence from deformation and shell effects exist, it should not be so significant.

Compared to other methods, e.g. the nuclear giant resonances or nucleus-nucleus collisions at high energies, the method presented here is free of uncertainty related with two body dissipation or by low lying nuclear structure. To go even further and get even more stringent restriction of EOS parameterization more data are demanded, as well improvement of computational power could help significantly. Even the fact that BUU model offers possibilities to study the EOS, it does not take into account quantum fluctuation. In order to evaluate influence of quantum mechanical fluctuations, we performed equivalent simulations but using another Boltzmann equation approximation as is the CoMD model.

4.2.1 Constrained Molecular Dynamics simulations (CoMD)

In the previous investigation on constraint and refinements of EOS parameters K_0 and γ, BUU simulations were performed for experimentally measured reactions leading to synthesis of SHE. In this chapter, Constrained Molecular Dynamics model (CoMD) is applied on the same reaction set to confront BUU simulations. Very briefly, the CoMD model represents microscopic dynamical model derived from QMD model, which is extensively used for simulations of heavy-ion collisions at high and intermediate energies [Pap01], [Mar02], [Pap05]. Similar to BUU also CoMD model was derived from the Boltzmann equation at non-equilibrium state, as one of the approximation for nuclear matter. The model is long-term use to simulate processes characteristic by large nucleon exchange. Besides similarities with BUU model, there are few differences, mainly approximation of quantum mechanical fluctuations resulting from Heisenberg principle of uncertainty. While in the BUU model nucleonic density fluctuations are simulated by test particle method by Wong [Won82], in the CoMD model this effect is delivered via consideration of wave packets. Also both of models differ in collision integral. Whereas in the CoMD model the collision integral implements experimentally measured nucleon-nucleon scattering cross sections, in the latter one it is defined as EOS dependent and changing with different parameter set. The Pauli exclusion principle for protons and neutron and Coulomb interaction between protons is described in a similar way by both of models. Short range repulsion between nucleons is considered as nucleon-nucleon collisions, using appropriate scattering cross section [Bon94]. For realistic description of heavy-ion collisions, the total angular momentum has to be conserved, so this is included in the latest version of CoMD as well.

Contrary to BUU simulations, the EOS parameterization is investigated in four dimensions. Namely, besides K_0 and γ parameters, surface parameter CSUP (describing surface properties) and σ_r (width of nucleonic wave packet defined over the $(\vec{r}, \vec{p})$ phase) space has to be considered, following an incorporation of quantum mechanical fluctuations. Only recently it was proved that CoMD code enables to reproduce fission dynamics at high and intermediate energies [Von16]. Therefore, there is an expectation on reliable description of fusion vs. quasi-fission dynamics. In order to investigate fusion and quasi-fission competition, some initial conditions and assumptions were established.

Assumptions & settings of CoMD simulations

We come out from various assumptions on the stiffness of EOS of nuclear matter and assumptions on properties of studied reactions.

- We considered parameter of incompressibility from sufficient wide range of values, i.e. $K_0 = 200 - 290$ MeV, consistent with possibilities of CoMD model. We make an assumption that the density dependence of symmetry energy should vary within $\gamma = 0.5 - 1.0$, based on previous BUU simulations.
- The same set of reactions as in BUU simulations were investigated by CoMD model, extended by few others, e.g. $^{48}Ca + ^{176}Yb$ reaction. Collision energy 5 AMeV / projectile correspondence to the available experimental data within few MeV per projectile nucleus.
- We expected that quasi-fission is dominant at central collisions of small impact parameter, similar as we observe in fusion.

- Only central collisions were considered, i.e. maximal taken impact parameter is 0.5 fm. In this way it is possible to cut off all peripheral nuclear reactions, mainly deep-inelastic transfers, typically spreading over the impact parameter range 4 - 16 fm.
- Time window for observation of each collision event was set to t = 3 000 fm/c, long enough to observe to formation of fusion or quasi-fission products.
- Each reaction was simulated 40 times at a given parameter set [K_0, γ].

Simulations were performed by Xeon Phi coprocessor cards, each of them equipped by 61 cores, and enable to run hundreds of parallel simulations, up to ~ 1 000 parallel collisions.

Experimentally deduced fusion probabilities P_{CN}

Experimentally derived fusion probabilities are taken from the sub-chapter 4.1.1, i.e. deduced in similar way.

Simulations of nucleonic density

In contrary to BUU simulations, there are two extra terms in Boltzmann equation to be optimized in order of reproduction of the measured data. Along with the parameter of incompressibility K_0 and the density dependence of the symmetry energy γ also the surface term CSUP (CSUP = $C_{s,\,the}$ equation 2.21) and width of Gaussian wave packet σ_r are introduced in CoMD. The surface term is given by Skyrme-like effective potential, describing nucleon-nucleon effective interaction. In general, it has been found to be -2.0 MeV/fm^2, valid for nuclei with A > 150. Such a value allows to properly reproduce binding energy, radius, and collective properties of projectile and target nucleus at ground state [Pap01], [Pap05]. Just recently, the investigation on proton induced fission of U and Th at intermediate and high energies shown that CSUP = - 2.0 MeV/fm^{2}is not appropriate. To observe fission, and get reasonable fission cross sections, the surface term had to be decreased from the original values to almost 0.0 [Von15].

In the context of our simulations, a dominance of quasi-fission for almost pure quasi-fission systems ^{64}Ni + ^{208}Pb, ^{64}Ni + ^{238}U and ^{48}Ca + ^{249}Cf was not observed at the setting with CSUP = -2.0. The simulations were performed for constraint derived from BUU simulations, i.e. [K_0, γ] = [240 – 260 MeV, 0.6 – 1.0]. However, even after lowering the CSUP value down to -1.0 and subsequently to 0.0, quasi-fission had remained suppressed. This discrepancy was finally resolved by varying σ_r. The default setting for σ_r in CoMD was 1.15 fm. Once we have changed it to σ_r = 1.0 fm, the quasi-fission occurs. Hence, the correct CSUP and σ_r combinations had to been found while testing the EOS. We also observed that CSUP and σ_r parameters are in counterbalance and the EOS have been tested four dimensionally as [K_0, γ, CSUP, σ_r]. Evolution of nucleonic density is depicted on the figures Fig. 4.6 – 4.11, where time step was set to 200 fm/c.

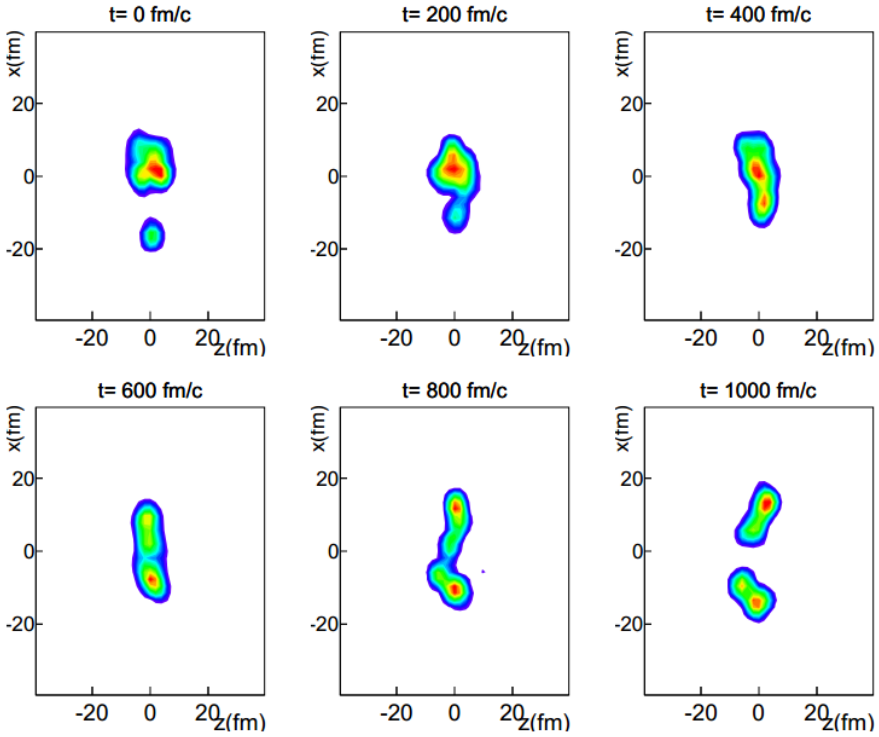

Fig. 4.6: An evolution of nucleonic density for the most central collisions ^{48}Ca + ^{249}Cf at 5 AMeV. The probability of quasi-fission is close to P_{QF} = 100 [%].

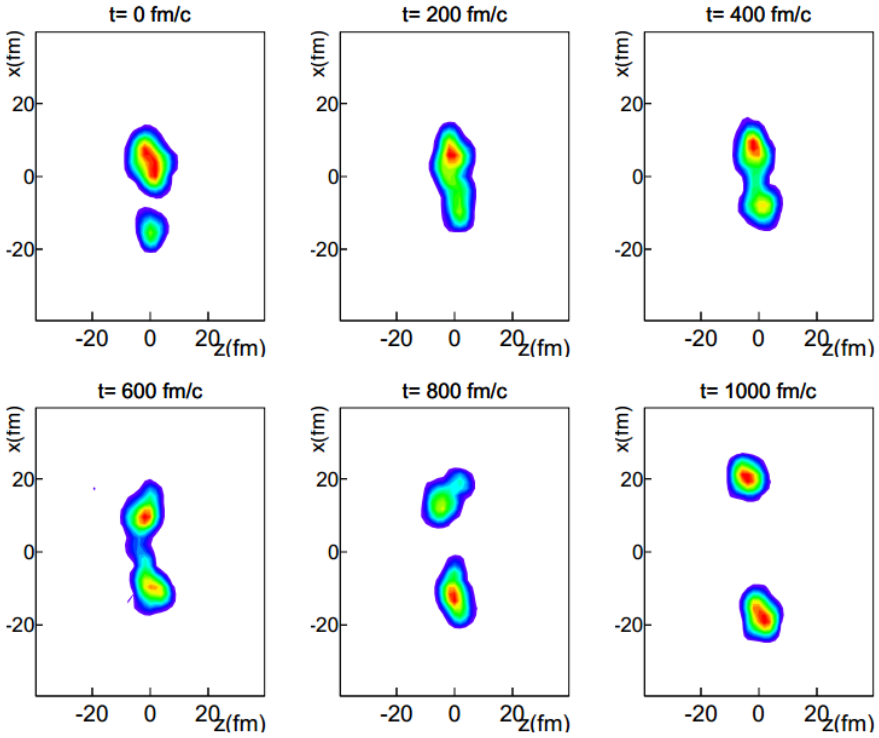

Fig. 4.7: An evolution of nucleonic density for the most central collisions ^{64}Ni + ^{238}U at 5 AMeV. The probability of quasi-fission is close to P_{QF} = 100 [%].

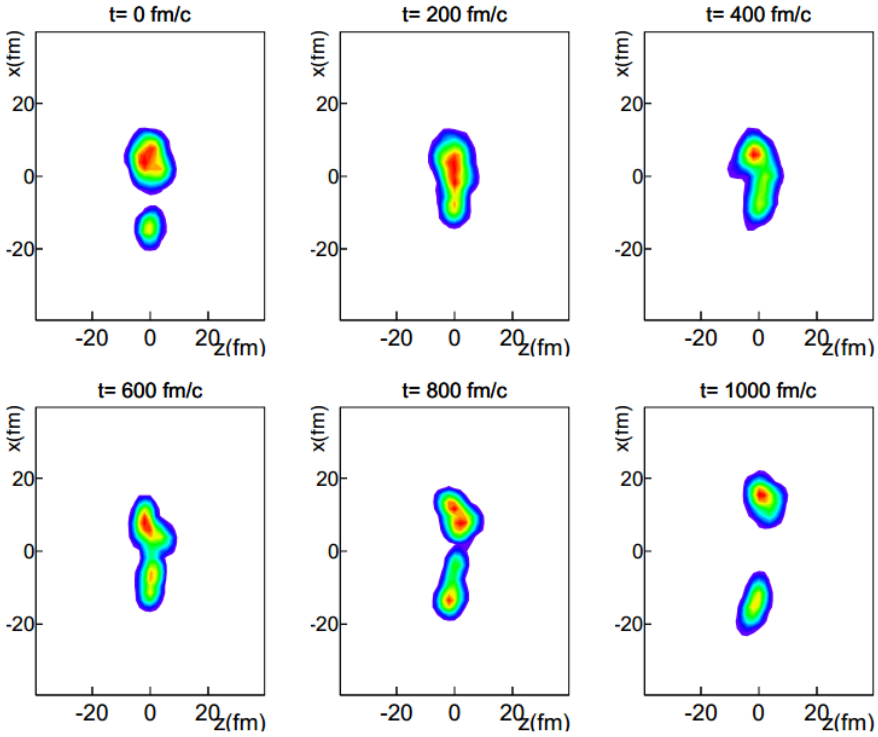

Fig. 4.8: An evolution of nucleonic density for the most central collisions ^{64}Ni + ^{208}Pb at 5 AMeV. The probability of quasi-fission is close to P_{QF} = 100 [%].

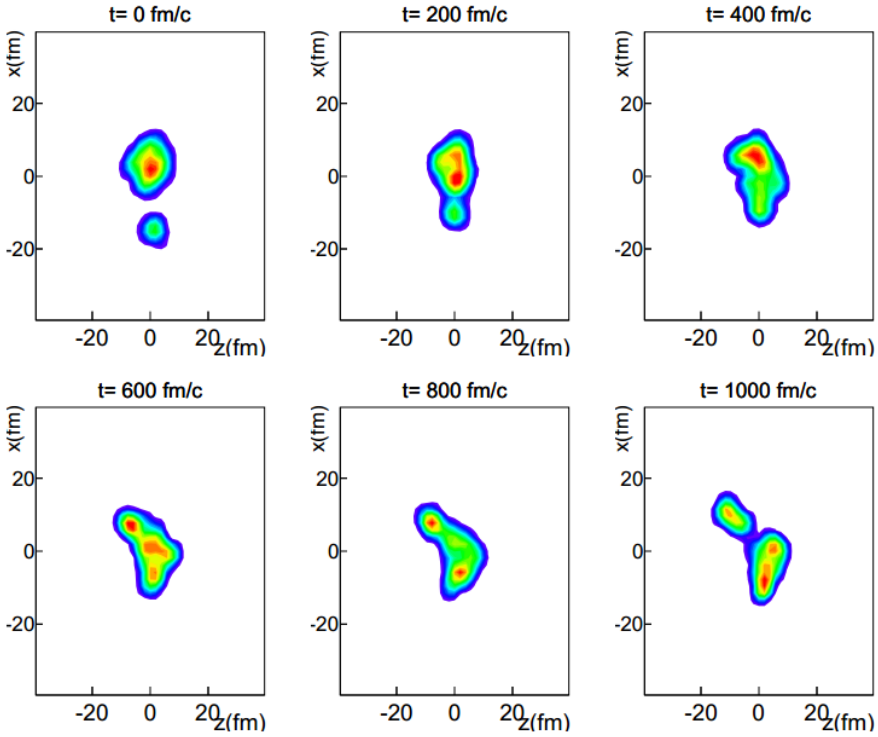

Fig. 4.9: An evolution of nucleonic density for the most central collisions ^{48}Ca + ^{238}U at 5 AMeV. The upper limit for fusion varies within P_{CN} = 20 - 50 [%].

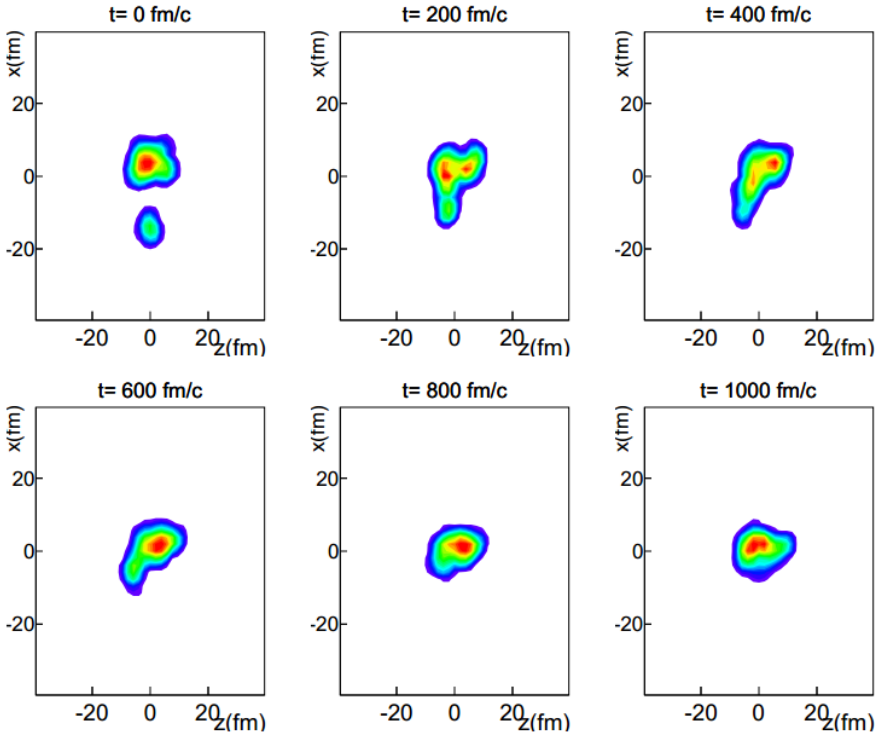

Fig. 4.10: An evolution of nucleonic density for the most central collisions ^{48}Ca + ^{208}Pb at 5 AMeV. The probability of quasi-fission close to P_{QF} = 0 [%], as fusion dominate with probability close to P_{CN} = 100 [%].

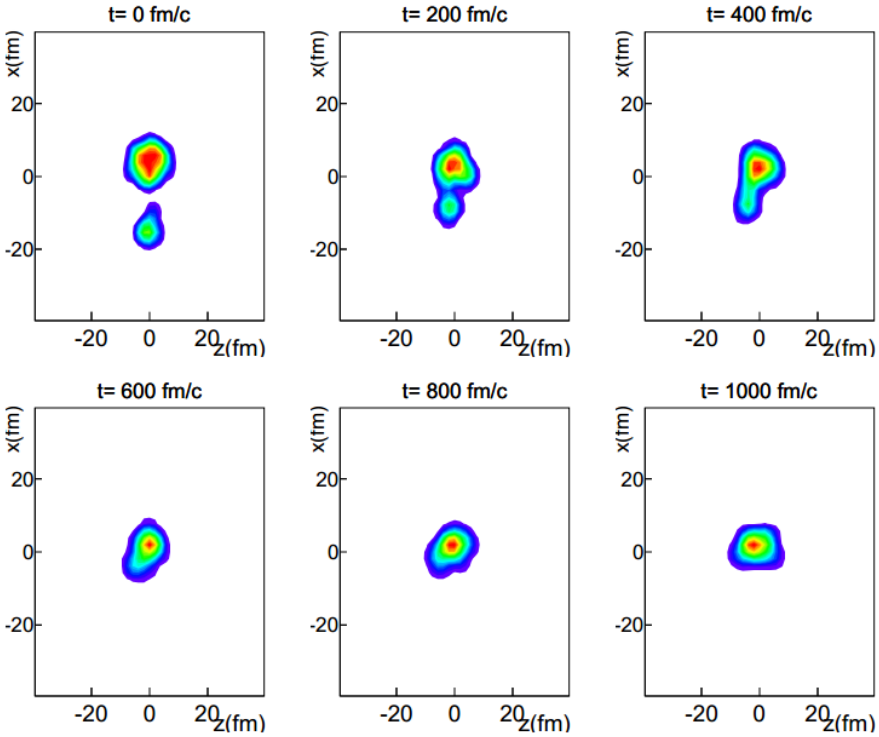

Fig. 4.11: An evolution of nucleonic density for the most central collisions ^{48}Ca + ^{176}Yb at 5 AMeV. The probability of quasi-fission close to P_{QF} = 0 [%], as fusion dominate with probability close to P_{CN} = 100 [%].

4.2.2 Constraining equation of state of nuclear matter, CoMD model

In a similar vein to BUU simulations, also CoMD model has been used to well reproduce available fusion vs. quasi-fission data, aiming to confront the BUU results. In contrary to BUU simulations, CoMD ones were performed four dimensionally as [K_0, γ, CSUP, σ_r]. Namely, K_0 is incompressibility parameter, γ density dependence of nuclear matter, CSUP is surface energy coefficient and σ_r represents width of Gaussian wave packet. In order to successfully describe the quasi-fission for the heaviest DNS systems, the surface term and the nucleonic Gaussian wave packet were optimized together with EOS parameters K_0 and γ. Eventually, the following set of reactions has been tested:

- *^{48}Ca + ^{249}Cf, ^{64}Ni +^{208}Pb, ^{64}Ni + ^{238}U at 5AMeV ("pure" quasi-fission)*
- *^{48}Ca + ^{208}Pb, ^{48}Ca + ^{176}Yb at 5 AMeV ("pure" fusion)*
- *^{48}Ca + ^{238}U, ^{64}Ni + ^{186}W at 5 AMeV (fusion and quasi-fission are comparable)*

In this case, we paid more attention on the pure quasi-fission systems, and condition to reproduce the fusion data was not considered as strictly. Consequently, the CSUP and σ_r parameters can describe a nucleonic evolution for quasi-fission reactions well, but it results to lower fusion probability for the lighter DNS systems, e.g. ^{48}Ca + ^{176}Yb. Also other systems with comparable mass manifest typically lower fusion cross section. Finally, the maximal fusion probability for almost pure fusion reaction has not exceeded more than 30 [%]. Hence, full consensus for both fusion and quasi-fission reactions was not achieved.

Such a discrepancy for pure fusion reaction could be explained by an influence of the Gaussian width on a position of fusion barrier and by surface energy term, which has an direct impact on the single particle mean field. In general, the change of default setting, i.e. [CSUP, σ_r] = [-2.0, 1.15], to other combinations leads to instability of compound nucleus CN, as we have observed in reactions with lower mass and atomic number of CN. On the other hand, almost pure quasi-fission DNS systems are reproduced reasonably. Other aspects can relate with the spin-orbital interaction and shell effects, not incorporated in CoMD model [God19].

The systematic CoMD simulations have been performed with the assumption on incompressibility parameter and density dependence of the symmetry energy as the following, K_0 = 200 – 290 MeV (range acceptable by CoMD) and γ = 0.5 – 1.0. And we got the best result for two parameter sets:

- [K_0, γ, CSUP, σ_r]$_1$ = [245 MeV, 0.5-1.0, 0.0 MeV/fm^2, 1.085 fm], also as (*qbs0*)
- [K_0, γ, CSUP, σ_r]$_2$ = [254 MeV, 0.5-1.0, -1.0 MeV/fm^2, 1.000 fm], also as (*ybf1*)

Only weak influence of density dependence of the symmetry energy was observed on the final fusion and quasi-fission statistics. This conclusion is valid considering the interval γ = 0.5 – 1.0. Thus our observation confirms the similar results on proton induced fission at intermediate energies by CoMD model [Von15], where weak influence of γ on fission was observed for similar interval.

Comparing previous BUU simulations with CoMD ones, we have got comparable constraint. Due to four dimensional simulations, the constraint achieved from CoMD model is not as stringent as we got from BUU. Still, more investigation is needed to distinguished between two possible combinations, i.e. [K_0, γ, CSUP, σ_r]$_1$ and [K_0, γ, CSUP, σ_r]$_2$.

4.2.3 Verification of equation of state of nuclear matter

Both of parameter sets [K_0, γ, CSUP, $\sigma_r]_1$ and [K_0, γ, CSUP, $\sigma_r]_2$ were subsequently tested on the recently measure multi-nucleon transfer reaction ^{136}Xe + ^{197}Pt at 8 AMeV. We supposed that if these sets are not out of the physical reality, they should be valid for the peripheral collisions too. Although peripheral reactions differ from central collisions leading to fusion or quasi-fission, the nuclear matter density should be changing in a similar way. In analogy to neck region driving the nucleon exchange of DNS in fusion vs. quasi-fission process, the window region is considered in peripheral reactions in order to dissipation of energy and nucleon transfer.

The comparison of projectile-like cross sections from DIT model of Tassan-Got [Tas91] and the one from CoMD model is depicted on the figure 4.12. Both of pick-up and striping channels from DIT and CoMD model were confront with not only each other but with recently measured experimental data as well, Watanabe et al. [Wat13]. Two suitable parameterization of EOS resulting from CoMD simulations were tested for deep-inelastic transfer ^{136}Xe + ^{197}Pt at 8 AMeV, in particular [K_0, γ, CSUP, $\sigma_r]_1$ (as *qbs0* on the figure) and [K_0, γ, CSUP, $\sigma_r]_2$ (as *ybf1* on the figure), also stated in the chapter 4.2.2. In order to see the level of agreement between data of Watanabe et al. [Wat13]

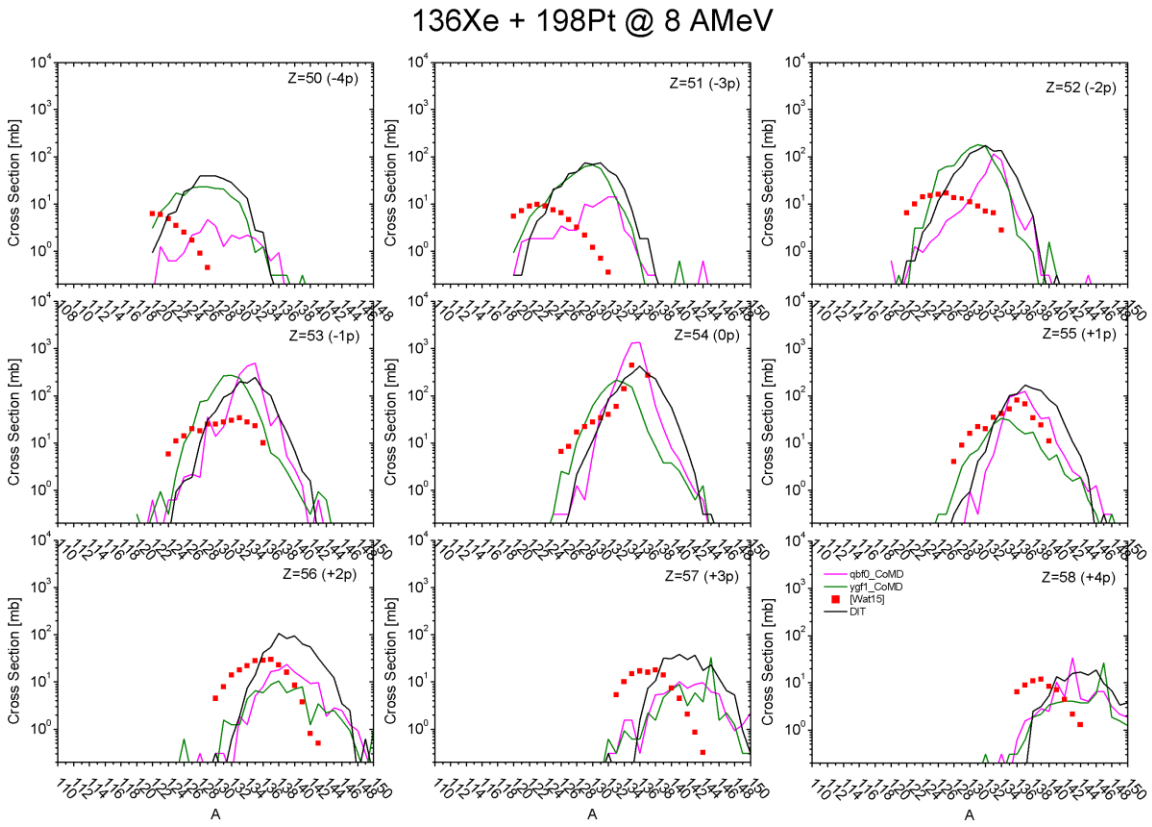

Fig. 4.12: The PLF mass distributions ^{136}Xe + ^{198}Pt at 8 AMeV. Experimentally measured cold PLF fragments [Wat13] (red points). Simulated hot PLF fragments: *qbf0_CoMD (purple line), ygf1_CoMD (green line), DIT (black line).* [K_0, γ, CSUP, $\sigma_r]_1$= *qbf0*, [K_0, γ, CSUP, $\sigma_r]_2$= *ygf1*, see the chapter 4.2.2.

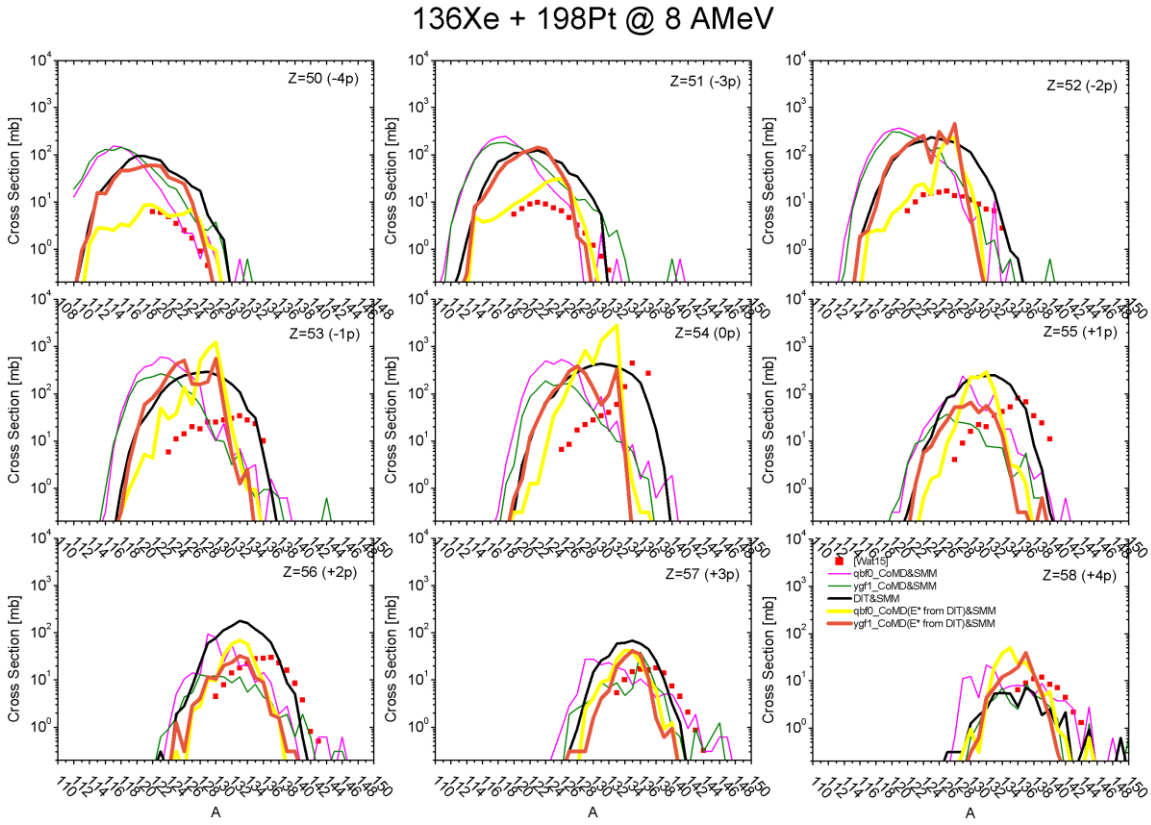

Fig. 4.13: The PLF mass distributions ^{136}Xe + ^{198}Pt at 8 AMeV. Experimentally measured cold PLF fragments [Wat13] (red points). Simulated cold PLF fragments with excitation levels taken from CoMD: *qbf0_CoMD&SMM (purple line), ygf1_CoMD&SMM (green line).* Simulated cold PLF fragments with excitation levels taken from DIT: *qbf0_CoMD(E*fromDIT)&SMM (yellow line), ygf1_CoMD(E*fromDIT)&SMM (red line), DIT&SMM (black line).* [K_0, γ, CSUP, σ_r]$_1$= *qbf0,).* [K_0, γ, CSUP, σ_r]$_2$= *ygf1*, see the chapter 4.2.2.

and models predictions, the hot projectile-like fragments (PLF) from DIT and CoMD simulations had to be de-excited. The cold PLF fragments are shown on the figure 4.13. The de-excitation phase was handled by Simultaneous Multi-fragmentation Model SMM [Bon95]. After de-excitation of DIT data by SMM code, the experimental data could be reproduced within one order of magnitude. As for de-excitation of CoMD, we made some adjustment on the excitation energy and angular momentum for each hot PLF fragment. The reason is that neither [CSUP, σ_r]$_1$ parameter set nor [CSUP, σ_r]$_2$ can describe the ground state of nuclei in realistic way. So one can see shift in energy of ground state of each nucleus, and discrepancy in the angular momentum. This resulting to overvaluing excitation energy for hot PLF fragments. Hence, the average value of excitation energy and angular momentum from DIT model were eventually used. This was applied separately for particular isotopes. After this procedure, the CoMD + SMM mass distributions of the cold fragments corresponded to DIT + SMM predictions. A bit more loosely we were able to reproduce the experimental data.

We can conclude that the two most appropriate sets of EOS parameters fitted on fusion vs. qausi-fission reactions are in good agreement with extensively used multi-nucleon transfer model and with experimental data as well. The CoMD model can reproduce dynamic of such complex investigated processes as fusion and quasi-fission, still same improvement will be needed in the future.

4.2.4 Discussion

This chapter was dedicated to investigation of equation of state of nuclear matter via the Constrained Molecular Dynamics (CoMD) as microscopic simulations complementary to BUU. The CoMD and the BUU model, both arisen as approximations of Boltzmann equation for nuclear matter, with different description of nucleonic density fluctuations, nucleon-nucleon cross section determining the collision integral, and differ in single particle mean field. In addition, each code is based on the different numerical method. In spite of all these differences, the constraint of the incompressibility parameter from CoMD model is consistent with BUU simulations, i.e. K_0 = 245 – 254 MeV [Kli19]. No significant sensitivity of EOS on density dependence of the symmetry energy was observed within the interval γ = 0.5 – 1.0. Also it is well known that shell effects and deformation of participating nuclei play a significant role on sub-barrier fusion. In case of collisions with energy above the Coulomb barrier, their impact on the entrance channel dynamics and compound system does not seem to be dramatic. Neither CoMD nor BUU model considered shell effects or deformed shape of nuclei.

In order to verify the two most suitable EOS parameters extracted from CoMD, they have been tested on deep-inelastic transfer reaction of ^{136}Xe + ^{198}Pt at 8 AMeV [Wat13]. The CoMD model enables to reproduce the experimental data in principle on the same level as extensively used deep-inelastic transfer model DIT.

Just recently, the simulations of two neutron star mergers point out that at incompressibility of K_0 = 245 MeV [Per19] should lead to formation of neutron star, while the softer EOS parameterization creates conditions for formation of black hole. The simulations were subsequently confirmed in the recent astronomical event GW170817, where a massive neutron star (magnetar) was formed [Abb19], [Put19]. Therefore, one can expect that EOS should be stiffer than softer, resulting from observation of nuclear matter on macro and micro scale.

4.3 Deep-inelastic transfer reactions & HIE - ISOLDE facility

About 3000 isotopes were investigated until present, and only 252 of them are of primordial origin, and are simultaneously considered as experimentally stable isotopes (based on the theory only 146 of them are stable). Another 34 primordial isotopes of 3000 investigated nuclides are not stable as they have experimentally measurable half-life. In addition to naturally occurring primordial nuclides there are group of 347 radionuclides, which are naturally occurring as well but are considered as non-primordial, generated by cosmic rays or in radioactive decay of the primordial elements. The most of isotopes which had to been studied so far have been prepared in the laboratory conditions artificially through the appropriate nuclear reactions. However, the mentioned 3000 isotopes represent only one half of the total 6000 nuclei which are predicted by the theoretical models as nuclides stable against proton or neutron emission. All of them are lying between the neutron and proton drip line in the nuclear landscape.

As for the nuclei on the left from the β-stability line, so-called proton rich nuclei, many of them were investigated through the compound nucleus reactions around the Coulomb barrier, up to the region of fissile nuclei behind lead. Another fruitful reaction mechanism to reach proton rich area are spallation reactions of massive targets, e.g. ^{238}U, ^{232}Th or lighter materials. Within the last decades, spallation becomes a very strong tool for production of radioactive ion beams on the both of sides of the β-stability line. Those compound nucleus reactions and spallation played a key role in experimental study of the proton drip line below Z = 83.

On the neutron rich side the situation is a bit different. The neutron drip line has been thoroughly examined only up to the oxygen element, Z = 8, where the spallation and fragmentation reactions play a significant role in production of light exotic nuclei. In the area of the medium mass nuclei, the neutron induced fission around the fission barrier is the leading tool in investigation of the most neutron rich isotopes, but it is still far away from the neutron drip line. Typically, the mass distribution from fission decay is relatively narrow. A larger diversity of atomic numbers can be reached in high energy fission following by spallation reactions in configuration with classical spallation target or with neutron converter, see figures 4.23 or 4.24 in the chapter 4.4. The lack of neutron rich data is even more obvious in the region above fission fragments region, Z = 60, which is not covered by low or high energy fission. Similarly, in spallation or in fragmentation of heavy targets, mass distributions of neutron rich nuclei are relatively close to the β-stability line. Beside this fact, the typical production cross section for neutron rich nuclei produced in the fragmentation ^{238}U + ^{9}Be at 1 AGeV (inverse kinematics at FRS facility in GSI, Darmstadt) varies within the range of few nb [Kur12], [NNDC]. In order to get neutron rich nuclei with even higher neutron excess, a new method should be developed.

The deficiency of neutron rich data for Z > 60, and low production cross sections, can be explained by binding energy of neutrons. The lack of Coulomb barrier for neutrons leads to neutron emission, becoming more probable for neutron rich nuclei. Therefore, to increase survival probability against neutron emission the excitation energy of nuclei has to be relatively low, especially in the nuclear reaction leading to production of neutron rich radioactive isotopes [Ves13], [Zag11], [Art02]. Consequently, the minimum possible excitation energy of excited nuclei leads to the minimum loss of neutrons. The very efficient nuclear reaction fulfilling such condition are nucleus-nucleus reactions of nucleon exchange characteristic for the collisions in the Fermi-energy domain, i.e. 15 - 50 AMeV, [Ves00], [Ves02] [Sou02], [Sou03].

We can expect two scenarios based on the value of impact parameter of collision at the Fermi-energy domain, i.e. central or peripheral collisions. Central collisions take place in the case the impact parameter is sufficient small. At the Fermi-energy domain pre-equilibrium emission (PE) and incomplete fusion (ICF) contribute to the total production cross section, where projectile like and target like fragments are produced. Typical impact parameters for central nucleus-nucleus collisions varies within the range of 0 – 3 fm, depending on the radius of interacting nuclei. The interaction time is relatively long ($>10^{-20}$s) as the process has adiabatic character through the formation of compound system. However, projectiles at the Fermi-energy domain mainly interact at the distance greater than ~ 3 fm, thus leading to semi-peripheral or peripheral collisions, so-called deep inelastic transfer reactions (DIT). The interaction time is short, approximately ~ 10^{-21}s.

A lot of experimental data have been collected on the many nucleon transfer reaction up to the present and a very reliable description of the peripheral collisions observed in experiments is provided by deep inelastic transfer model of Tassan-Got DIT [Tas91]. The model is based on the Monte Carlo method, and has to be combined with de-excitation code such as the statistical model of multi-fragmentation SMM. If we take into account all the mentioned processes at the Fermi-energy domain then we can link particular codes together as PE + ICF/DIT + SMM in order to get the best interpretation of experimental data and physical reality. Over the years some modification and enhancement of DIT model were done for Fermi-energy domain and for lower energies as well. In the context of energies below 10 AMeV the main improvement was done by adjustment of nuclear mean field in the so-called “window“ created in neck region of di-nuclear system (DNS). The “window” allows transfer of nucleons between two parts of DNS, and thus energy and angular momentum can be dissipated [Ves11]. Another enhancement of DIT model is given by incorporation of shell structure, i.e. microscopic effects and thus to consider effect of neutron skin [Ves06]. Many years of development of DIT model results that experimental data are in very good agreement with DIT simulations if the input parameters are handled well, depending on the particular reaction and collision energy.

The low energy of the beam at multi-nucleon transfer reactions is demanded in order to produce and study neutron rich residues around Z ~ 70 with reasonable cross sections [Zag11]. This chapter is dedicated to simulations of production cross section of some neutron rich isotopes towards the neutron drip line. For this purpose the following model framework has been used at the energy under Fermi-energy domain, i.e. 8 AMeV: PE + ICF/DIT + SMM. Because the excitation energy of projectile like fragments typically do not exceed 1 AMeV, at the collision energy below 10 AMeV, no pre-equilibrium emission is taken into the account. Thus the model framework reduces to shorten version: ICF/DIT + SMM. This combination of codes can be utilized to predict production cross section. The simulations shown in the following chapter were dedicated to peripheral collisions induced by exotic nuclei. Such nuclei can be potentially prepared as post-accelerated radioactive ion beams from HIE-ISOLDE (High Intensity and Energy ISOLDE) facility at CERN. Where choosing right combination of projectile and target nucleus with appropriate energy, a new way to produce isotopes with a large neutron excess can be opened up. The isocaling studies on production cross sections imply that even larger neutron excess in projectile like fragments is achievable by using the projectiles with higher isospin asymmetry [Ves11]. Therefore, we suggest the following reactions ^{170}Ho + ^{238}U, ^{177}Yb + ^{238}U, ^{180}Hf + ^{238}U at the energy of post-accelerated beams around 8 AMeV. The radioactive ion beams (RIBs) were chosen with respect on their intensity (2016). The present status of the

HIE-ISOLDE facility is that the Phase 2 (energy upgrade) of its upgrade has reached completion in 2018. This allows accelerating exotic nuclei up to 10 AMeV, and after completion of the Phase 3 it will reach even higher intensities. Once the ISOLDE facility will be completely transformed to HIE-ISOLDE, this device will remain at the forefront of nuclear physics. Then the HIE-ISOLDE will be only in the world capable of accelerating medium to heavy radioactive isotopes in this energy range [Kad17], [Kad18].

4.3.1 Simulations of Deep Inelastic Transfer reactions

As was discussed in the previous section, the present capabilities of the ISOLDE physics program are in the process of extension as for energies and intensities of RIBs as well. We can expect a wider range of physics could be studied after completion of the ISOLDE upgrade to the HIE-ISOLDE. After that the post-accelerator can provide wide spectrum of RIBs accelerating up to 10 AMeV. The secondary reactions such as Coulomb excitations, transfer reactions or deep-inelastic transfer reactions at higher energies are possible to use as a tool to do detailed nuclear structure research. A new way for production of isotopes which are currently produced at relative low production cross sections or have not been produced yet is now achievable with the HIE-ISOLDE infrastructure.

In this section the simulations of production cross sections of some neutron rich projectile like fragments (PLF) behind Z = 60 are presented. Within the framework of the model combination DIT + SMM, we have done calculations of PLF production cross sections for the following reactions $^{170}_{67}$Ho + $^{238}_{92}$U, $^{177}_{70}$Yb + $^{238}_{92}$U, $^{180}_{72}$Hf + $^{238}_{92}$U at the energy 8 AMeV, Tab.4.3. The radioactive ion beams of ^{170}Ho, ^{177}Yb and ^{180}Hf were selected with regards on the beam intensity and neutron excess of these nuclei. The higher neutron excess of target nucleus the more neutron reach PLF isotopes can be expected in the output channel. This fact is confirmed from the isoscaling studies on deep-inelastic transfer products [Ves11]. The pre-equilibrium reactions do not play role below 10AMeV and peripheral collisions (DIT + SMM) are significantly dominant over central encounters (ICF + SMM). From previous studies on the DIT model parameterization we can conclude its independence on the energy within the Fermi-energy domain, i.e. 15 - 50 AMeV. However, in order to ensure DIT can work properly

Isotop	T1/2 [m]	Spallation	Target	Ion Source SC PSB	Intensity [μC] SC PSB
^{170}Ho	2.76	SC ---	Ta	Surface-W ---	1.3×10^{8} ---
^{177}Yb	114.6	SC PSB	Ta	Surface-W RILIS	8.3×10^{7} 2.5×10^{4}
^{180}Hf	330	SC ---	Ta	Hot-Plasma ---	2.8×10^{6} ---

Tab. 4.2: The yields provided by ISOLDE Thalium target in spallation induced by protons with energy of 0.6 AMeV and 1.4 AGeV [ISO12]. SC – 0.6 AGeV proton beam, PSB – 1.4 AGeV proton beam.

even at lower energies, i.e. 5 – 10 AMeV, it is necessary to modify some model parameters. Especially, the trapezoidal density profile in the "window" region, within the neck of the di-nuclear system, has to be enlarged. Such extension allows opening of transfer "window" at larger distances of interacting nuclei. Otherwise, theoretical cross sections are suppressed compared to experimental ones [Ves11]. Therefore, the maximum full density radius R_0 based the liquid drop model prediction was enlarged by 0.525 fm, and also the inverse slope of the linear density tail was extended from 0.65 to 1.8125 fm. Such modifications were consistent at any flight out angle (0 - 180°) of hot PLFs. Similar DIT parameterization for trapezoidal density profile was applied for differential cross sections around grazing angles in the reactions ^{22}Ne + ^{232}Th or ^{22}Ne + ^{90}Zr at 7.99 AMeV [Ves11].

Such kind of adjustment of the trapezoidal density profile results from the assumption that the low density nuclear matter is evolving during the first stage of the reaction. This is driven by the changes of the mean filed in the neck region of di-nuclear system. The reason is longer interaction time between interacting nuclei. This effect is observed only in the deep-inelastic transfer reactions with massive targets, and the effect is more significant as beam energy is decreasing.

On the figures 4.14 – 4.16 the mass distributions of cold fragments at the full angular range (0 - 180°) are presented. De-excitation of hot PLFs and TLFs is described via the multi-fragmentation model SMM. Because of excitation energy of hot fragments do not exceed 1 AMeV at the energies below 10 AMeV, the main de-excitation way of hot PLFs is mostly by evaporating of neutrons. Besides this, also charged particles or light clusters can be emitted, but contribution of these channels to the final PLF peak is much lower. On the figures 4.14 – 4.16 the middle peak represents all channels from (-xp) to (+xp). Within all simulated spectra relatively wide mass distributions is visible, spreading over the interval $\Delta A \approx 40 - 45$ u at the collision energy set to 8 AMeV. Only events with PLF production cross section higher than 10^{-5} mb were taken into the account, Tab. 4.4. As far as TLFs, they dominantly de-excite through fission or by evaporation. However, the fission fragment peaks originating from high energy fission,

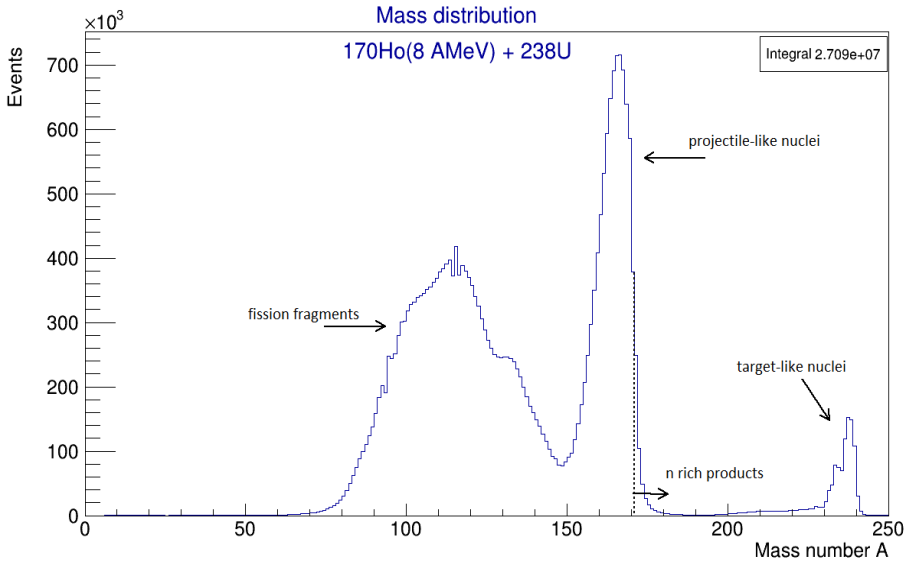

Fig. 4.14: The mass distribution of cold fragments for the peripheral collisions $^{170}_{67}$Ho + $^{238}_{92}$U at 8 AMeV. The simulations were performed within the model framework of DIT + SMM.

point to dominance of fission decay over evaporation of particles. Masses of fission products are distributed over the middle mass region of nuclear landscape, typically positioned around A = 115. Some of the hot TLFs also can survive splitting into two fragments, but such scenario is more probable for events with lower angular momentum or if the excitation energy after reaching the thermal equilibrium of nucleus is lower than the fission barrier height. In that case particle emission is becoming dominant. The mass distributions on the figures 4.14 – 4.16 also indicate that only small fraction of PLFs are produced with mass number higher than projectile mass. Therefore, mass

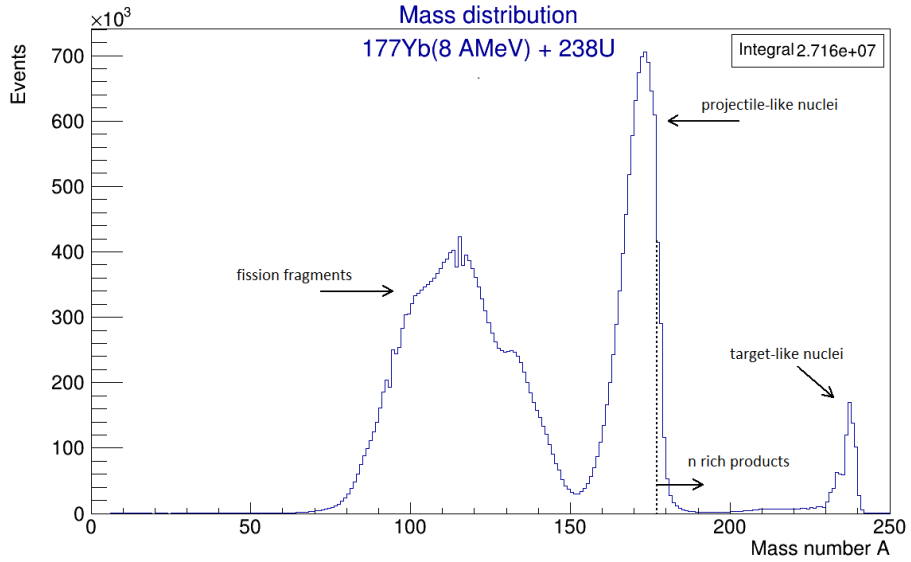

Fig. 4.15: The mass distribution of cold fragments for the peripheral collisions $^{177}_{70}$Yb + $^{238}_{92}$U at 8 AMeV. The simulations were performed within the model framework of DIT + SMM.

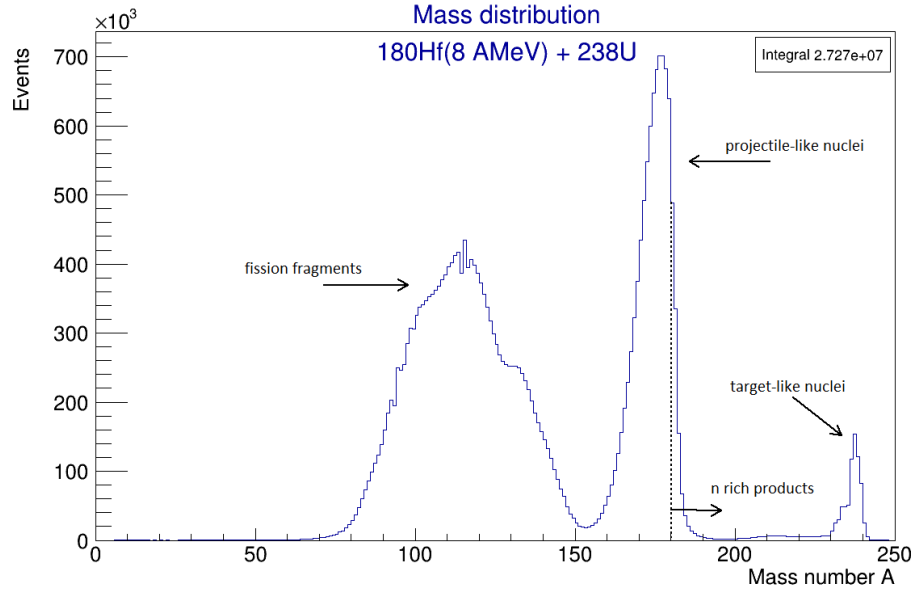

Fig. 4.16: Figure 4.36: The mass distribution of cold fragments for the peripheral collisions $^{180}_{72}$Hf + $^{238}_{92}$U at 8 AMeV. The simulations were performed within the model framework of DIT + SMM.

mass distributions on the figures 4.14 – 4.16 also indicate that only small fraction of PLFs are produced with mass number higher than projectile mass. Therefore, stripping channels (–xp) are much more perspective to reach neutron rich isotopes (the left tile of PLF peaks), which are characteristic by higher isospin asymmetry, compared to proton pick up channels (+xp).

4.3.2 Production cross sections in the region Z_{PLF} = 60 – 72, ^{170}Ho, ^{177}Yb, ^{180}Hf + ^{238}U at 8 AMeV

The simulations of selected reactions: ^{170}Ho + $^{238}_{92}$U, ^{177}Yb + $^{238}_{92}$U, ^{180}Hf + $^{238}_{92}$U were carried out with parameterization similar to those used in the previous studies [Ves11]. Particularly, the maximum full density radius R_0 was enlarged by 0.525 fm and the inverse slope of the linear density tail was extended from 0.65 to 1.8125 fm. Each combination projectile and target was performed for 5 million events of peripheral collisions, and after de-excitation by SMM code the residual cross sections were finally evaluated. The geometrical cross section was calculated based on the maximum angular momentum $\ell_{max.}$ at the contact configuration radius + 1 fm, separately for each of the three reactions. Then we got the mean value $< \ell_{max.} >$ for a given reaction, calculated by averaging of $\ell_{max.}$ values over all (+/- xp) channels. Within these simulations the attention was paid on the neutron rich PLFs from (-xp) channels with Z_{PLF} = 60 – 72. The mass distributions of PLFs from (-xp) channels are stated in the table Tab. 4.4. The table contains the following (-xp) channels, (-7p) – (0p) for ^{170}Ho + $^{238}_{92}$U, (-8p) – (0p) for ^{177}Yb + $^{238}_{92}$U, (-8p) – (0p) for ^{180}Hf + $^{238}_{92}$U. The (+xp) transfers are not included in the Tab. 4.4 as their isospin asymmetry is relatively low.

The comparison of our calculations with available fragmentation data on the most neutron rich isotopes, from Z_{PLF} = 60 to Z_{PLF} = 72, indicates much higher cross sections for DIT + SMM deep-inelastic transfers. Particularly, we observe from one up to three orders of magnitude higher production cross sections than those measured by Kurcewicz et al. in the fragmentation ^{9}Be + ^{238}U (1 AGeV) [Kur12], [NNDC], Tab. 4.3.. However, this is definitely valid only for some neutron rich isotopes, as in the fragmentation much wider region of isotopes can be investigated. In the Kurcewicz experiment, production cross sections were measured from Neodymium to Platinum. These comparisons lead us to the conclusion that deep-inelastic transfers can be opened with significantly higher cross sections as were observed in the fragmentation ^{9}Be + ^{238}U (1 AGeV). The mass distributions and cross sections, the figures. 4.17 a) – f), with few possible new isotopes were evaluated for the future ISOL type experiments. From

Cross section [ubarn]		$^{161}_{60}$Nd	$^{163}_{61}$Pm	$^{165}_{62}$Sm	$^{168}_{63}$Eu	$^{170}_{64}$Gd	$^{172}_{65}$Tb	$^{173}_{66}$Dy	$^{176}_{67}$Ho	$^{178}_{68}$Er	$^{181}_{69}$Tm	$^{185}_{70}$Yb	$^{188}_{71}$Lu	$^{190}_{72}$Hf
$^{9}_{4}$Be +	$^{238}_{92}$U (1 AGeV)	0.003	0.0045	0.0078	0.002	0.0026	0.001	0.018	0.0022	0.0055	0.006	0.00007	0.0001	0.00027
$^{238}_{92}$U +	$^{170}_{67}$Ho (8 AMeV)	---	---	0.3	0.6	0.6	1.2	28	1.3	---	---	---	---	---
	$^{177}_{70}$Yb (8 AMeV)	---	---	---	---	---	0.3	11	5.7	29	3.8	---	---	---
	$^{180}_{72}$Hf (8 AMeV)	---	---	---	---	---	---	1.4	0.3	4.4	1.6	0.7	---	---

Tab. 4.3: The production cross sections for the heaviest neutron rich isotopes from Z = 60 to Z =72. ^{9}Be + ^{238}U (1 AGeV) - fragmentation data [Kur12], ^{170}Ho, ^{177}Yb, ^{180}Hf + ^{238}U (8 AMeV) – our DIT + SMM simulations.

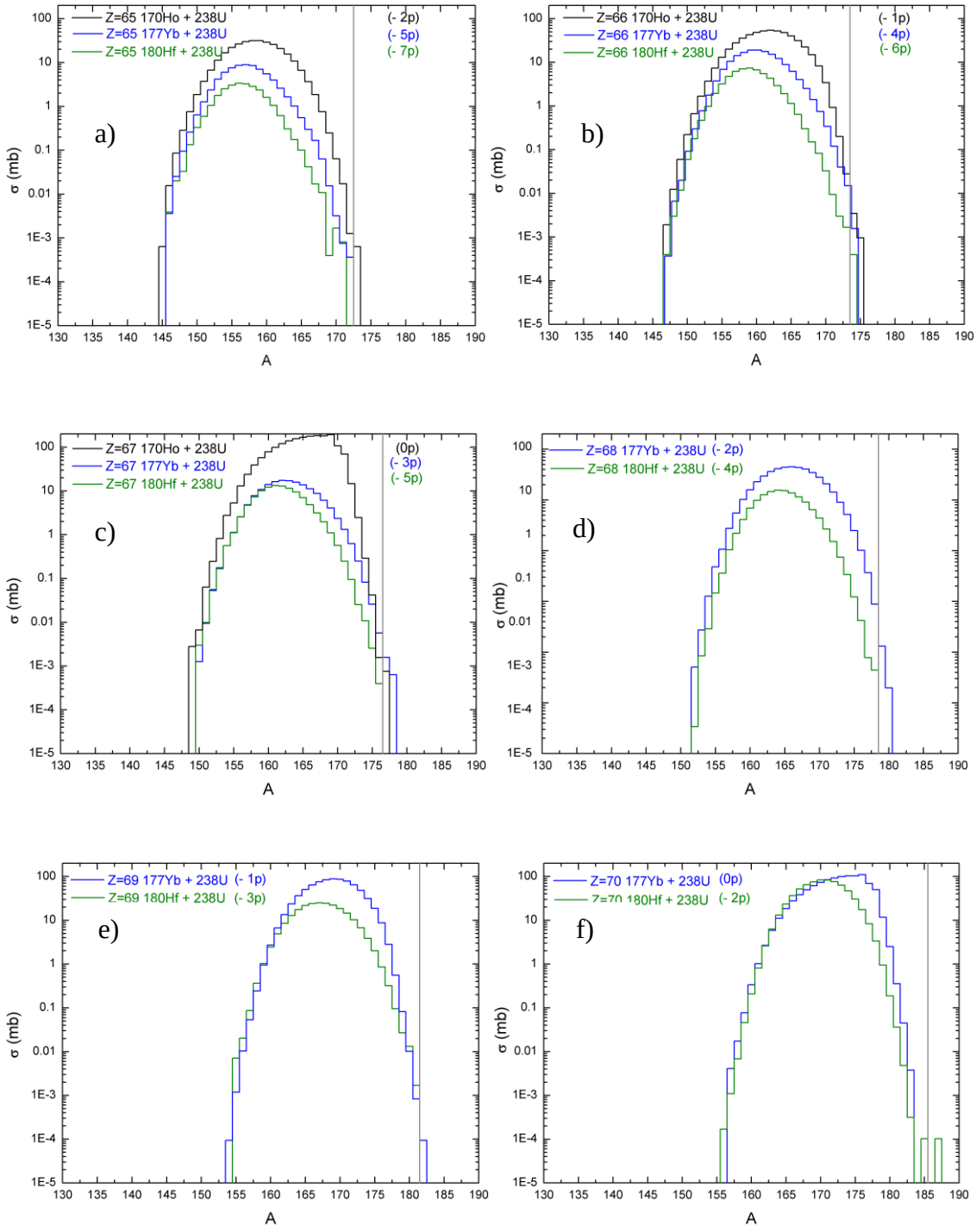

Fig. 4.17 a) – f): DIT + SMM simulations of production cross sections for elements Z = 65 – 70 produced in the deep-inelastic transfer reactions: ^{170}Ho + ^{238}U (black line), ^{177}Yb + ^{238}U (blue line), ^{180}Hf + ^{238}U (green line). All the reactions were calculated at the collision energy 8AMeV. On the right side from the gray vertical line the isotopes with no available experimental data are distinguished. The new isotopes can be found in the color cells in the table Tab. 4.4.

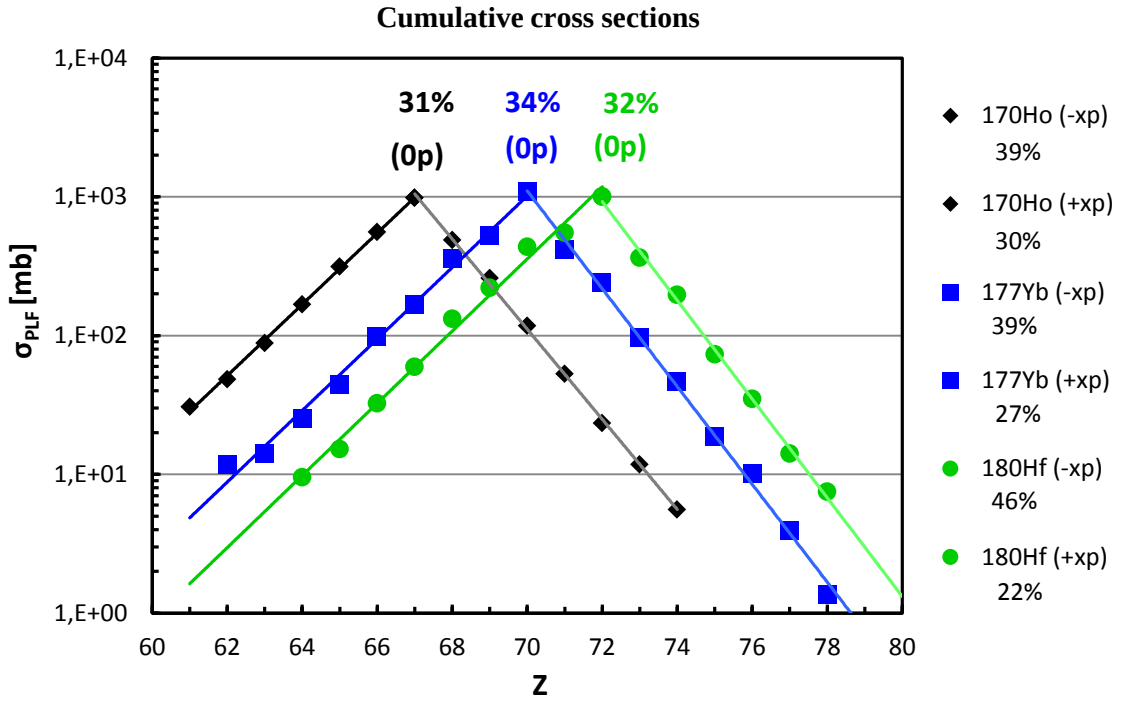

Fig. 4.18: DIT + SMM cumulative cross sections: ^{170}Ho + ^{238}U (black points/lines), ^{177}Yb + ^{238}U (blue points/lines), ^{180}Hf + ^{238}U (green points/lines) at the collision energy of 8 AMeV. The yields for (-xp) and (+xp) channels are stated in the legend (right).

the chosen exotic RIBs in a combination with the massive ^{238}U target, DIT + SMM simulations show 4 new isotopes in deep-inelastic transfer from ^{170}Ho, 7 new isotopes from ^{177}Yb, and 2 isotopes from the reaction with ^{180}Hf beam at the energy of 8 AMeV. The production cross section for the new PLFs varies from 10^{-1} to 10 μb.

From the stated PLF cumulative cross sections, the figure 4.18, one can observe the exponential decrease of their values as more protons are stripping or picking up from the given projectile nucleus. It is seen, that all three distributions are fitted by exponentials with very similar parameters. This overlap relates with the same choice of the target material for all the three reactions, also with similar projectile isospin asymmetry and projectile masses, and the collision energies are the same as well. Because, there are no data to compare with our simulations, our simulations have to be handled carefully. It should be mentioned that the DIT model is in really good agreement with many experimental data, but it is necessary to test this model for energies just above Coulomb barrier. The measurement of discussed reactions could be a very good chance testing also other models describing deep-inelastic transfer reaction at energies above the Coulomb barrier. However, in order to measure PLF, complete identification, and A, Z separation is necessary. Consequently, a spectrometer with a large magnetic acceptance to detect PLF fragments at a large solid angle with energies of fragments below the Fermi-energy domain is demanded. The present magnetic spectrometers with such excellent separation capability are VAMOS++ [Sav99], MAGNEX [Cun02] or PRISMA [Ste02]. Nonetheless, no of them presently provides neutron rich beams like ^{170}Ho, ^{177}Yb or ^{180}Hf. On the other hand, this aim looks more probable for the HIE-ISOLDE facility equipped with the ISOLDE Solenoidal Spectrometer (ISS). As the ISS is a new device it is still under development, it can offer measurement of transfer products kinematics, including Q value.

4.3.3 The comparison of DIT simulations with the experimental data

To get a better clue about the precision of DIT simulations at the energy region below the Fermi-energy domain, the comparison with recently measured data on the reaction ^{136}Xe + ^{198}Pt at 8AMeV are presented on the figure 4.19. The same parameterization of the nuclear profile was used as in [Ves11] or in the discussed reactions with following exotic beams: ^{170}Ho, ^{177}Yb or ^{180}Hf. The total cross sections for PLF fragments produced in all (+/- xp) including (0p) channels are 2.7 ± 1 mb and 2.9 mb from the experiment [Wat13] and from the model prediction, respectively.

The comparison on the figure 4.19 shows the good agreement in peak centroid positions between measured and simulated data only for (-xp) channels. For the pick up channels (+xp), the measured mass distributions are not reproduced by simulations so well, and the simulation prediction looks shifted to the more neutron deficient region against the experimental data. Whereas, the measured maxima for (+xp) channels are around the pure proton pick up, i.e. <A> ≈ 136 + ((+xp) + 1), and the simulated distributions are typically of few mass units lower. The shift in the centroid position is also obvious for the most intensive channel (0p), where no protons are stripped or picked up from the projectile.

Even though the total PLF cross sections from the experiment and from the simulation are in good agreement, the simulated PLF production cross sections for given transfer channels are up to one order of magnitude over the data. This was observed for the most of channels, except (0p) and (+4p). For the most intensive channel (0p), the experimental cumulative cross section is more than 200 mb higher

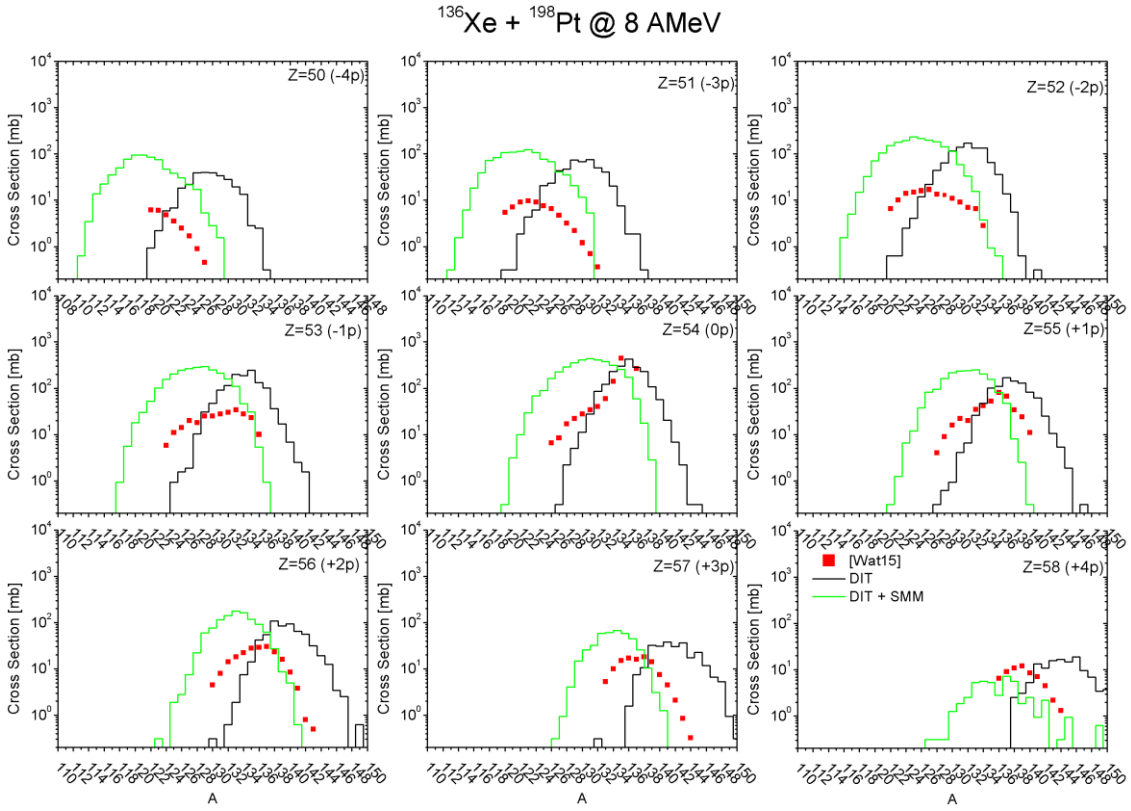

Fig. 4.19: The PLF mass distributions ^{136}Xe + ^{198}Pt at 8 AMeV: experimental cross sections [Wat13] (red points) – cold PLF fragments, DIT + SMM (green histograms) – cold PLF fragments, only DIT (black histograms) – hot PLF fragments.

compared to our model simulation, Fig. 4.20. The fractions of PLF cumulative cross

section, particularly the yields $\sum Y_{PLF\ (-xp)}$ / $Y_{PLF(0p)}$ / $\sum Y_{PLF(+xp)}$ [%] are as following: 44 % / 28 % / 28 % based on DIT + SMM, and 22 % / 45 % / 33 % from [Wat13], see the figure 4.20.

In summary, the model prediction is in good agreement with the experiment as for the position of peak centroids only in (-xp) channels, but cumulative cross sections are deviating and for (-xp) are actually higher then measured values. Also we have to take into account that for the channels (-4p), (-3p) and (-2p) the data are incomplete as the PLF fragments with lower isospin asymmetry have not been detected and eventually the effect of discrepancies could be less significant. In the case of pick up channels (+xp), the main discrepancy is in given by centroids positions, where the DIT + SMM simulations predict too high loss of neutrons for arisen cold PLF fragments. If we try to extrapolate these results to the reactions of our interest: ^{170}Ho, ^{177}Yb, ^{180}Hf + ^{238}U at 8 AMeV, the simulated mass spectrum of PLF should not differ from reality so much and some new isotopes could be produced in some of (-xp) channels in the given reactions. As for the amplitude of PLF production cross section, one can expect that the real values could be predicted within in one order of magnitude.

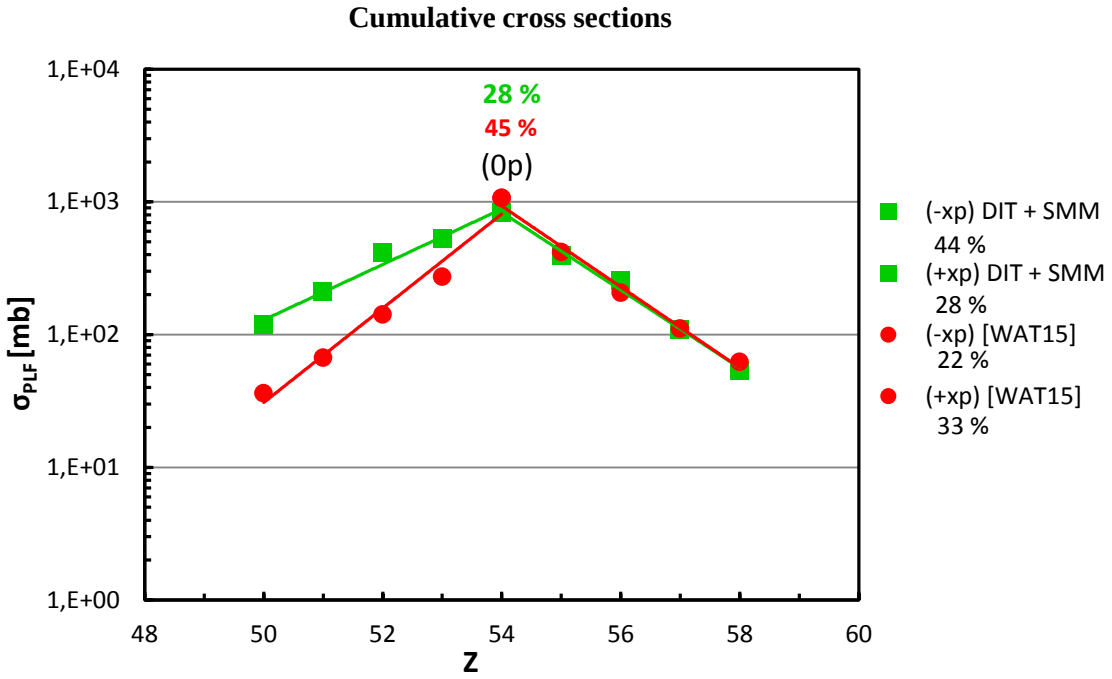

Fig. 4.20: PLF cumulative cross sections ^{136}Xe + ^{198}Pt at 8 AMeV: experimental cross sections [Wat13] (red points) – PLF fragments, DIT + SMM (green points) – cold PLF fragments.

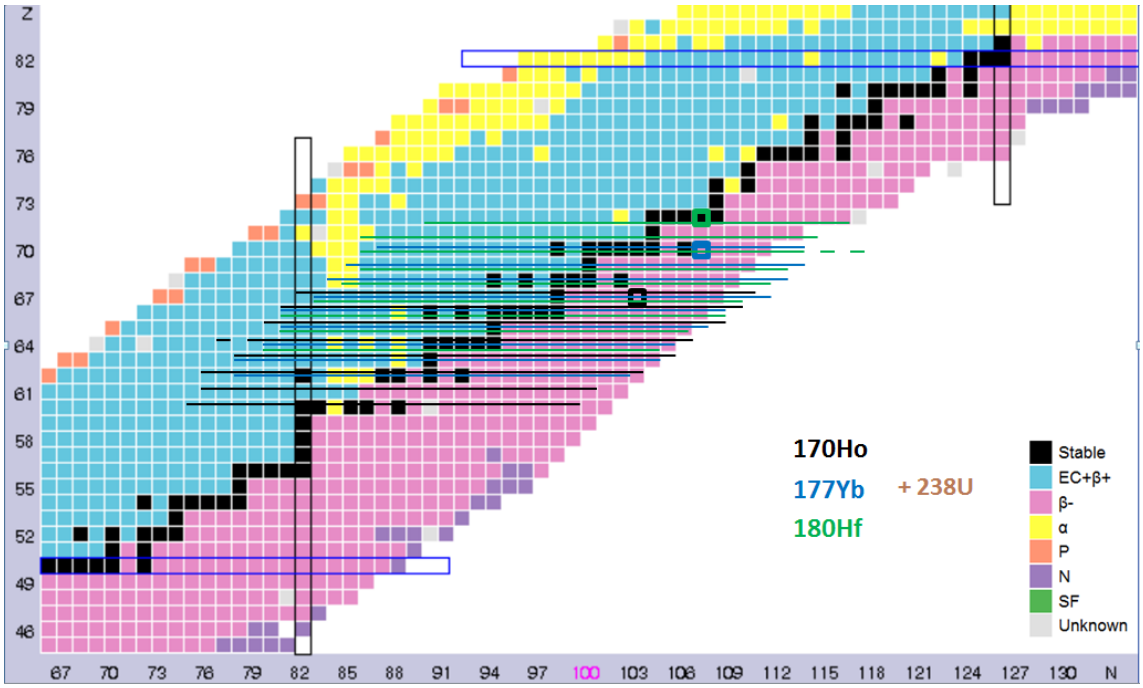

Fig. 4.21: DIT + SMM simulations: the area of PLF products from ^{170}Ho + ^{238}U (black lines), ^{177}Yb + ^{238}U (blue lines), ^{180}Hf + ^{238}U (green /lines) at the collision energy of 8 AMeV. Some new isotopes from stripping channels (-xp) are drawn in the white area.

4.3.4 Discussion

Selecting the right combination of projectile and target nucleus with appropriate energy, a new way on production of isotopes with a large neutron excess can be opened up via deep-inelastic or multi-nucleon transfer reactions above the Coulomb barrier. This idea is supported by the previous studies on isoscaling, which results that low excitation energy of pre-fragments and even larger neutron excess in the projectile and target nucleus lead to more neutron rich nuclei [Ves11], [Zag11], [Ves13].

Therefore, we suggest the following reactions ^{170}Ho + ^{238}U, ^{177}Yb + ^{238}U, ^{180}Hf + ^{238}U at the energy of post-accelerated radioactive ion beams around 8 AMeV with respect on the relatively high intensity at the HIE-ISOLDE facility in CERN. In this chapter, the DIT + SMM simulations of deep-inelastic transfer reaction leading to production of new isotopes were presented. Particularly, 4 new isotopes from ^{170}Ho, 7 new isotopes from ^{177}Yb, and 2 isotopes from the reaction with ^{180}Hf beam on the ^{238}U target at the energy of 8 AMeV. The production cross section for the new isotopes (projectile-like fragments PLF´s) was evaluated and depending on the particular isotop varies from 0.1 to 10 μb.

In this work we underlined that the only one device in the Europe equipped with spallation source and post-accelerator, capable to accelerate radioactive ion beams to induce given secondary reactions is HIE-ISOLDE facility. In combination with the ISOLDE Solenoidal Spectrometer (ISS) it can ensure complete identification of isotopes and measurement of kinematics of transfer products, including Q values. Hence some very neutron rich isotopes from Z = 65 to 70 could be measured first time ever in the laboratory conditions. Consequently, nuclear models could be tested for a new region of neutron rich nuclei, the figure 4.21.

Tab. 4.4: The PLF elemental production cross section [mb] from DIT + SMM simulations (Z_{PLF} = 60 – 72). ^{170}Ho, ^{177}Yb, ^{180}Hf beams + target ^{238}U at 8 AMeV. The cross sections of new elements are marked in colors. Only (-xp), (0p) are considered.

A ↓	Z →	60			61			62			63			64		
		170Ho	177Yb	180Hf	170Ho	177Yb	180Hf	170Ho	177Yb	180Hf	170Ho	177Yb	180Hf	170Ho	177Yb	180Hf
134																
135		1,E-03														
136		2,E-02														
137		5,E-02			5,E-03											
138		1,E-01			1,E-02			6,E-04								
139		3,E-01			5,E-02			1,E-03								
140		6,E-01			2,E-01			1,E-02	1,E-03							
141		1,E+00			4,E-01			6,E-02	7,E-03		2,E-03	1,E-03		3,E-04		
142		2,E+00			9,E-01			2,E-01	4,E-02		2,E-02	6,E-04		4,E-06		
143		2,E+00			2,E+00			7,E-01	1,E-01		8,E-02	8,E-03		1,E-03	3,E-04	7,E-04
144		2,E+00			2,E+00			1,E+00	2,E-01		3,E-01	6,E-02		1,E-02	4,E-03	2,E-03
145		3,E+00			3,E+00			2,E+00	3,E-01		9,E-01	1,E-01		8,E-02	2,E-02	8,E-03
146		3,E+00			3,E+00			3,E+00	6,E-01		2,E+00	2,E-01		3,E-01	6,E-02	3,E-02
147		3,E+00			3,E+00			4,E+00	8,E-01		3,E+00	5,E-01		8,E-01	1,E-01	7,E-02
148		2,E+00			3,E+00			5,E+00	9,E-01		4,E+00	7,E-01		2,E+00	3,E-01	2,E-01
149		2,E+00			3,E+00			6,E+00	1,E+00		6,E+00	9,E-01		3,E+00	6,E-01	3,E-01
150		2,E+00			3,E+00			5,E+00	1,E+00		9,E+00	1,E+00		5,E+00	1,E+00	4,E-01
151		1,E+00			2,E+00			5,E+00	1,E+00		8,E+00	1,E+00		8,E+00	2,E+00	7,E-01
152		1,E+00			1,E+00			4,E+00	1,E+00		1,E+01	2,E+00		1,E+01	2,E+00	9,E-01
153		6,E-01			1,E+00			4,E+00	1,E+00		1,E+01	2,E+00		1,E+01	3,E+00	1,E+00
154		3,E-01			6,E-01			2,E+00	7,E-01		9,E+00	1,E+00		2,E+01	3,E+00	1,E+00
155		1,E-01			4,E-01			2,E+00	5,E-01		7,E+00	1,E+00		2,E+01	3,E+00	1,E+00
156		3,E-02			2,E-01			1,E+00	3,E-01		6,E+00	8,E-01		2,E+01	3,E+00	1,E+00
157		1,E-02			1,E-01			6,E-01	1,E-01		4,E+00	5,E-01		2,E+01	2,E+00	9,E-01
158		4,E-03			4,E-02			3,E-01	7,E-02		3,E+00	3,E-01		1,E+01	2,E+00	6,E-01
159		2,E-03			2,E-02			2,E-01	3,E-02		2,E+00	1,E-01		1,E+01	1,E+00	4,E-01
160					6,E-03			9,E-02	1,E-02		1,E+00	8,E-02		8,E+00	7,E-01	2,E-01
161					2,E-03			4,E-02	6,E-03		6,E-01	5,E-02		6,E+00	4,E-01	9,E-02
162								1,E-02	6,E-03		3,E-01	3,E-02		4,E+00	2,E-01	4,E-02
163								4,E-03	2,E-03		1,E-01	1,E-02		2,E+00	1,E-01	2,E-02
164								3,E-04	6,E-04		5,E-02	1,E-02		1,E+00	8,E-02	7,E-03
165								3,E-04			2,E-02	5,E-03		5,E-01	4,E-02	5,E-03
166											3,E-03	9,E-04		2,E-01	1,E-02	7,E-04
167											1,E-03	6,E-04		7,E-02	7,E-03	2,E-03
168											6,E-04			2,E-02	3,E-03	3,E-04
169														3,E-03	6,E-04	
170														6,E-04		
171																
172																
173																
174																
175																
176																
177																
178																
179																
180																
181																
182																
183																
184																
185																
186																
187																
188																
189																
190																

A ↓ / Z →	65			66			67			68			69		
	170Ho	177Yb	180Hf	170Ho	177Yb	180Hf	170Ho	177Yb	180Hf	170Ho	177Yb	180Hf	170Ho	177Yb	180Hf
134															
135															
136															
137															
138															
139															
140															
141															
142															
143															
144															
145	6,E-04														
146	2,E-02	3,E-03	3,E-03												
147	9,E-02	2,E-02	1,E-02	2,E-03	3,E-04	3,E-04									
148	3,E-01	7,E-02	2,E-02	1,E-02	5,E-03	2,E-03									
149	8,E-01	2,E-01	9,E-02	6,E-02	1,E-02	9,E-03	2,E-03								
150	2,E+00	4,E-01	2,E-01	2,E-01	6,E-02	4,E-02	5,E-03	1,E-03	2,E-03						
151	4,E+00	8,E-01	4,E-01	7,E-01	2,E-01	1,E-01	4,E-02	9,E-03	7,E-03						
152	7,E+00	1,E+00	7,E-01	2,E+00	5,E-01	3,E-01	2,E-01	5,E-02	4,E-02		9,E-04	3,E-04			
153	1,E+01	2,E+00	1,E+00	4,E+00	1,E+00	6,E-01	5,E-01	2,E-01	1,E-01		7,E-03	8,E-03			
154	2,E+01	3,E+00	2,E+00	7,E+00	2,E+00	1,E+00	2,E+00	6,E-01	4,E-01		4,E-02	3,E-02		6,E-04	
155	2,E+01	4,E+00	2,E+00	1,E+01	4,E+00	2,E+00	3,E+00	1,E+00	7,E-01		2,E-01	1,E-01		5,E-03	7,E-03
156	3,E+01	5,E+00	2,E+00	2,E+01	6,E+00	3,E+00	7,E+00	3,E+00	2,E+00		5,E-01	4,E-01		3,E-02	2,E-02
157	3,E+01	5,E+00	2,E+00	3,E+01	8,E+00	4,E+00	1,E+01	5,E+00	3,E+00		1,E+00	1,E+00		1,E-01	9,E-02
158	3,E+01	5,E+00	2,E+00	4,E+01	9,E+00	4,E+00	2,E+01	8,E+00	4,E+00		3,E+00	2,E+00		4,E-01	4,E-01
159	3,E+01	4,E+00	1,E+00	4,E+01	1,E+01	4,E+00	3,E+01	1,E+01	6,E+00		6,E+00	4,E+00		1,E+00	1,E+00
160	3,E+01	3,E+00	1,E+00	5,E+01	1,E+01	4,E+00	4,E+01	1,E+01	7,E+00		1,E+01	7,E+00		3,E+00	2,E+00
161	3,E+01	2,E+00	7,E-01	5,E+01	1,E+01	3,E+00	5,E+01	2,E+01	7,E+00		2,E+01	1,E+01		6,E+00	5,E+00
162	2,E+01	2,E+00	4,E-01	5,E+01	8,E+00	3,E+00	6,E+01	2,E+01	7,E+00		2,E+01	1,E+01		1,E+01	8,E+00
163	2,E+01	1,E+00	2,E-01	5,E+01	7,E+00	2,E+00	7,E+01	2,E+01	6,E+00		3,E+01	1,E+01		2,E+01	1,E+01
164	1,E+01	6,E-01	1,E-01	5,E+01	5,E+00	1,E+00	8,E+01	2,E+01	5,E+00		3,E+01	2,E+01		2,E+01	2,E+01
165	7,E+00	3,E-01	7,E-02	4,E+01	4,E+00	7,E-01	8,E+01	1,E+01	4,E+00		3,E+01	2,E+01		3,E+01	2,E+01
166	4,E+00	2,E-01	3,E-02	3,E+01	2,E+00	4,E-01	9,E+01	1,E+01	3,E+00		4,E+01	1,E+01		4,E+01	2,E+01
167	2,E+00	1,E-01	1,E-02	2,E+01	2,E+00	2,E-01	9,E+01	9,E+00	2,E+00		3,E+01	1,E+01		5,E+01	2,E+01
168	8,E-01	4,E-02	8,E-03	1,E+01	9,E-01	1,E-01	9,E+01	6,E+00	1,E+00		3,E+01	9,E+00		5,E+01	2,E+01
169	2,E-01	1,E-02	3,E-04	8,E+00	5,E-01	6,E-02	1,E+02	4,E+00	7,E-01		3,E+01	6,E+00		5,E+01	2,E+01
170	6,E-02	3,E-03	1,E-03	3,E+00	2,E-01	2,E-02	5,E+01	2,E+00	4,E-01		2,E+01	4,E+00		5,E+01	2,E+01
171	2,E-02	6,E-04	7,E-04	9,E-01	8,E-02	7,E-03	4,E+01	1,E+00	2,E-01		1,E+01	3,E+00		5,E+01	1,E+01
172	1,E-03	3,E-04		2,E-01	3,E-02	2,E-03	8,E+00	6,E-01	6,E-02		9,E+00	2,E+00		4,E+01	1,E+01
173	6,E-04			3,E-02	1,E-02	1,E-03	1,E+00	3,E-01	2,E-02		5,E+00	7,E-01		3,E+01	7,E+00
174				3,E-03	1,E-03	3,E-04	2,E-01	8,E-02	8,E-03		3,E+00	3,E-01		2,E+01	4,E+00
175				1,E-03			3,E-02	3,E-02	2,E-03		1,E+00	1,E-01		1,E+01	2,E+00
176							1,E-03	6,E-03	3,E-04		4,E-01	4,E-02		8,E+00	9,E-01
177							6,E-04	2,E-03			1,E-01	8,E-03		3,E+00	3,E-01
178								6,E-04			3,E-02	4,E-03		8,E-01	1,E-01
179											3,E-03			2,E-01	3,E-02
180											3,E-04			3,E-02	1,E-02
181														4,E-03	2,E-03
182														6,E-04	
183															
184															
185															
186															
187															
188															
189															
190															

A ↓	Z →	70			71			72		
		170Ho	177Yb	180Hf	170Ho	177Yb	180Hf	170Ho	177Yb	180Hf
134										
135										
136										
137										
138										
139										
140										
141										
142										
143										
144										
145										
146										
147										
148										
149										
150										
151										
152										
153										
154										
155										
156				1,E-03						
157			4,E-03	5,E-03						
158			2,E-02	2,E-02			1,E-03			
159			8,E-02	1,E-01			2,E-03			
160			3,E-01	4,E-01			1,E-02			
161			1,E+00	1,E+00			6,E-02			
162			3,E+00	3,E+00			2,E-01			6,E-03
163			6,E+00	6,E+00			9,E-01			4,E-02
164			1,E+01	1,E+01			2,E+00			2,E-01
165			2,E+01	2,E+01			5,E+00			7,E-01
166			3,E+01	2,E+01			1,E+01			2,E+00
167			4,E+01	3,E+01			2,E+01			4,E+00
168			5,E+01	4,E+01			2,E+01			9,E+00
169			6,E+01	4,E+01			3,E+01			2,E+01
170			7,E+01	5,E+01			4,E+01			3,E+01
171			8,E+01	5,E+01			5,E+01			4,E+01
172			9,E+01	5,E+01			6,E+01			5,E+01
173			1,E+02	4,E+01			6,E+01			6,E+01
174			1,E+02	3,E+01			6,E+01			8,E+01
175			1,E+02	2,E+01			6,E+01			9,E+01
176			1,E+02	1,E+01			5,E+01			1,E+02
177			7,E+01	7,E+00			4,E+01			1,E+02
178			5,E+01	3,E+00			3,E+01			1,E+02
179			1,E+01	1,E+00			2,E+01			1,E+02
180			2,E+00	3,E-01			6,E+00			9,E+01
181			4,E-01	8,E-02			2,E+00			6,E+01
182			4,E-02	2,E-02			4,E-01			2,E+01
183			4,E-03	2,E-03			7,E-02			4,E+00
184							2,E-02			7,E-01
185				7,E-04			3,E-03			1,E-01
186										1,E-02
187				7,E-04						4,E-03
188										3,E-04
189										
190										

4.4 Spallation & HIE-ISOLDE facility

The ISOLDE (Isotope Separation On-Line DEvice) facility presently can produce over 700 different isotope beams for over 70 different chemical elements [ISO12] and nuclei with high isospin-asymmetry. This makes ISOLDE the leading ISOL-type facility in the world. The main principle of ISOL method is based on collision of proton beam that impinges onto a thick target with extremely high temperature. Before the recoils being ionized and subsequently separated in a mass separator they should be stopped. The name of such nuclear reaction is spallation. This technique is complementary to the second method of isotope beam production, the so-called in-flight fragmentation. The in-flight fragmentation is characterized by heavy ion beam impinging onto a thin target after that the fast recoil fragments undergo separation by a series of large acceptance dipoles. After isotopic separation of particular recoils, the beam can be subsequently injected and accelerated in a LINAC in the REX-ISOLDE post-accelerator. The uniqueness of ISOLDE facility to produce a very wide range of isotopes, and elements is because of advanced research program on spallation targets, ion source and proton beam characteristics given by Proton Synchrotron Booster (PSB). The proton beam presently delivered to ISOLDE by PSB can be set to 1 or 1.4 AGeV energy, as a result of the last upgrade of the PSB in 1999 [PSB12]. Interaction of a proton beam with target nuclei of thick spallation target, such as ^{238}U, can trigger three main nuclear reaction channels: spallation-evaporation, spallation-fission and spallation-fragmentation. The contribution of particular de-excitation channels such as evaporation, fission and fragmentation in the total cross section depends on the target nuclei and on the specific isotope to be produced. At the last years about 70 % of the scheduled beam time at ISOLDE was delivered from ^{238}U based targets [ISO12]. Based on the experimental data and Monte Carlo simulations on production cross section for different elements in the spallation reaction p + ^{197}Au, at energies ranging from 200 AMeV to 30 AGeV, there is physical possibility to increase that cross section by increasing proton energy up to 10 AGeV [Kau80], [Koe02]. One of previous studies shown that increasing the proton energy from 1.4 to 2 AGeV will lead to the following gains: fission x1.4, fragmentation x2 to x5 and evaporation x6 [Geo02]. The upgrade of the PSB to higher energy and beam intensity of protons would be beneficial for all CERN experiments. Besides the way to increase cross section of spallation reactions, the ISOLDE group is still looking for solutions to produce higher quality beams at the level of spallation target, ion source, mass separator, ion optical system.

The following part of my thesis is dedicated to simulation of production cross section of spallation products where protons or neutrons are incident particles. Calculations are based on the demand of ISOLDE target group during my stay at CERN in 2016. The work was focused on Monte Carlo simulations with standard heavy element target, ^{238}U, and with some new targets based on very light elements. The important part of the simulations is investigation of impact of higher energy protons on (HIE-) ISOLDE program. For such kind of simulations ABRABLA had been chosen as the reliable Monte Carlo code [Sch91], [Sch02], [Kel08], [Kel09]. From recent experiments performed at GSI in inverse kinematics [Vil03], [Nap04], [NapPhD], [Tai03], [Ber03], [Ric06], [Arm04], there is a good empirical knowledge of the general characteristics of spallation and fragmentation reactions. Three types of collisions have been measured in that experiments, i.e. ^{238}U + ^{1}H, ^{136}Xe + ^{1}H and ^{56}Fe + ^{1}H at 1 AGeV. Based on these results ABRABLA parameterization has been adjusted as well. In order to demonstrate a prediction power of ABRABLA07 simulations, it can be seen the comparison between simulations and GSI data Fig. 4.22. Recently ISOLDE measurement with direct target and with neutron converter configuration confirmed a lower discrepancy between cross

sections achieved with the ABRABLA07 code compared to Monte Carlo code FLUKA, as transport code previously used by ISOLDE target group [Lui12]. The code is mostly used for high energy physics calculations. However, because the FLUKA code cannot describe statistical decay of spallation remnants in reliable way, it is not suitable for prediction of cross sections of exotic nuclei produced at ISOLDE facility.

a)

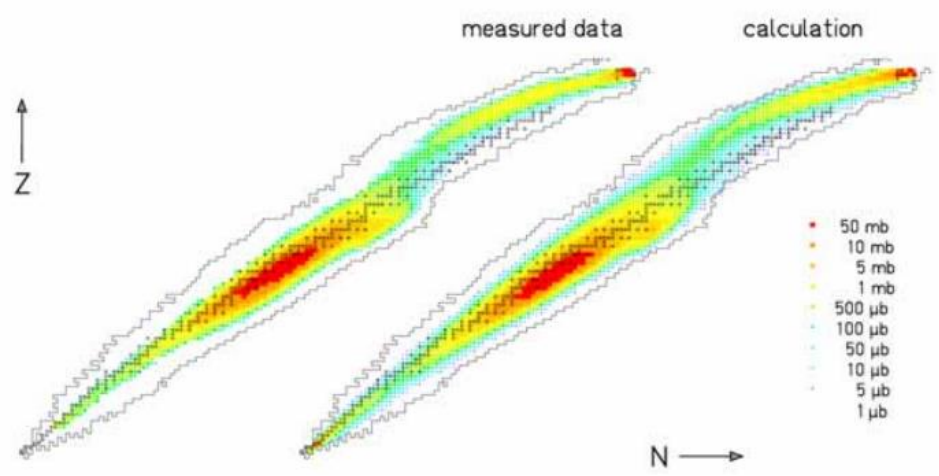

b)

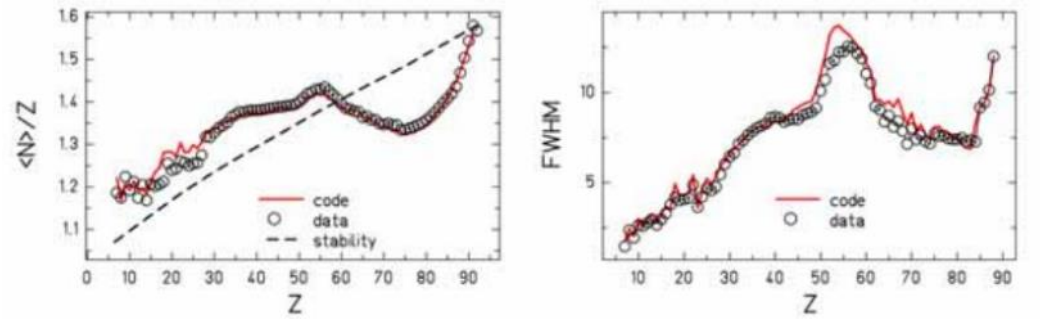

Fig. 4.22: Isotopic production cross sections of nuclei produced in p + ^{238}U at 1 AGeV:
a) The nuclear chart of spallation products, FRS data vs. theoretical prediction. In-flight technique was used during the measurement of p + ^{238}U at 1 AGeV [Arm04], [Ber03], [Ber06] (left) vs. simulations BURST + ABLA07 [Ric06].
b) from the left, the ratio of mean neutron <N> to atomic number Z as a function of Z, on the right picture FWHM distribution as a function on Z is depicted.

4.4.1 Incident energy of protons vs. cross section of spallation products

The reaction of spallation allows us to measure and observe many unstable nuclei with high statistics by advanced ISOL technique. In this context, proton energy plays a crucial role in collisions where beams of protons are colliding with a massive uranium target in ISOLDE target station. Further increase of the energy of protons from 1.4 AGeV to 2.0 AGeV can provide not only higher production cross section for available radioactive beams, but can open new possibilities for new isotopic beams, and for secondary post-accelerated beams. These assumptions we investigated with ABRABLA07 simulations. One can find a comprehensive description of the latest version of the code ABLA07 (de-excitation code) [Kel09], discussed in the IAEA report [IAE08] as well.

The figure 4.23 presents the atomic number distribution for 0.6, 1.0, 1.4 and 2.0 AGeV proton-induced reactions on thin target of ^{238}U. All the simulations are performed in inverse kinematics, as ABRABLA was designed for in-flight inverse kinematics. The black points on the pictures represent a total cumulative cross section for every element from uranium below. If we decompose the total cross section to particular channels, we can quantify contributions from de-excitations like evaporation, fission and IMF emission (intermediate mass fragment), which we also call fragmentation. However, the most of particles are produced in the first stage of reaction, in spallation phase. In this phase, a proton entering a nucleus subsequently induce intra-nuclear cascade when big amounts of neutrons and light charged particles (LP, z = 1, 2), as proton and helium, are typically ejected from nucleus. Before thermally equilibrated residue is produced a pre-

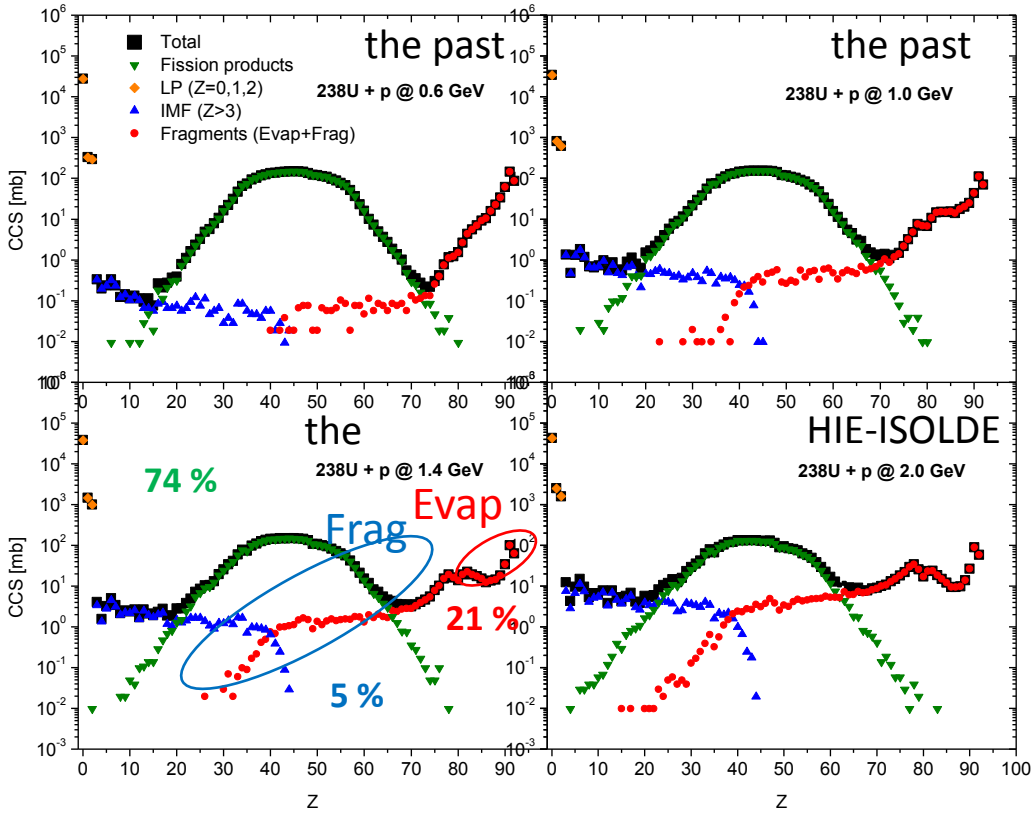

Fig. 4.23: The evolution of atomic number distributions of cold recoils produced in spallation reaction: p + ^{238}U at collision energy of: 0.6, 1.0, 1.4, 2.0 AGeV. Towards the higher energies more diverse beams with higher isospin-asymmetry are available.

equilibrium emission of neutrons is possible too. The impact of collision energy on the particular particles and fragments is evident from the figure 4.24.

As a consequence of higher proton energy excitation energy of hot residue is higher as well. This opens up the way for higher branching ration for spallation-fragmentation, when IMF fragments are produced. Because fragmentation is a threshold process and starts at excitation energy above 1 MeV/u, it is obvious that higher beam energy leads to rising trend of IMF distribution. Complementary to IMF, the cross section of fragments produced in fragmentation (Z<87) has ascending trend too. In general, if excitation energy of residue is even higher, i.e. above 2 MeV/u, nucleus can undergo multi-fragmentation and break up to many IMF fragments. The threshold is dependent on the mass number of the given target. It is evident, that at higher proton energy there is stronger impact of multi-fragmentation on total cross section. Nevertheless, the contribution of multi-fragmentation to the total cross section is almost negligible, and should not exceed 0.5 % at energy proton of 1.4 AGeV. For 2.0 AGeV protons multi-fragmentation branching ratio is very similar. Quantitatively, the ABRABLA07 simulations show that IMF production cross section can increase by factor of 2.43 at 2.0 AGeV/protons, compared to spallation at 1.4 AGeV/protons, the figure 4.25. In summary, within spallation-fragmentation de-excitation phase elements from Z = 3 to Z = 86, can be produced experimentally.

As for evaporation channel, data analyses of 1.4 AGeV spallation results that intersection of fragmentation and evaporation atomic number distributions is around Z = 75. Forward to higher atomic numbers, fragmentation distribution is decreasing to negligible value at Z = 86. On the other hand, evaporation is dominant at the interval Z,

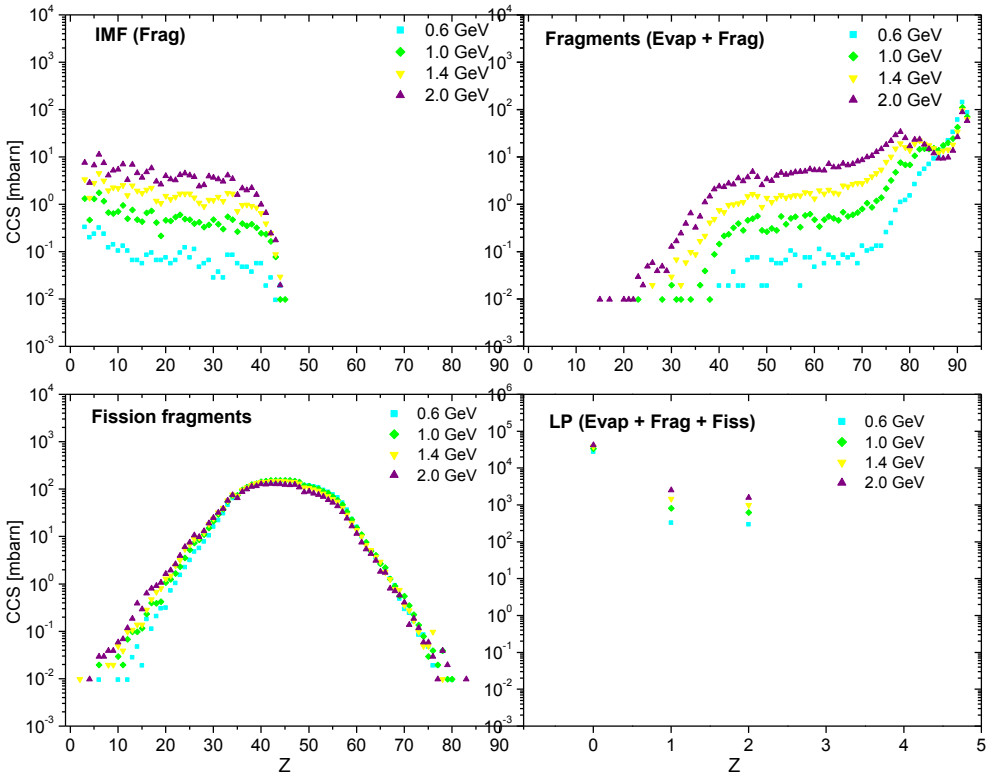

Fig. 4.24: Decomposition to particular de-excitation channels. The atomic number distribution of recoils is evolving with increasing incident energy: p + ^{238}U at collision energy of: 0.6, 1.0, 1.4, 2.0 AGeV.

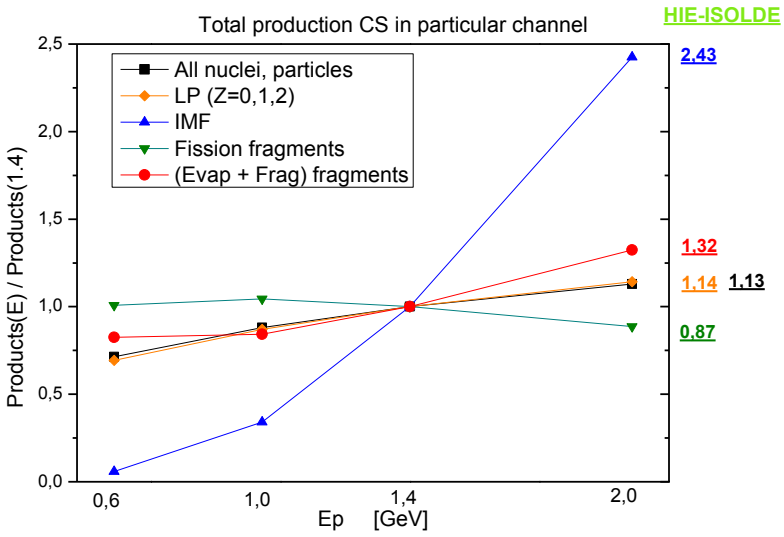

Fig. 4.25: ^{238}U + p: Comparisons of total cross section for particular de-excitation channel at four different collision energies. The Y values are normalized to cross section at the energy of 1.4 AGeV. Absolute values are stated in the table 4.5.

Energy [AGev]	$\sum_{z=0}^{z=92}(CCS)_Z$ [barn]				
	TOTAL	LP	IMF fragments	FISSION fragments	FRAG. + EVAP fragments
2.0	50,20	46,76	0,16	2,61	0,66
1.4	44,46	40,95	0,07	2,94	0,50
1.0	39,15	35,64	0,02	3,07	0,42
0.6	31,76	28,38	0,00	2,96	0,41

Tab. 4.5: The cumulative cross section integrated over the whole range of atomic numbers at different beam energy: 0.6, 1.0, 1.4, 2.0 AGeV. The specific case Z = 0 corresponds to one or more neutron emission.

= 75 - 92, and this interval is even narrower at 2.0 AGeV. Unlike to IMF production positive impact of 2.0 AGeV proton beam on cross section is obvious. This process represents another contribution to light charged particles so-called LP. As PSB synchrotron has been upgraded from 0.6 AGeV up to 1.4 AGeV evaporation channel cross section increased only gradually, figure 4.24. The combination of figures 4.24 and 4.25 can clarify evaporation process a bit more. Whereas, cross section of evaporation is going down with increasing energy at the interval Z = 85-92, on the interval Z = 72-85 it grows. Eventually, the total gain in cross section of heavy fragments produced in fragmentation and evaporation at 2.0 AGeV leads to gain of 1.32.

While excitation energy of pre-fragments has the most significant impact on evaporation and fragmentation, it is an angular momentum which has the strongest influence on fission process. Therefore, any stagnation or decrease of spallation-fission cross section with increasing collision energy will affect fission branching ratio, where downward trend is visible from the figure 4.25. On the other hand, one should mention that spallation-fission reactions with uranium target or with other actinides represents a strong tool in production of n-rich isotopes in a wide element range in the interval Z = 10-80. In order to enhance production of fission fragments, the proton-neutron converter configuration seems to be the best option for ISOLDE experiments [Got14], [Lui12].

4.4.2 Yields of spallation products Mg, Ca, Zn, Tl, Pb, Bi, At, Ra

In order to further examine an impact of 2 AGeV proton beam on yields of particular isotopes, we bring simulations where n-rich isotopes of Mg, Ca, Zn and Ra were investigated. Thus, ABRABLA simulations can help to get insight to experiments where mentioned isotopes are demanded for study of nuclear structure with higher statistics or to produce secondary beams with higher intensity in REX-ISOLDE experiments. Besides that set of n-rich isotopes we extended the interest of our research to n-deficient heavy isotopes of Tl, Pb, Bi and At. The most of them can be used as post-accelerated secondary beams in transfer induced fission (d, pf). Such kind of experiments is IS581 experiment where new state-of-art active targets can bring measurement of fission barriers with exceptional precision, which has not been reached in any experiment yet.

In our calculations we assumed spallation of a thick ^{238}U target with density of 19.05 g/cm3 where 99% of all simulated protons interact. In real ISOLDE conditions, just about 10% of all protons from beam can interact with target nuclei at 1.4 AGeV to be caused by restricted length of targets. The standard ISOLDE uranium UCx targets are 20 cm in length and have radius of 0.7 cm with standard density of 3.5 g/cm^3 [Lui12]. Because of isotopes yields are scalable by beam intensity and density of UCx target, the results of our simulations can be adjusted to real experimental conditions. In the framework of ABRABLA simulations we worked with 2x10^5 collisions in total. The present proton beam injected by LINAC2 to PSB, has pulse length of 2.4 μs, and can provide up to 3.3x10^{13} protons per pulse [Cat03]. After upgrade of LINAC2 to higher intensity one can expect count rate about 1x10^{14} particles per pulse.

As a beam is spreading through a massive target its kinetic energy and corresponding position inside a target is changing. Reliable tool for evaluation of particle kinetic energy and its range and intensity provides AMADEUS program. Since AMADEUS

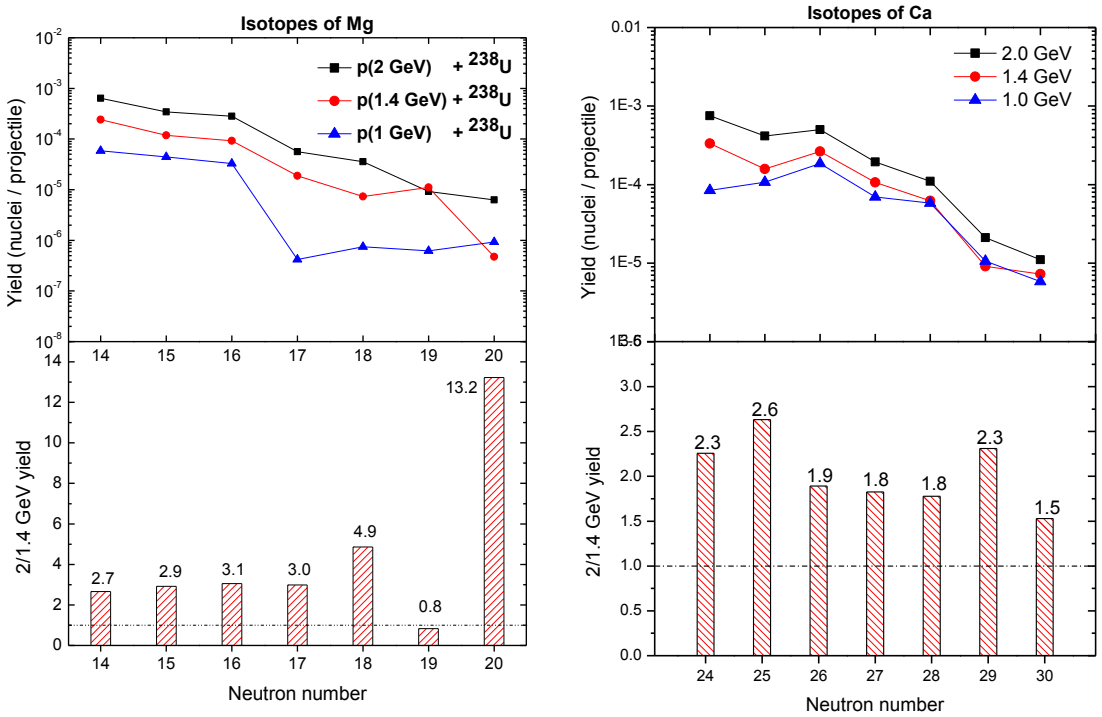

Fig. 4.26: Yields of n-rich Mg, Ca isotopes. Spallation: p + ^{238}U at 2.0, 1.4, 1.0 AGeV.

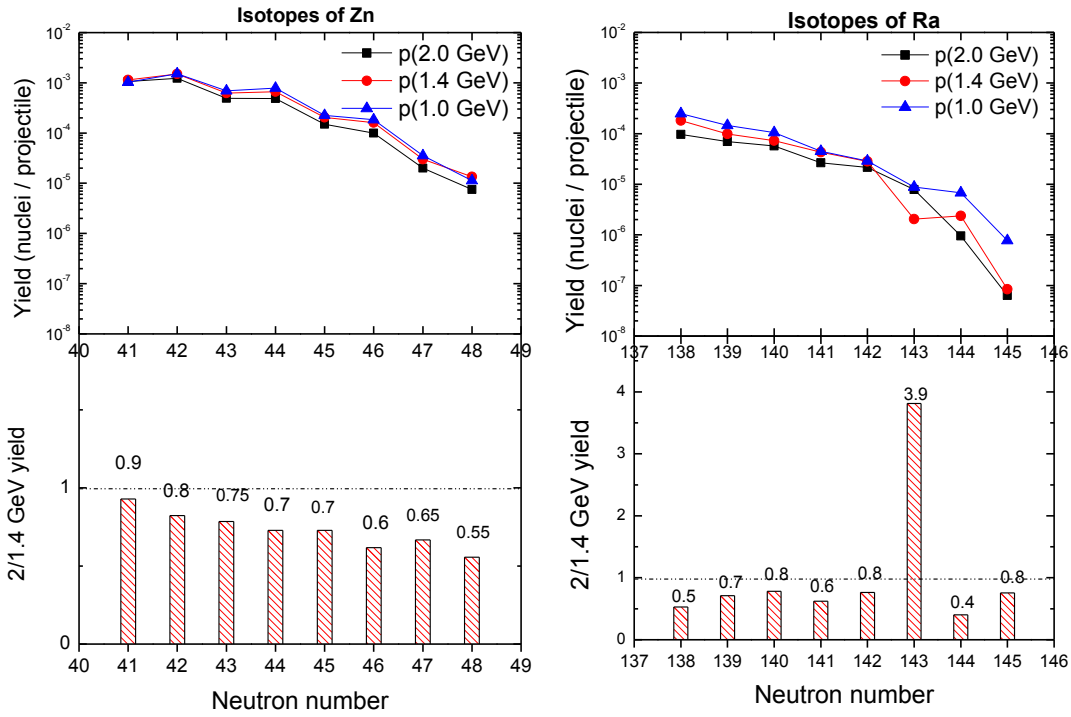

Fig. 4.27: Yields of n-rich Zn, Ra isotopes. Spallation: p + ^{238}U at 2.0, 1.4, 1.0 AGeV.

allows to calculate with discrete beam energies, the energy step was set to ΔEp = -100 MeV. These simulations finally result to comparison of yields for given n-rich and n-deficient isotopes at energies 2.0, 1.4 and 1.0 AGeV, figures 4.26, 4.27, 4.28, 4.29.

The increase of yields for Mg and Ca isotopes is very clear with increasing collision energy, figure 4.26 and 4.27. Looking back to the graphs 4.23 and 4.24, such behavior relates with reinforced spallation-fragmentation channel and both of the elements are IMF products of fragmentation predominantly. However, this is not the case of Zn and Ra isotopes, those are produced mainly in spallation-fission and in spallation-evaporation, respectively. The lower cross sections for Zn isotopes, as a fission product, results from the figure 4.24. The lower yields of Ra isotopes is a consequence of higher amount of neutrons and protons emitted during the intra-nuclear cascade. Subsequently, more pre-fragments further from the target nucleus region are formed. The second reason is the higher excitation energy for pre-fragments leading to increasing multiplicity of evaporated nucleons in de-excitation phase. From our simulations we observed that the spallation-evaporation distribution extends to lighter masses and smaller atomic numbers when the collision energy is increased. The similar results can found in previous works [Kau80], [Enq02], [Kau02], [Fer05], [Aud05].

For isotopes of Tl, Pb, Bi and At, we can apply the same explanation as for Rn isotopes. Therefore, a significant enhancement of production cross sections is evident for the n-deficient isotopes of Tl and Pb, the figure 4.28. The positive impact of the higher incident energy of the system is also visible on the side of very n-deficient isotopes of Bi, the figure 4.29.

The second option to enhancement of cross section of some very n-deficient isotopes in ISOLDE experimental conditions lies in use of targets element slightly above the desired products. However, the limited choice of target elements or materials imposes a severe restriction on this option. The third option relates with the beam, when ^{2}H or ^{3}He beam can significantly enhance cross section of very n-deficient isotopes at the same center-of-mass energy [Enq02]. The last one is probably the least realistic at the present.

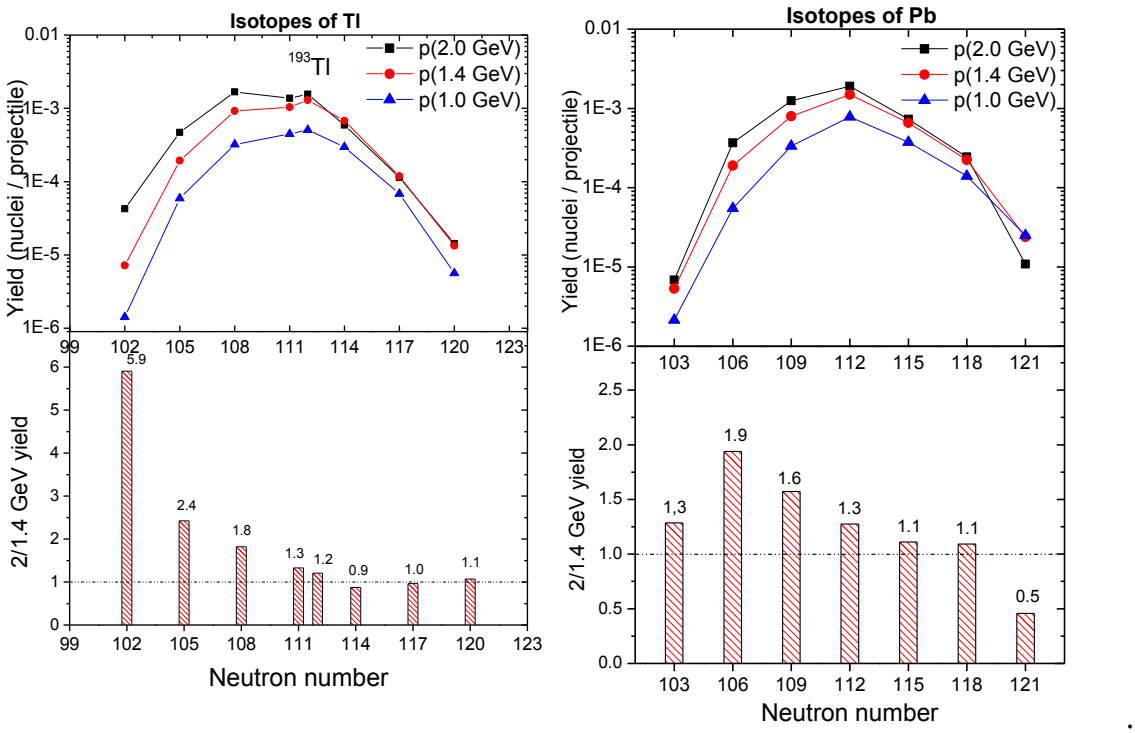

Fig. 4.28: Yields of n-rich Zn, Ra isotopes. Spallation: p + ^{238}U at 2.0, 1.4, 1.0 AGeV.

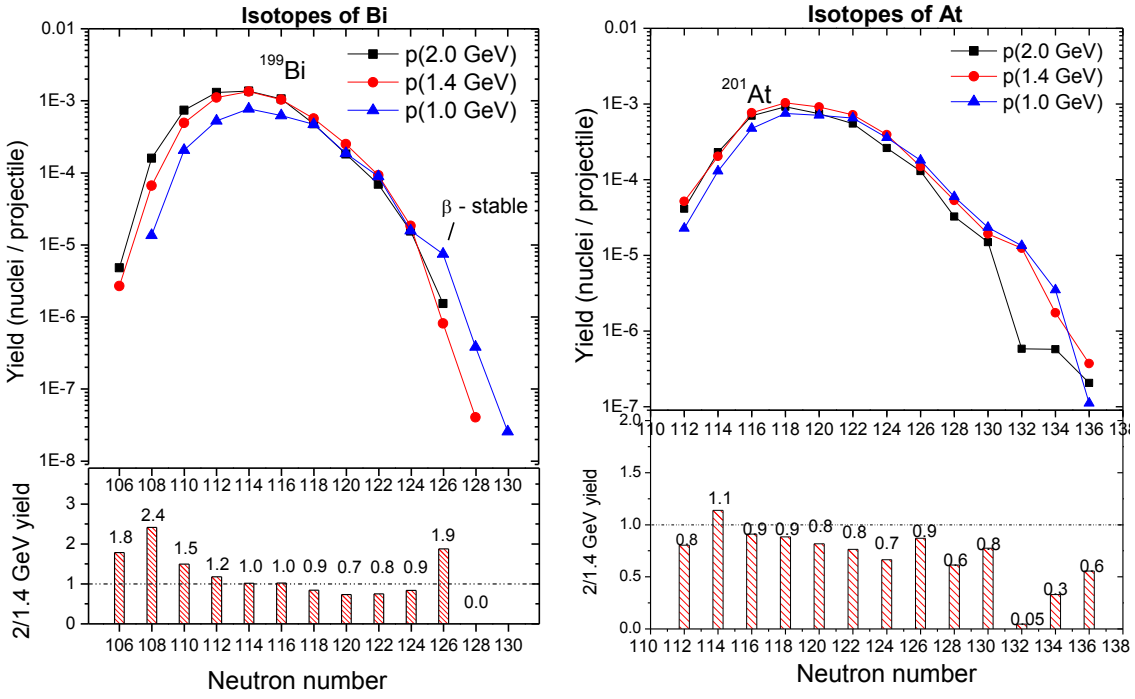

Fig. 4.29: Yields of n-rich Bi, At isotopes. Spallation: p + ^{238}U at 2.0, 1.4, 1.0 AGeV.

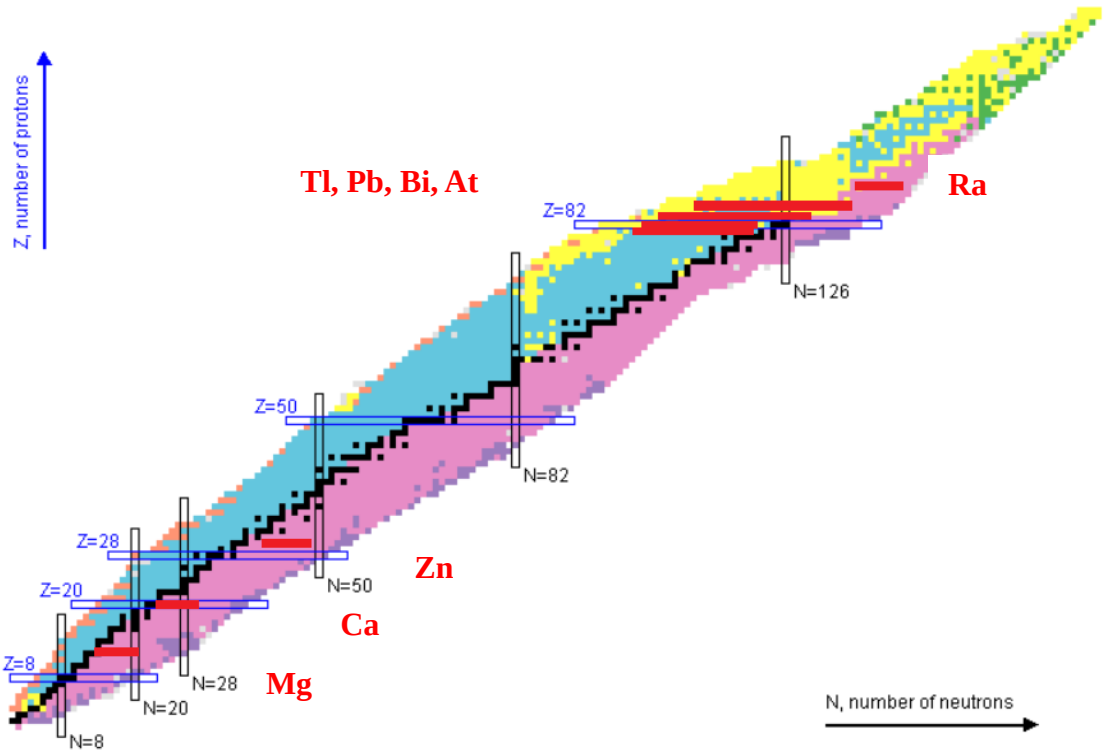

Fig. 4.30: Chart of the nuclides: isotopes of Mg, Ca, Zn, Tl, Pb, Bi and At were investigated in the framework of impact of high collision energy on production yields in proton induced spallation with uranium target.

4.4.3 Spallation of light targets ^{12}C, ^{28}Si, ^{40}Ca, ^{48}Ti

In order to produce light isotopes at higher production cross section in spallation and to produce isotopes even closer to proton drip line, the use of light targets could be alternative to heavy actinides targets. The results on the figure 4.32 confirm that statement. We have investigated the spallation of 1.4 AGeV protons on following targets: ^{12}C, ^{28}Si, ^{40}Ca and ^{48}Ti, the figure 4.31. These target elements are used in ISOLDE experiments where high flux of n-deficient radioactive ion beam, especially light isotope beams is required. The conclusion of spallation simulations of light targets is that spallation-evaporation and spallation-fragmentation are only channels contributing to production of any possible fragments, the figure 4.31. The total production gain for fragments is of one order of magnitude in this nuclide chart region, the figure 4.32. The mentioned light targets offer a possibility to make experiments with light radioactive ion beams more time effective, with shorter beam time, and thus more experiments can be performed at ISOLDE facility over a year. All isotopes produced in our simulations can be seen on the figure 4.33. Moreover, for chosen elements one can expect following gains of cumulative cross sections compared to standard ^{238}U based targets:

- O ~ 17x, produced in reaction: 1.4 AGeV proton + ^{28}Si
- Mg ~ 38x, produced in reaction: 1.4 AGeV proton + ^{28}Si
- Ar ~ 48x, produced in reaction: 1.4 AGeV proton + ^{48}Ti

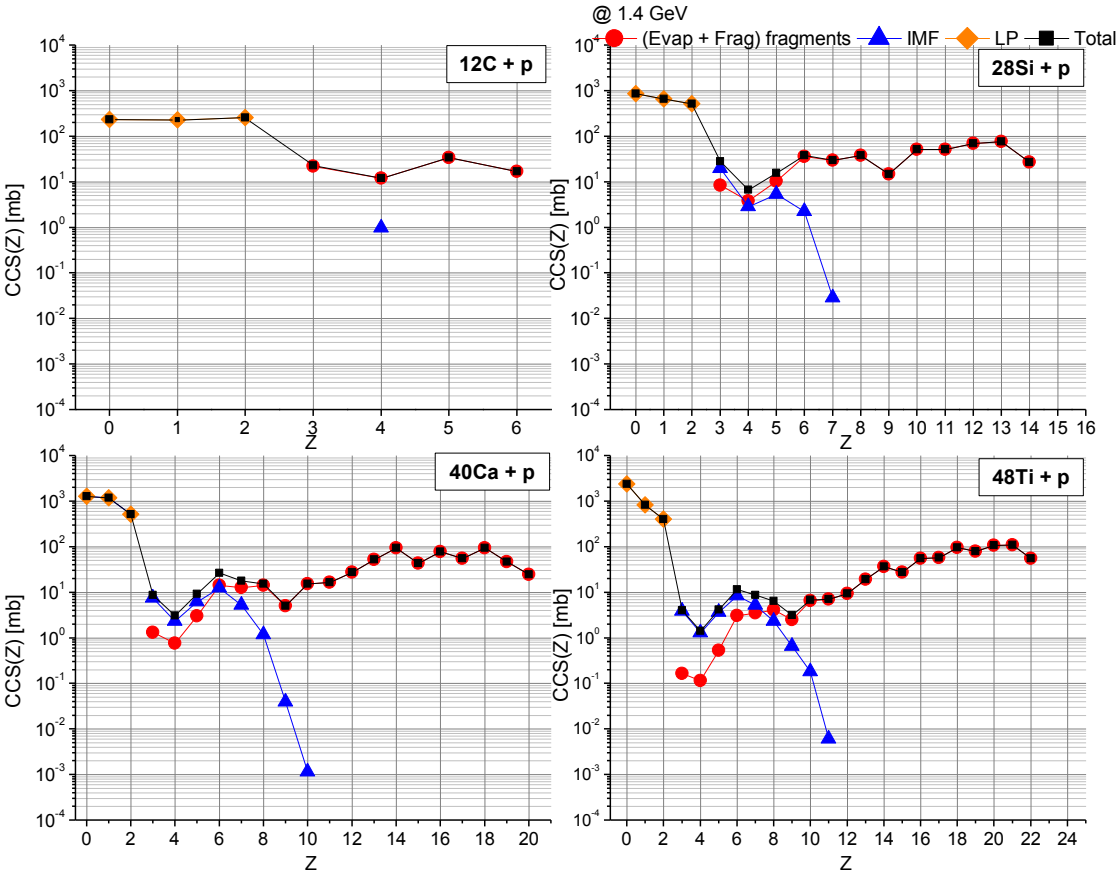

Fig. 4.31: Spallation of light targets ^{12}C, ^{28}Si, ^{40}Ca, ^{48}Ti at collision energy of 1.4 AGeV.

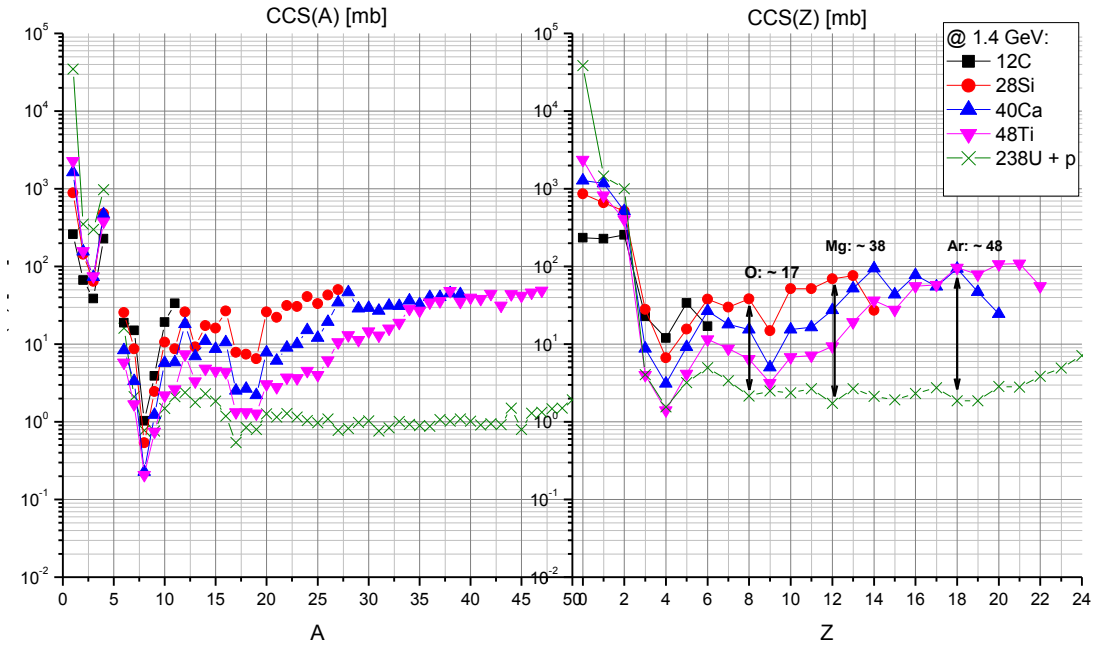

Fig. 4.32: Comparison of A, Z distributions at proton energy of 1.4 AGeV on light and heavy mass target materials. Instead of spallation with uranium target, spallation induced on light targets can bring significant enhancement of production cross section.

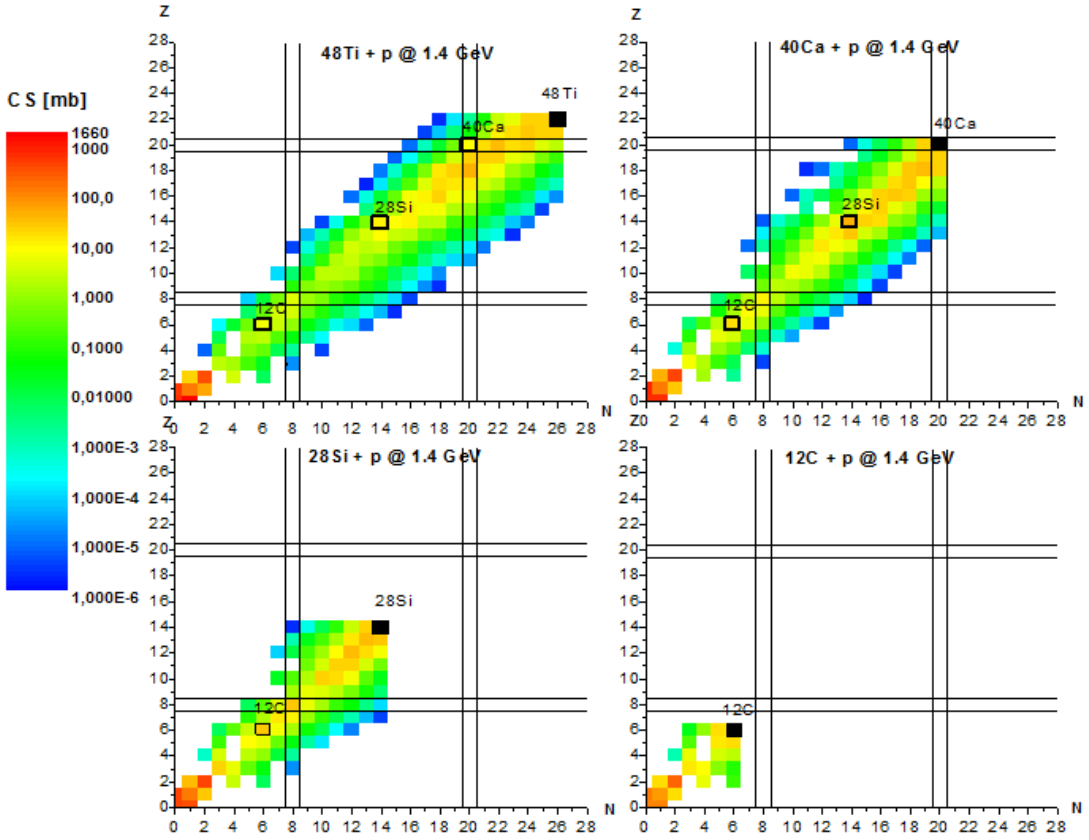

Fig. 4.33: Nuclide distribution of residues produced in the spallation of ^{48}Ti, ^{40}Ca, ^{28}Si, ^{12}C by 1.4 AGeV protons simulated using ABRABLA code. A target element slightly above the desired product gives the highest cross section, including the most n-deficient ones.

4.4.4 Proton vs. neutron induced spallation

One of the leading ISOLDE research program relates with the study of nuclear structure around the double shell closures of ^{78}Ni and ^{132}Sn. Emphasis is focused on fundamental understanding of nuclear structure or to determine the path of the r-process which plays a significant role in nucleosynthesis of about half of the heavy nuclei. The main process allows producing n-rich radioactive ion beams with Z=20-65 is spallation-fission. Such fission in direct target configuration is high energy fission and is also accompanied by a huge contribution from n–deficient isobars. These isobars create a strong contamination. The way to suppress contamination in n-rich isotopes experiments at ISOLDE relates with use of neutron converter configuration consists of primary UCx target, and secondary target based on W or Pb. By this technique high energy fission can be replace by low energy mass asymmetric fission characteristic by mean neutron energy of about 2 MeV. In principle, this represents the way to suppress big amount of isobaric contaminants and to investigate n-rich isotopes even closer the neutron drip line.

In this chapter the comparison between spallation of ^{12}C, ^{28}Si, ^{40}Ca, ^{48}Ti and ^{238}U by protons and neutrons at energies ranging from 200 AMeV up to 1.4 AGeV are presented. Such kind of simulations allows us to test ABRABLA07 code in condition that neutrons initiate spallation. The evolutions of A, Z cumulative distributions for p + ^{238}U and n + ^{238}U reactions are depicted on the figure 4.32 a). Both of the reactions imply a week dependence of spallation-fission on incident energy. Much stronger

impact of collision energy is visible in region of fragments from evaporation and fragmentation channel. As one can see, the simulations result to 2 times higher production cross sections in proton induced spallation compered to spallation by neutrons. That ratio p/n (proton to neutron cross section) is more or less constant in fission and evaporation region with larger variability in region typical for fragmentation. The similar behavior is obvious from simulations with light targets such as ^{48}Ti or ^{12}C, the figures 4.35 a), b) and 4.36 a), b). In the case of p + ^{48}Ti the ratio p/n for both of A, Z distributions ranges in the interval 2.60 - 3.30. For even lighter target, based on the isotope ^{12}C, the ratio p/n would be shifted to the interval 3.65 - 4.25. If one considered collision energy more than 200 AMeV the influence of coulomb barrier itself could be neglected. Besides others, we expect very weak influence of baryon electric charge on intra-nuclear cascade inside the target nucleus as well. Therefore, approximately systematic shift in cross sections between proton and neutron induced spallation reactions have to be verified by other model framework. We suggest to repeat simulations by use of intra-nuclear cascade code INCL++ linked to de-excitation code ABLA07.

4.4.5 Discussion

Few aspects of enhancement of fragment production cross sections in spallation reaction were discussed in the framework of that chapter. All cross sections were simulated using the Monte Carlo code ABRABLA07, capable to calculate spallation and de-excitation phase of reactions. An influence of incident energy of proton on cumulative production cumulative cross sections of n-rich and n-deficient isotopes were investigated on standard ISOLDE target, made of ^{238}U(Cx) using ABRABLA07. It was shown that increase of proton incident energy from 1.4 AGeV to 2 AGeV can improve fragments production capability of uranium targets, mainly for light and heavy fragments arisen in spallation-fragmentation, and n-deficient heavy fragments produced via spallation-evaporation. The most significant enhancement was observed above and below fission fragment region Z = 25-60. Within this interval the fission is dominant de-excitation mode and the incident energy of 2.0 AGeV does not lead to increase of fragment cumulative cross sections. Isotopic cross section of many isotopes of Mg, Ca, Zn, Tl, Pb, Bi, At and Ra have been investigated and discussed at various incident energies within the same model framework of ABRABLA07.

The possibly enhancement of production cross section of light fragments Z < 22 (Ti) was examined in proton induced spallation reactions of few light isotopic targets ^{12}C, ^{28}Si, ^{40}Ca and ^{48}Ti. The simulated cross sections were compared with standard uranium target. That results point to gain in cumulative production cross sections for elements O, Mg and Ar, in one order of magnitude at least. Isotopes belonging to the so-called “Island of inversion”, e.g. some n-rich isotopes of Li, Na, Mg, Si and Ca, are possible to study with better statistics by ISOL methods using light spallation targets..

The development of neutron converters promising enhancement of n-rich yields of spallation-fission and suppress isobaric contaminations is still topical at ISOLDE facility. Proton and neutron induced spallation reactions of heavy and light targets at wide incident energies have been examined, in order to test ABRABLA code for neutron projectiles in a pair with isotopic target of light and heavy elements. The results point to systematic shift of proton vs. neutron induced spallation cross sections, the most obvious in the region of fragmentation products.

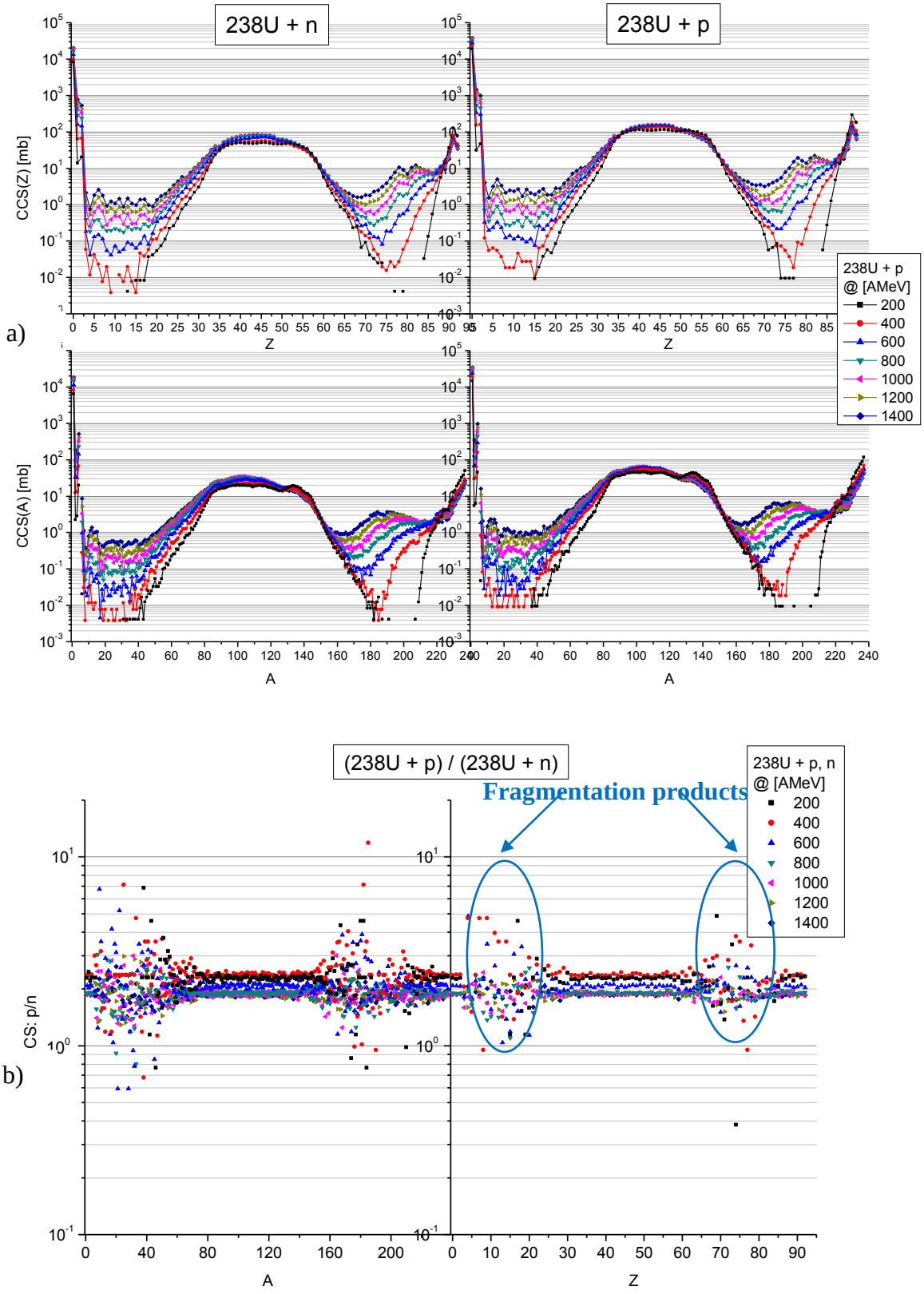

Fig. 4.34: p, n + ^{238}U at 0.2-1.4 AGeV a) left: neutron induced spallation, right: proton induced spallation. b) the ratio proton to neutron induced spallation cross section at given A, Z.

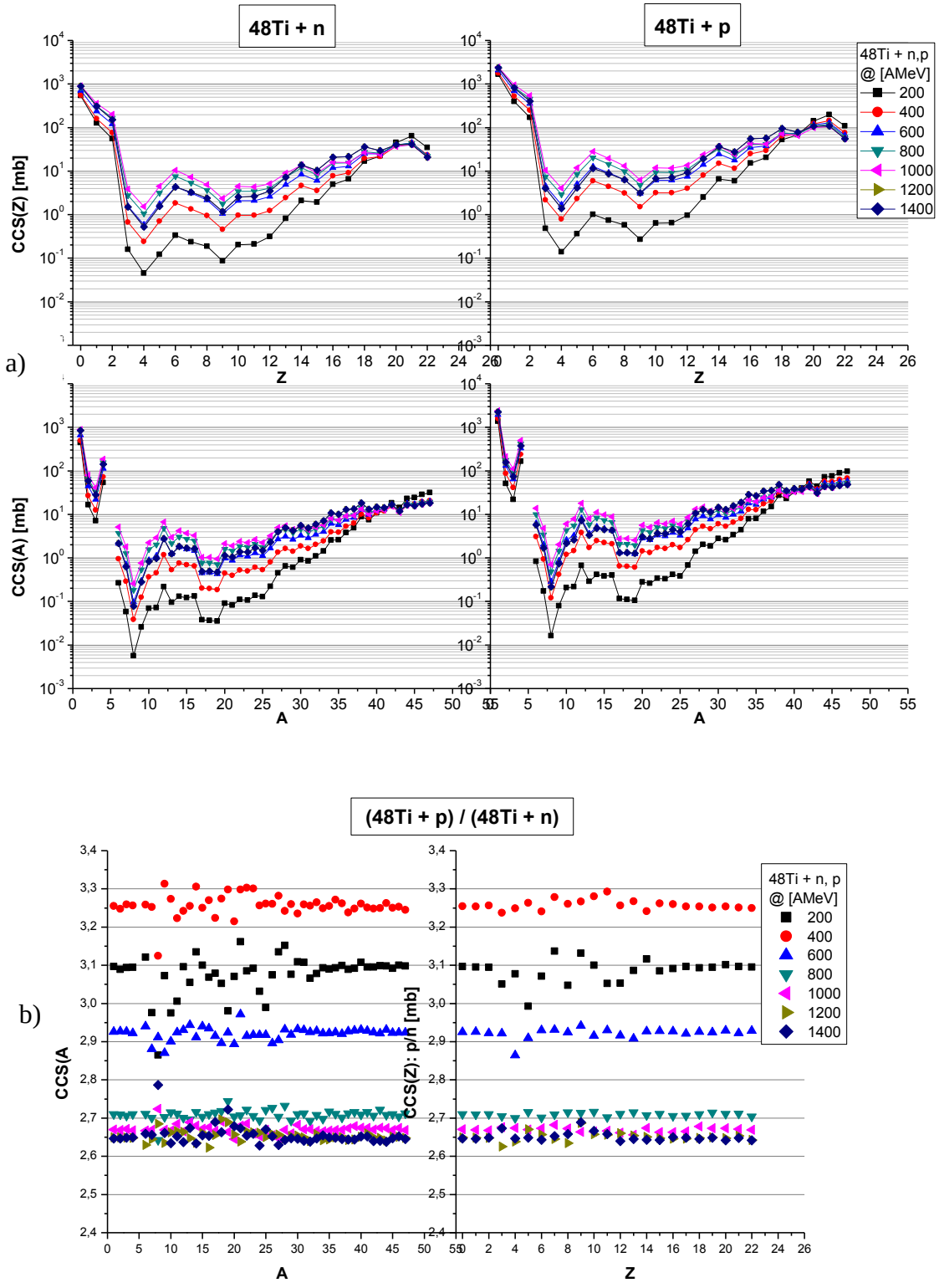

Fig. 4.35: p, n + ^{48}Ti at 0.2-1.4 AGeV a) left: neutron induced spallation, right: proton induced spallation. b) the ratio of proton to neutron induced spallation products.

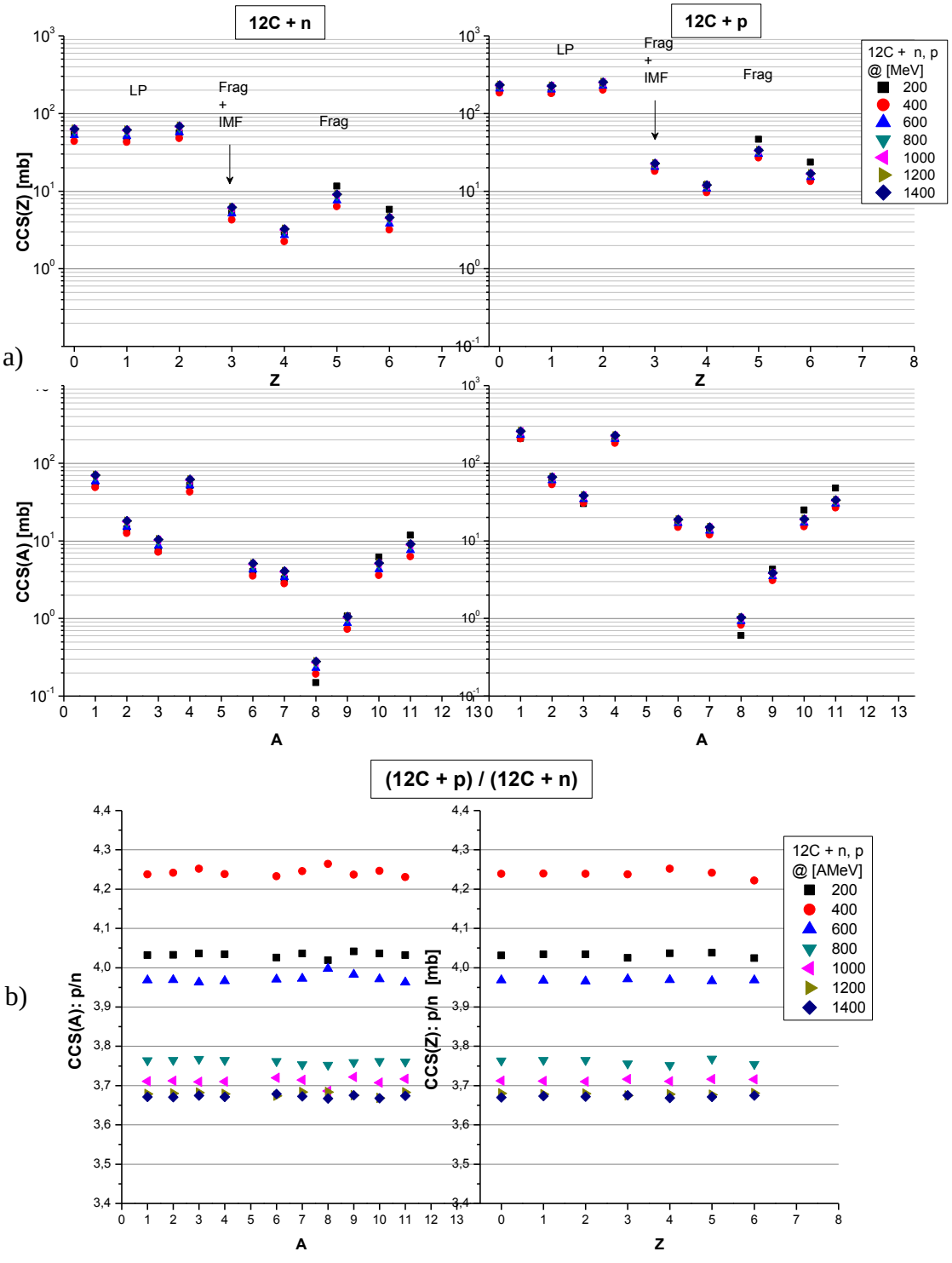

Fig. 4.36: p, n + ^{12}C at 0.2-1.4 AGeV a) left: neutron induced spallation, right: proton induced spallation. b) the ratio of proton to neutron induced spallation products.

4.5 SPALADiN experiment, ^{136}Xe + p and ^{136}Xe + ^{12}C at 1AGeV

Spallation reaction is usually described and modeled as two-stage process, where each step corresponds to different time scales in the reaction. There are several types of models for physical description of a first-stage. Based on different degrees of complexity we distinguish from microscopic models or codes, like as pure quantum-mechanical dynamics, quantum-molecular dynamics (QMD), Boltzmann-Uehling-Uhlenbeck equation (BUU) and intra-nuclear cascade (INC) to macroscopic abrasion-like models. The most important feature is that after a first stage of a reaction a remnant or pre-fragment nucleus can have changed its nucleon content, acquired a certain excitation energy, linear momentum and angular momentum.

From the point of view of the INC models the first step of reaction could be described by the intra-nuclear cascade consisting in series of incoherent nucleon-nucleon collisions on the timescale of 10^{-22} s. In a cascade phase the total initial kinetic energy can be transferred from the projectile to the target nucleus. The cascade stops once the energy from the projectile is homogenously dissipated among all the nucleons of the remaining nucleus. During intra-nuclear cascade energetic particles may escape from the nucleus and remaining nucleus, so-called pre-fragment stay still highly excited. INCL++ code (the Liège intra-nuclear cascade model) is considered as a one of the most reliable intra-nucleon cascade codes [IAE08] [Bou02], which is implemented in GEANT4 as well [GEANT], [Ago03]. Another reasonable choice is intra-nuclear cascade code BURST, which is a part of abrasion model ABRA as first stage code of ABRABLA07 code, capable to reconstruct spallation reaction over whole timescale of the reaction up to formation of cold fragments [Sch91], [Sch02], [Kel08], [Kel09]. Depending on the thermo-dynamical temperature of nucleus the system can experience pre-equilibrium emission or thermal instabilities and break-up into several pre-fragments or evolve to a single compound nucleus.

The second stage treats the further evolution of the pre-fragment or compound nucleus, i.e. its de-excitation down to the cold fragments experimentally observed. De-excitation is considered as a long process where one or more cold fragments are formed. The second stage is always treated by means of statistical models applying thermo-dynamical pictures. Depending on the excitation energy and transferred angular momentum pre-fragment can undergo evaporation, fission or fragmentation. Emission of gammas becomes dominant in the last phase of the de-excitation disposing a big amount of angular momentum. The picture of the full spallation reaction is depicted in simplified form on the figure 4.37.

The two stage picture of spallation comes out from the assumption that de-excitation process is independent on the way pre-fragment is created because de-excitation is collective process of nucleus. Therefore, one can used global variables to described pre-fragment, i.e. mass, charge, excitation energy and total angular momentum.

It is one of the aims of SPALADiN experiment to test the two-step hypothesis and measure the contribution of different pre-fragment decay channels in the reactions ^{136}Xe + p and ^{136}Xe + ^{12}C at the energy 1 AGeV [Gor19]. Both of the reactions have been measured in inverse kinematics at SPALADiN setup in GSI, Darmstadt, see the figure 4.38. The big-aperture dipole magnet together with large acceptance detectors of SPALADiN setup allows to measure final state of charged particles and projectile residue with $Z \geq 2$ in coincidence with neutrons. Such coincident event-by-event measurement permits to estimate the excitation energy of pre-fragments and to analyze their de-excitation channels. Based on the measured data the elemental production cross sections were compared with existing data and theoretical models. Besides these characteristics, the total multiplicity and the fragment production cross section

depending on the excitation energy were studied and models were confronted with measurement. In the framework of this chapter I will not discuss all the details and results of SPALADiN experiment and analysis. Instead of that I focus more on comparison of different first stage models linked to different de-excitation models in order to confront them with experimental data. To be able to compare simulations of spallation reactions with SPALADiN data the outputs of nuclear models were linked to GEANT4 environment where whole SPALADiN setup is simulated, i.e. dipole magnet, detection system and so on.

Besides fundamental research of spallation reaction, there is a strong motivation coming from application research with high–intensity GeV proton beams impinging on targets with high Z. Few of them are nuclear-waste transmutation to build a high-flux neutron sources, like European Spallation Source [ESS], or to construct subcritical fast-neutron research reactor MYRRHA [Abd01].

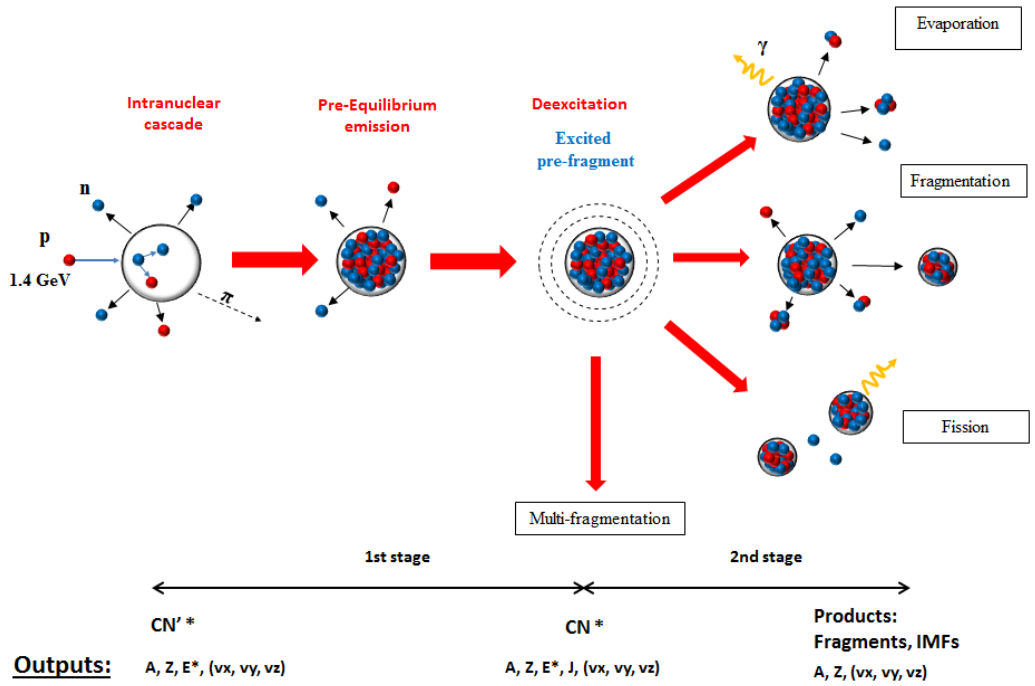

Fig. 4.37: Evolution of the high energy collision leading to final cold fragments by different channels.

4.5.1 SPALADiN setup

The beam of ^{136}Xe is delivered from synchrotron SIS18 at energy of 1 AGeV, with charge state of 48 and subsequently ionized by plastic scintillator to 54+. The average beam intensity was about of 3.10^3 ions/s, so the dead-time for data acquisition is at the level below 30%. Two targets were employed: a cryogenic liquid hydrogen target LH_2 [Che07], 80.53 mg/cm^2 thick, and graphite foil ^{12}C, 386 mg/cm^2 thick. Residues of the projectiles were detected by two multiple-sampling ionization chambers (MUSIC), filled with P10, the mixture of 90% Ar and 10% methane. Upstream of ALADiN dipole, the "Forward MUSIC" (FM) was placed and downstream of ALADiN two sectors chamber "Twin MUSIC" (TwM) to reconstruct tracks was in operation. TwM detector provides additional detection and identification of fragments close to beam axis, and allows to measure velocity spectra in the projectile rest frame. Total detection

efficiency of FM, including an acceptance, was evaluated to 100% for charge identification down to Z = 12. Because of geometrical losses of TwM, those are charge dependent and are not negligible, we evaluated them as 75% for Z = 12, 20% for Z = 40 and 15% for the heaviest residues. Beyond ALADiN dipole TOF wall equipped with two walls is installed, with 96 plastic scintillators. The size of each scintillator is 10 x 1100 x 25 mm (thickness, length, width). The hole in the middle of TOF wall ensures identification of light fragments with Z = 2 - 11, so the scintillators are not damaged by heavier fragments detected in TwM. TOF time resolution after calibration and correction is 300 ps (RMS) for fragments of $Z \geq 4$, and about 500 ps for Z = 2, 3. TOF detection efficiency is constant with any Z. The acceptance of each TOF plane scintillators is 95% and the probability for charged fragments in TOF in SPALADiN experiment was 81% ± 3%. In order to detect neutrons in SPALADiN experiment, LAND detector was positioned 10 m downstream of ALADiN's exit in 2π azimuthal homogenous configuration around the beam axis. Reconstruction of neutrons is based on amount of tracks inside the LAND detector. The LAND detection efficiency for single neutrons was evaluated as 80% ± 3%.

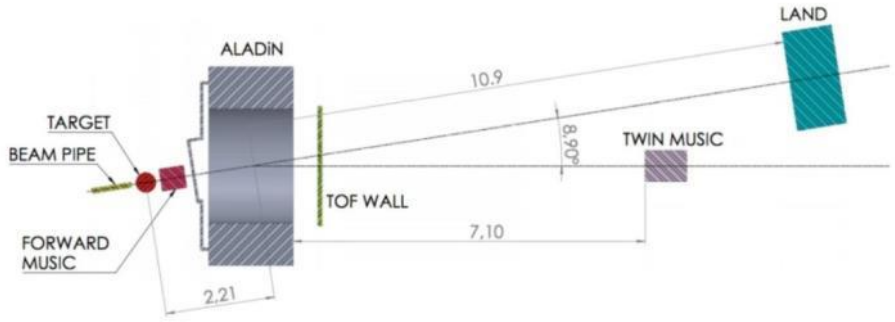

Fig. 4.38: SPALADiN experimental setup from experiment in 2009. The setup is equipped with two ionization chambers "Forward MUSIC" (FM), upstream ALADiN dipole magnet, and "Twin MUSIC" (TwM), downstream the dipole magnet. TOF in coincidence with TwM allow to measure charged fragments. Neutron detection system LAND, positioned downstream of the magnet, gives the opportunity for neutron multiplicity measurement.

4.5.2 Kinematics and acceptance of particles and ions

In order to compare models with experimental data for reactions ^{136}Xe + p and ^{136}Xe + ^{12}C at the energy of 1 AGeV, we have done simulations considering detection efficiencies of each part of the setup. We were capable to simulate whole transport of particles and ions leaving collision point using GEANT4 environment as the geometry of SPALADiN setup was included in details to the simulations. The second reason of kinematics simulations of both of spallation reactions is the fact that we just rely on the estimation of acceptance of SPALADiN setups. Especially, simulations play a key role in computation a probability that ions pass through the active volume of TOF scintillator wall. Two spallation or collision models were compared in combination with tree de-excitation models. One of the collision models is intra-nuclear cascade code INCL++, the second one is fast excitation model ABRA, also implemented inside the ABRABLA07 code [Sch91], [Sch02], [Kel08].. As de-excitation models, tree standalone codes were tested: ABLA07 (from ABRABLA07), GEMINI++ [Cha88], [Cha10] and SMM code [Bon95]. These three de-excitation models in pair with

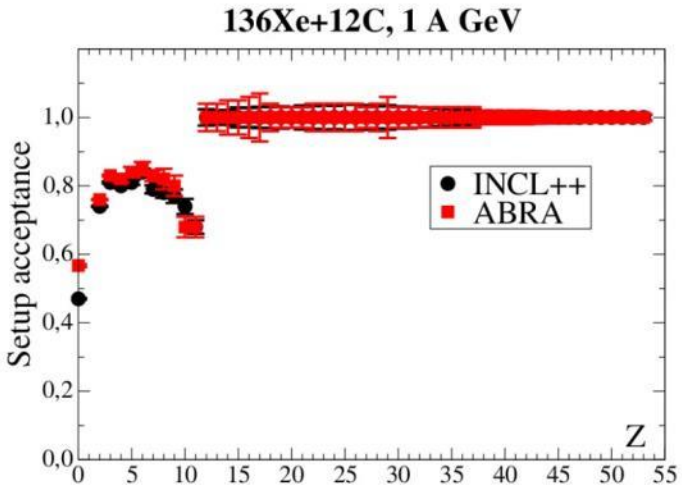

Fig. 4.39: The geometrical acceptance of SPALADiN as a function on Z, simulated in GEANT4 and fed by two different collision codes for ^{136}Xe + ^{12}C at 1 AGeV are presented here. The black points: acceptance for INCL++ + ABLA07, the red points: acceptance for collision model implemented in ABRABLA07. The results are similar for proton induced spallation ^{136}Xe + p at AGeV.

INCL++ cascade model were recognize among the best performing models by IAEA [IAE08], [Dav11], [Ler11] for description of spallation reaction. We utilize the assumption of intra-nuclear independence on de-excitation phase of reaction. Therefore, both of first stage codes either INCL++ or ABRA could be linked to very de-excitation code such as ABLA07 or to another.

On the figure 4.39 one can see comparison of SPALADiN setup acceptance depending on Z, for the reaction ^{136}Xe + ^{12}C and for ^{136}Xe + p at 1AGeV as well. Both of them are very comparable but for simplicity we attached just one graph. The geometry of SPALADiN implemented in GEANT4 was one and the same for each simulation. The acceptance is given by the ratio between the number of particles passing through the detection system (TOF, FM, TwM or LAND) and number of particles produced in event-by-event generator. The simulations using either INCL++ or ABRA linked to ABLA07 result to comparable dependence of acceptance on variable Z, especially above Z = 12. However, the kinematics by INCL++ + ABLA07 differs from one interpreted by ABRA + ABLA07 = ABRABLA07, as is shown on the figures 4.40 - 4.43. The kinematics, particularly vertical linear momentum components of alpha particles, IMF fragments, fragments with Z = 50 - 54 and neutrons, in the rest frame of ^{136}Xe, are presented on these graphs. It is obvious that for charged particles ABRA spectra are broader than the INCL++ ones. However, this is not the case of neutron spectra, where INCL++ model gives broader distribution.

The acceptance of the TOF wall as a function of Z, for Z < 12, can be seen from the figure 4.39. The dependence was obtained by GEANT4 simulations pairing INCL++ model with ABLA07. The sharp decrease of TOF acceptance beyond Z > 12 is caused by the hole in TOF wall, so the most of the fragments are passing through the TOF without any interaction, and they are additionally detected by TwM detector. Finally, we can evaluate the acceptance of TOF wall for light charged particles to 81% ± 3%, as was discussed in the previous sub-chapter.

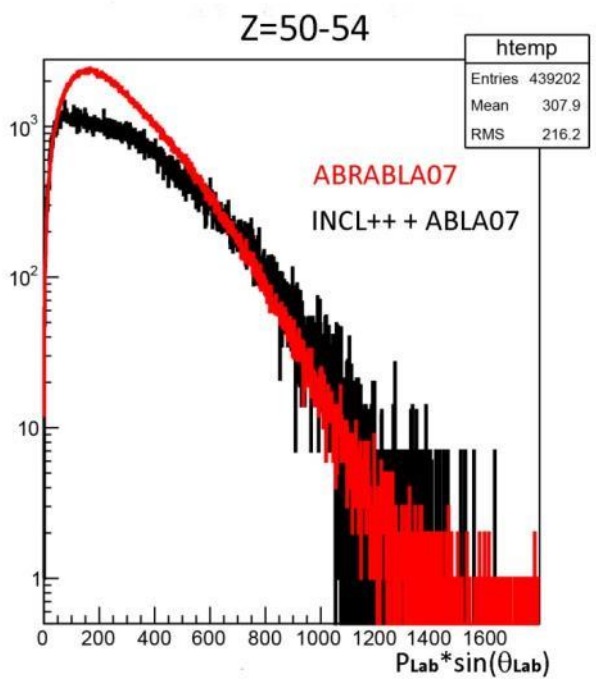

Fig. 4.40: Kinematics of fragments Z = 50 - 54 in ^{136}Xe + p at 1AGeV. The projection of linear momentum to the beam axis represented by axis x [MeV/c]. The θ_{lab} as the angle alpha vs. beam.

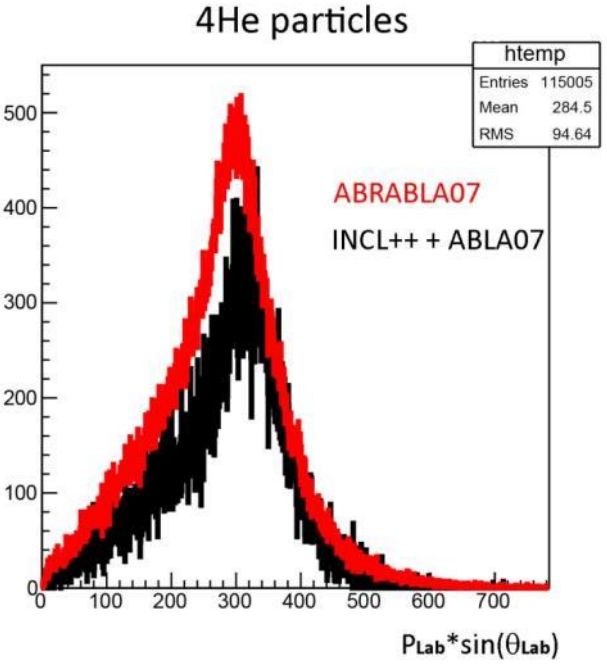

Fig. 4.41: Kinematics of the alphas in ^{136}Xe + p at 1AGeV. The projection of linear momentum to the beam axis represented by axis x [MeV/c]. The θ_{lab} as the angle alpha vs. beam.

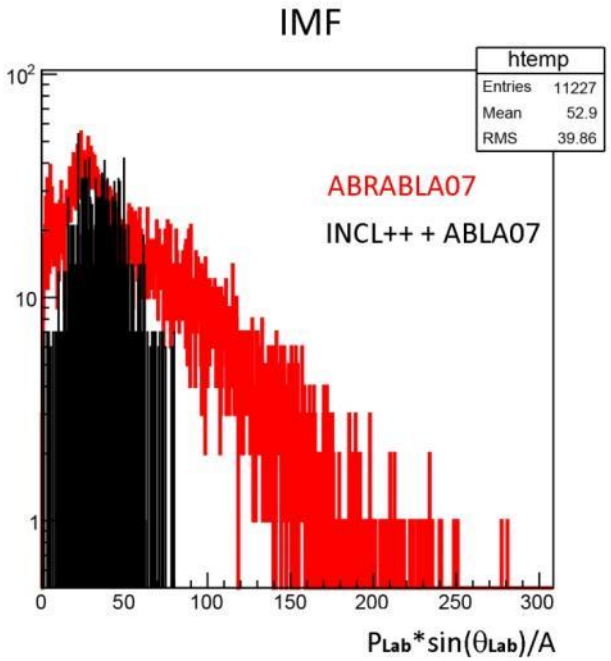

Fig. 4.42: Kinematics of IMF fragments in ^{136}Xe + p at 1AGeV. The projection of linear momentum to the beam axis represented by axis x [MeV/c]. The θ_{lab} as the angle alpha vs. beam.

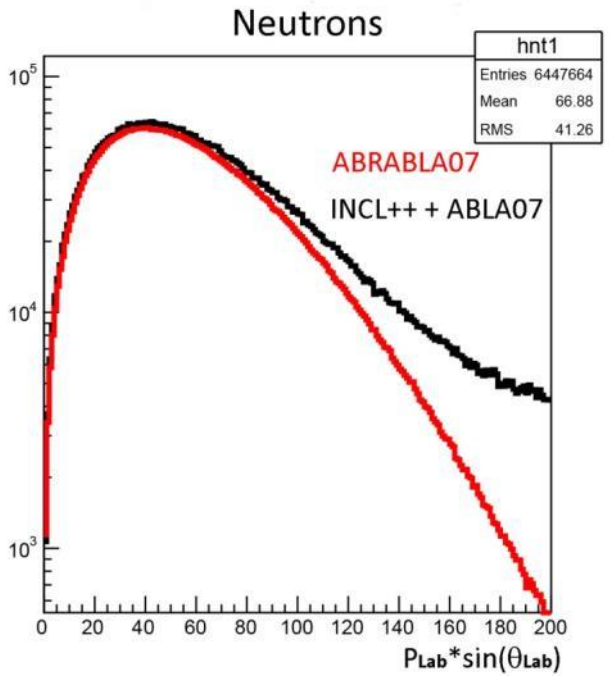

Fig. 4.43: Kinematics of neutrons in ^{136}Xe + p at 1AGeV. The projection of linear momentum to the beam axis represented by axis x [MeV/c]. The θ_{lab} as the angle alpha vs. beam.

4.5.3 Measured elemental production cross sections

The production cross sections in SPALADiN experiment in both of reactions were measured from two independent data sets, i.e. we rely on the identification by TOF in case of lighter charges and by FM used for larger charges. The cross section as a function of Z is shown on the figure 4.44 a) and b), for ^{136}Xe + p and ^{136}Xe + ^{12}C at 1 AGeV, respectively. First of all, one can see the good agreement between data collected from TOF and FM detection system in the overlap region. These overlaps are positioned within Z = 23 – 26, the collision with hydrogen target, and within Z = 12 – 29 for spallation on the ^{12}C target.

Based on the comparison on the figure 4.44 a), the SPALADiN data with hydrogen target agrees with those from FRS experiment, measured by group of Napolitani et al. [Nap07] below Z = 6 and above Z = 30. Discrepancy is mostly evident in the interval of Z = 8 – 26, where FRS data are above SPALADiN one. The explanation for such variance is not clear for us. On the other hand, looking at the data measured in direct kinematics and different identification technique provided by Kotov et al. [Kot95], one can see relatively good agreement with SPALADiN experiment. Due to direct kinematics measurement of Kotov, the heaviest elements were not registered, only light IMF fragments. The acceptance correction and correction for detection efficiency in SPALADiN experiment is handled well, as TOF and FM cross sections are overlapping in IMF fragments region. Therefore, Kotov and SPALADiN data appear more trustworthy in the region of IMF's.

From the comparison of elemental production cross sections on the graphs 4.44 b) for the second reaction ^{136}Xe + ^{12}C, SPALADiN data vs. data of Binns et al. [Bin87] results systematic shift of about 30%. This shift is more or less constant over whole Z interval. In spite of bit different beam energies in experiments, it could not lead to 30% shift in cross sections as its dependence on the beam energy around 1AGeV is really small, see figure 4.25. The most probable explanation of cross section shift is different target thickness for SPALADiN and experiment performed by group of Binns as the target used in the latter experiment was three times thicker. However, this explanation should be verified by another spallation experiment with ^{136}Xe on with hydrogen target.

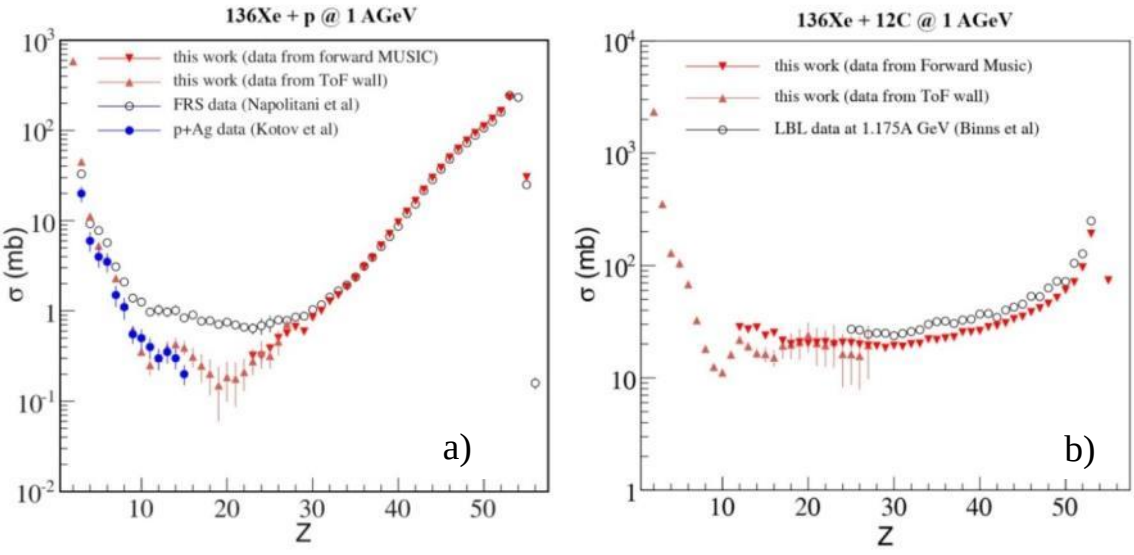

Fig. 4.44: Elemental production cross sections: a) ^{136}Xe + p at 1AGeV b) ^{136}Xe + ^{12}C at 1AGeV. Experimental data measured in SPALADiN experiment shown by red.

4.5.4 Comparison of experimental SPALADiN data with models

In the framework of the comparison of experimental SPALADiN data with our simulations we used only INCL++ as very reliable cascade model in pair with one of three statistical de-excitation models: ABLA07, GEMINI++ and SMM. The collision energy range for INCL++ to work properly was established as 0.15 – 3.0 AGeV, with assumption that following particles or ions are used as impinging projectiles: nucleons, pions, and light ions up to A = 18. More info related with INCL model could be found in [IAE08] [Bou02]. These collision simulations served us as event generator for GEANT4 simulations where whole SPALADiN setup is included. In orders to compare experimental and modeled data the total cross sections were normalized.

^{136}Xe + p @ 1 AGeV

The elemental production cross section for the reaction ^{136}Xe + p is depicted on the figure 4.45. The experimental data are compared with three models. The good agreement between SPALADiN data and models was reached in INCL++ + ABLA07 simulations for atomic numbers down to Z = 34. Other models provide comparable good results as ABLA07 within that region. As for GEMINI++ model, it provides extra good agreement with SPALADiN data at higher Z region. Below Z = 30 a cross sections by ABLA07 model are more comparable with GSI-FRS measurement measured by group of Alcántara-Núñez et al. [Nun15]. However, on the narrow interval Z = 28 – 34 SPALADiN data are better fitted by SMM model. From Z = 28 down to Z = 8, the best overlapping with SPALADiN experiment is provided by GEMINI++ simulations. In the

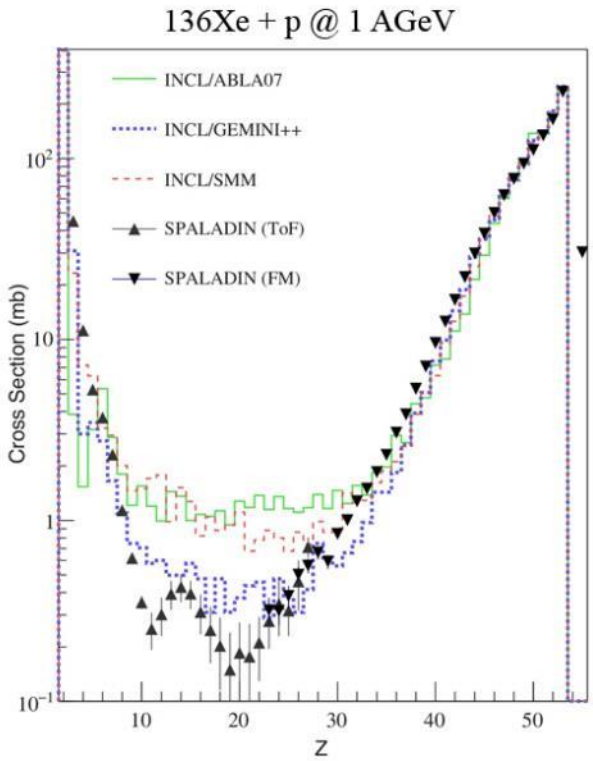

Fig. 4.45: Elemental production cross sections of ^{136}Xe + p at 1AGeV. SPALADiN experimental data by black compared with simulations by INCL++ inter-nuclear cascade model in combination with three different de-excitation models ABLA07 (green), GEMINI++ (blue), SMM (red).

range Z = 3 – 14 one can see good agreement of GEMINI++ simulations not just with SPALADiN experiment but also with measurement of Kotov et al. [Kot95], as it is depicted on the figure 4.44 a). As for ABLA07 and SMM models within the range of Z = 8 – 26 one can see better correspondence with FRS data measured by Napolitani et al. [Nap07] compared to those collected in SPALADiN measurement. However, such overlap of ABLA07 model with Napolitani data is not surprising for us, due to the fact that ABLA07 parameterization is based on the FRS data. The following three reactions served for ABRABLA07 parameterization: ^{238}U, ^{136}Xe and ^{56}Fe nuclei on hydrogen target and collision energy of 1AGeV at inverse kinematics [Vil03], [Nap04], [NapPhD], [Tai03], [Ber03], [Ric06], [Arm04].

^{136}Xe + ^{12}C @ 1 AGeV

Prediction power of models for spallation of hydrogen target is considerably more satisfactory than in the configuration with ^{12}C target, as can be seen 4.46. Down from the target atomic number to Z = 40, the most realistic results are given by SMM model. Unfortunately, from that point all de-excitation models in pair with INCL++ exhibit significant discrepancies. If we consider the systematic shift of about 30% between Binns et al. [Bin87] and SPALADiN data then we can conclude no agreement with available measured data and model predictions for ^{136}Xe + ^{12}C at 1 AGeV. The presented discrepancies in elemental production cross sections between experiment and models point to necessity of advanced analysis of SPALADiN and models data. The most significant results of such analysis are being discussed in the following sub-chapter.

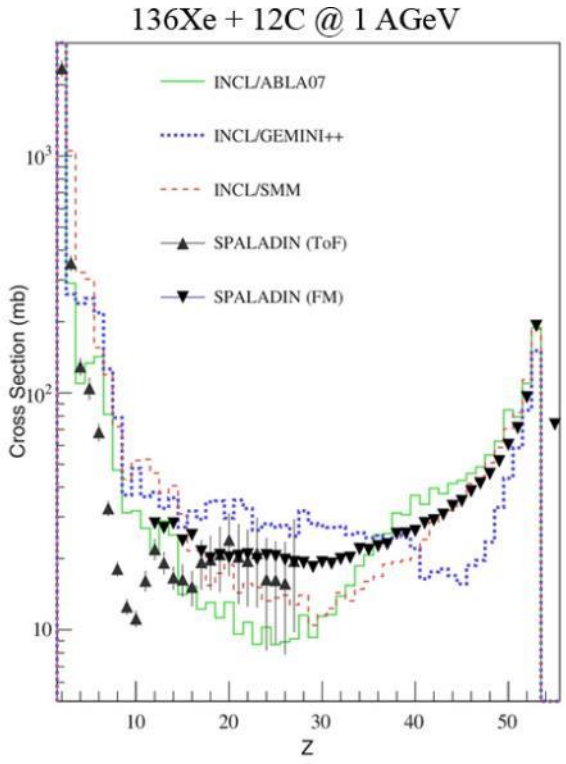

Fig. 4.46: Elemental production cross sections of ^{136}Xe + ^{12}C at 1AGeV. SPALADiN experimental data by black compared with simulations by INCL++ intra-nuclear cascade model in combination with three different de-excitation models ABLA07 (green), GEMINI++ (blue), SMM (red).

4.5.5 Decomposition of cross section to de-excitation channels

The graphs 4.45 and 4.46 show elemental production cross sections for both of investigating reactions. From the comparison of SPALADiN data and models it is evident that a large divergence between models and experimental data, mainly in nucleus-nucleus collisions, should be caused by how particular statistical models describes de-excitation phase of the reactions. Decomposition of final states to evaporation, fragmentation, multi-fragmentation and fission (in case of heavier pre-fragments), allow us to better comprehend the source of large discrepancies in discussed cross sections. With purpose to experimentally distinguish between particular de-excitation channels, detection of all particles in one collision event is needed. Than the sum over all registered atomic numbers Z_i ($Z_i \geq 2$) in one event should equal to so-called Z_{bound}. This Z_{bound} should correspond to pre-fragment atomic number, which is created at the end of intra-nuclear cascade. One of the most important characteristics of pre-fragment with particular Z_{bound} is its distribution of excitation energies per nucleon (E^*/A_{PF}), defined by some average value $< E^*/A_{PF} >$. It is an excitation energy which determines whether a given de-excitation channel is opened or closed.

We have used method of Gentil et al. [Gen08] to decompose element cross section $\sigma(Z_{bound})$ for pre-fragment produced in a given de-excitation channel. The method is based on registration of coincidences presented in the table 4.6. Based on the amount of neutrons, alphas particles and fragments ($Z \geq 3$) registered within one spallation event one can decide on de-excitation channel. We distinguished between 5 types of coincidences leading to given de-excitation channels, as are stated in the table 4.6. Coincidences of type (1) and (2) reproduced evaporation contributions. Types (3) – (5) are for fragmentation channel or multi-fragmentation.

Type	Residue	Neutrons	He	Fragments
(1)	1	≥ 1	0	0
(2)	1	≥ 1	≥ 1	0
(3)	1	≥ 1	0	≥ 1
(4)	1	≥ 1	≥ 1	1
(5)	1	≥ 1	≥ 0	≥ 2

Tab. 4.6: Coincidences of particles and ions to decompose of $\sigma(Z_{bound})$ to particular de-excitation channels. The label “Fragments” refers to nuclei with $Z \geq 3$.

^{136}Xe + p @ 1 AGeV

On the figure 4.47 are presented decompositions of $\sigma(Z_{bound})$ to de-excitation channels. Data measured in SPALADiN experiment are shown in upper left part of the figure. The experimental decomposition channels are then compared with three models as is shown in other frames of the figure. From the decomposition analysis of SPALADiN data for reaction ^{136}Xe + p, it appears that type (1) coincidences, typical for evaporation of neutrons, dominate in the interval Z_{bound} = 50 – 55 over other coincidences. The second dominating partial cross section comes from coincidences of type (2), corresponding to evaporation of He particles, with end point at Z_{bound} = 24. The remaining three coincidences (3) – (5) are less contributing to total cross section with distributions positioned around Z_{bound} = 48, similar to type (2). The main signature of emissions (3) – (5) is that at least one fragment is created despite heavier residue.

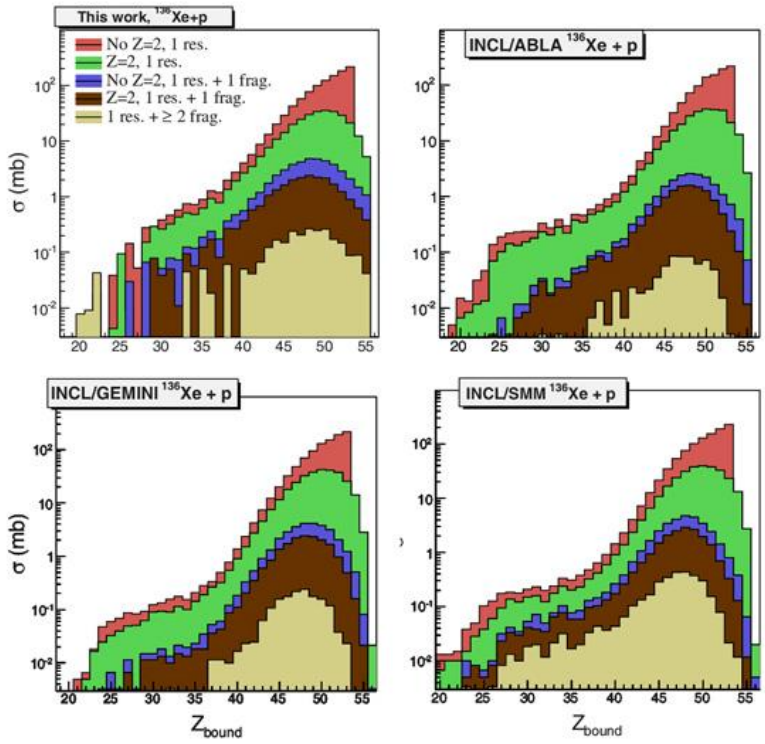

Fig. 4.47: ^{136}Xe + p at 1AGeV. SPALADiN data depicted in upper-left. Partial cross sections $\sigma(Z_{bound})$ contributing to elemental production cross sections from following de-excitations: evaporation (red, green), fragmentation (blue, brown colors) channels. No break-up or multi-fragmentation is included, only sequential emissions. Coincidence type: (1) – red, (2) – green, (3) – blue, (4) – brown, (5) – soft brown.

At that point, it is much easier to find out the reason of elemental production cross section discrepancy coming from model predictions as we can see in the interval Z_{bound} = 8 – 28, where evaporation channel of type (1) and (2) is the main source. This behavior is visible in case of ABLA07 and SMM model as well. The second important conclusion of that analysis is shift of fragmentation partial cross sections simulated by models which are systematically below SPALADiN experimental data.

Besides others we can discuss an influence of multi-fragmentation channel and how it is handled by given de-excitation models. Based on ABLA07 model prediction, multi-fragmentation channel stays still closed, because threshold is set to default value of E^* = 4.2 MeV/u, and it is still above average excitation energy of any $Z_{bound.}$ To set multi-fragmentation threshold to constant value is more simple than consider it as a function of pre-fragments mass (the systematics of Natowitz et al.[Nat02], [KEL08]). However such constant value will not cause any degradation in precision in that case, as mass dependence of multi-fragmentation threshold for both of reactions is leading to the same value of 4.2 MeV/u. As far as GEMINI++ model, simultaneously fragmentation or multi-fragmentation is not incorporated in the model. In case of SMM model break-up process is handled reliably and due to insufficient amount of excitation energy this channel stays closed.

$^{136}Xe + ^{12}C$ @ 1 AGeV

Partial cross sections observed in $^{136}Xe + ^{12}C$ show that evaporation of type (1) dominates over sum of all other types down to $Z_{bound} = 40$, figure 4.48. We can see that the coincidences of type (2) have very constant value of $\sigma(Z_{bound}) \approx 20$ mb over the interval $Z_{bound} = 23 – 48$. For coincidences (3) – (5), leading to emission of IMF's, we can observe higher cross sections compared to spallation on hydrogen target. Contribution of IMF channel to the total cross section is becoming more significant below $Z_{bound} = 50$. Also pre-fragment distribution is wider, and it is spreading over the interval $Z_{bound} = 18 – 54$, with peak maximum positioned around $Z_{bound} = 30$. Consequently, the lower average value of Z_{bound} means higher average of excitation

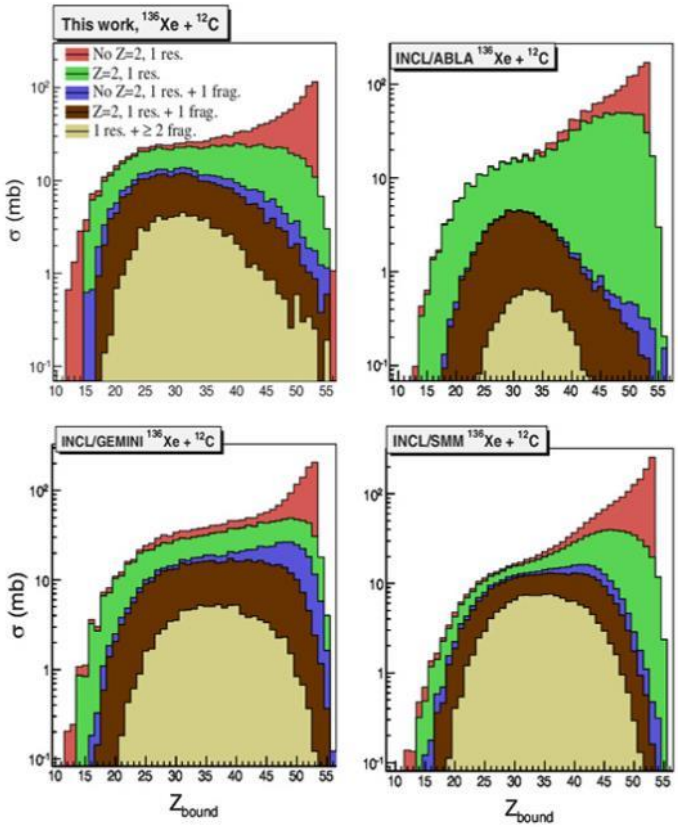

Fig. 4.48: $^{136}Xe + ^{12}C$ at 1AGeV. SPALADiN data depicted in upper-left. Partial cross sections $\sigma(Z_{bound})$ contributing to elemental production cross sections from following de-excitations: evaporation (red, green), fragmentation (blue, brown colors) and multi-fragmentation channels (soft brown). Coincidence type: (1) – red, (2) – green, (3) – blue, (4) – brown, (5) – soft brown.

energy per nucleon for pre-fragments $< E^*/A_{PF} >$. Such trend is more visible in correlation between $< E^*/A_{PF} >$ and Z_{bound}, and more details of such analysis can be found in the published article [Gor19].

The comparison of SPALADiN data with the simulated events by decomposition technique allows us to deduce a deficiency of the models in description of coincidences (1) and (2). Such statement is valid for following nucleus-nucleus collision $^{136}Xe + ^{12}C$ at 1 AGeV. Both types of emissions, either neutrons or neutron-alpha coincidences correspond to peripheral collisions characteristic for evaporation of light particles. The most significant divergence of models was observed for $Z_{bound} > 40$. In the case of events accompanied by emissions of types (3) – (5), i.e. fragmentation channel, we got

systematically under-predicted cross sections resulting from all models.

Appendix

Complete results of SPALADiN experiment are discussed in the paper T. Gorbinet et al. [Gor19]. In this sub-chapter I pointed out some of the most important results of the experiment and simulations. Besides elemental production cross sections also other properties of reactions can be found in the article, such as correlations between excitation energy per nucleon and pre-fragment atomic number, i.e. E^*/A_{PF} vs. Z_{bound}, and the total multiplicity of neutrons corresponding to average excitation energy of pre-fragments $<E^*/A_{PF}>$ was reconstructed. We observed very similar behavior for both of reactions in neutron multiplicity spectra. The results on neutron multiplicity provided a confirmation of the of two-step mechanism of spallation reactions, which is basic idea for any simulations. Reflecting the relatively high excitation energies for each Z_{bound} in spallation reaction, the evaporation cascade consists of many steps, and therefore multiplicity spectra is spreading over 30 neutrons. Moreover, the evolution of neutron multiplicity spectra observed for ^{136}Xe + p differs from simulated ones, mainly in the region of low neutron multiplicity of 1 - 10 neutrons per cascade. We found that if mass and charge mean values of pre-fragments, $<A_{PF}>$ and $<Z_{PF}>$, formed at the end of intra-nuclear cascade are shifted to lower ones, than simulated total multiplicity spectra by de-excitation models are better comparable to measured ones. This fact results from INCL++ properties. The effect of sharp decrease of neutron multiplicity was not observed in the reaction ^{136}Xe + ^{12}C in such strong way as in previous one reaction.

4.5.6 Discussion

In this study we confront models (INCL++, ABLA07, GEMINI++, SMM) with SPALADiN data [Gor19] measured recently in inverse kinematics and put them under the pressure, to see their strong and weak sides. The results demonstrated above indicate much weaker prediction power of investigated models in nucleus-nucleus collision ^{136}Xe + ^{12}C at 1 AGeV compared to nucleon-nucleus reaction ^{136}Xe + p at 1 AGeV. For the first reaction the best reproduction of SPALADIN data is provided by INCL ++ + SMM, but still with strong discrepancy below atomic number Z < 40. The latter reaction was relatively well reproduced for Z > 30 by all the de-excitation models combined with INCL++. In the best agreement with SPALADiN data at Z = 10-30 seem to be GEMINI++ model. On other hand, ABLA07 and SMM models at that interval were in good agreement with Napolitani et al. [Nap07]. The experimental results and simulation show that evaporation is still dominant at incident energy of 1 AGeV.

As for INCL++ model, the main discrepancy with SPALADiN data is observed in multiplicity spectra [Gor19]. Compared to SPALADiN data one can observed the lower multiplicity in de-excitation spectra of pre-fragments corresponding to lower excitation energies in the reaction ^{136}Xe + p. This effect can be explained as non-sufficient loss of nucleons within intra-nuclear cascade of INCL++ during spallation reaction. Such effect was not observed in the reaction ^{136}Xe + ^{12}C.

Each time when we use any model which is considered as reliable, it can work properly only at some conditions and for specific reactions. To improve prediction power of models and to expand application for larger amount of reactions, experiments such as SPALADiN will always play a crucial role in fixing of physical parameters of models.

Chapter 5

Conclusions

The presented work is closely connected with very topical fields of nuclear physics, such as properties of very asymmetric nuclear matter far off stability studied in the context of equation of state, and production possibilities of exotic nuclei. The results are divided to four topics related with investigation of equation of state of nuclear matter, and possibilities of production of radioactive ion beams via two most promising reaction mechanisms, i.e. spallation/fragmentation and deep-inelastic transfer reactions. The results of main topics of this thesis are discussed below:

- *Investigation of fusion hindrance in reactions leading to production of super heavy elements:*
  In the framework of the semi-classical microscopic model of Boltzmann-Uehling-Uhlenbeck (BUU), the equation of state of nuclear matter has been studied based on the reaction dynamics of heavy ion collisions above the Coulomb barrier leading to production of super-heavy elements. Pauli blocking for protons and neutrons is included and Coulomb interaction is considered as well. We prove that besides heavy ion collisions at intermediate and high energies, and collective excitation such as Isoscalar Giant Monopole Resonances (ISGMR), the equation of state of nuclear matter can also be studied in low energy heavy ion collisions. Specifically, we focused on central collisions leading to production of super-heavy elements or to quasi-fission, where equation of state parameters were refined to reproduce fusion probabilities P_{CN} stated in the table 4.1. Based on the presented study, fission and quasi-fission dynamics is evidently sensitive on modulus of incompressibility K_0 and density dependence of symmetry energy γ.

  Moreover, we went even further and from the experimental fusion probabilities P_{CN} of production of compound nucleus we constrain the equation of state of nuclear matter for reactions, where spherical and deformed target nuclei were used. The fusion vs. quasi-fission dynamics was studied at manifold initial conditions with various mass and charge asymmetry, leading to hot and cold fusion above the Coulomb barrier. The compound systems from Z = 102 (fusion still dominant) to Z = 120 (almost pure quasi-fission) were considered. The constraint what we derived varied within incompressibility parameter K_0 = 240 – 260 MeV and density dependence of symmetry energy γ = 0.6 – 1.0 [Ves16]. Such a result implies that di-nuclear system (DNS) formed in collision is governed by stiffer equation of state, where maximum compression density reaches 1.4 – 1.5 of saturation density. Evolution of nucleonic density shows that scission time, when DNS system usually splits two fragments, is around 1300 fm/c. This value is in a good agreement with TDHF simulations from Sekizawa et al. [Sek16] and ImQMD simulations of Choudhury et al. [Cho14]. Characteristics, such as kinetic energy of fragments of quasi-fission from ^{64}Ni +

^{208}Pb and ^{48}Ca + ^{238}U seem to be in compliance with [Sek16]. As spin dependence is not incorporated to single-particle mean field (isospin-dependent) in BUU model, shell effects are not considered. Hence, the influence of microscopic effects cannot be evaluated. Anyway, the dependence of dynamics on shell effect is probably not so simple, and can be manifested differently for fusion and quasi-fission channel, and differ from one reaction to another. As far as deformation of nuclei, the recent measurement had shown the dependence of quasi-fission probability on deformation in entrance channel of reaction [Wak14]. Because the constraint on equation of state derived in our wok is quite narrow, one can expect that shell effects should not contribute in very significant way. More experimental data are still necessary in order to make even more strict constraint. Besides the quality of data, some model improvements, related with shell effects and quantum-mechanical fluctuations are required as well.

In order to verify these results and evaluate the influence of quantum-mechanical fluctuations on fusion and quasi-fission dynamics the simulations using the Constrained Molecular Dynamics (CoMD) were performed. CoMD simulations are complementary to BUU model calculations. Both of models use approximation of the Boltzmann equation, incorporating single-particle mean field of Skyrme-type, and the Pauli principle separately for protons and neutrons is restored, with consideration of the Coulomb interaction. Similar to BUU, the shell effects and deformation of nuclei are not implemented in CoMD model. Main difference between models relates with handling of uncertainties in phase space of nucleons. In CoMD model each nucleon is considered as wave packet with dispersion in coordinate space σ_r, and dispersion in linear momentum space σ_p. This property is not included in BUU model, where fluctuations vanish due to test particle method of Wong [Won82]. Among others, in CoMD the effective nucleon-nucleon interaction is extended by the surface term and the Coulomb term, and also the collision integral is evaluated in a different way. Despite of quantum-mechanical fluctuations in CoMD model, and presented similarities and differences with BUU model, the constraint of equation of state of nuclear matter agrees with those from BUU simulations, i.e. K_0 = 245 – 254 MeV and γ = 0.6 – 1.0 [Kli19]. It should be noted that such compliance between models is not trivial. Also one should mentioned that the constraint set via CoMD simulations is a bit looser due to four parameters [K_0, γ, surface parameter C_s, σ_r] instead of two free parameters [K_0, γ].

The recent astrophysical event GW170817 [Abb17], [Put19], where a massive neutron star appear to be formed, is well reproduced by simulations where incompressibility of nuclear matter K_0 = 245 was considered [Per19]. Taking into account another constraints of equation of state, i.e. K_0 = 231 ± 5 MeV [You99], K_0 = 230 – 265 MeV [Gle00], [Web99], one can expect that stiffer parameterization suits the observable reality better than versions with softer parameters.

- *Deep-inelastic transfer reactions & HIE - ISOLDE facility:*
  Evident lack of of n-rich data for Z > 60 has not been resolved by fragmentation/spallation reactions or using induced fission till the present. The most n-rich isotopes from the region of Z = 60 – 70 have been produced via fragmentation reaction, ^{238}U + ^{9}Be at 1 AGeV, with cross sections of few nb for the most n-rich nuclei.

  In the present work three deep-inelastic transfer reactions are suggested to

improve production cross sections of nuclei with atomic numbers Z = 65 - 70: ^{170}Ho + ^{238}U, ^{177}Yb + ^{238}U, ^{180}Hf + ^{238}U at 8AMeV. The simulations performed using transport model DIT and statistical model SMM indicate that to more than 13 new isotopes (Z = 65 - 70) can be produced with production cross sections varies from 0.1 to 10 μb. Post-accelerator of new generation already installed at ISOLDE facility enables to re-accelerate low energy radioactive ion beams coming from spallation target up to 10 AMeV. Thus this goal can be achieved by secondary beams ^{170}Ho, ^{177}Yb and ^{180}Hf at available intensities ~ 10^6μC. From experimental point of view, very sensitive technique has to be applied for complete identification of transfer products. This could be possible with ISOLDE Solenoidal Spectrometer (ISS) capable of complete identification A, Z of transfer products, and measurement of reaction kinematics and Q values. The simulations presented in this work can be used for experiments with n-rich exotic nuclei using secondary deep-inelastic transfer reactions, and may provide guidance for real experiments in the future.

- *Spallation & HIE-ISOLDE facility:*
  The next generation of radioactive ion beam facilities, including HIE-ISOLDE, SPES-INFN and SPIRAL2 (leading to EURISOL-DF) will enable the study of reactions of astrophysical importance. Two aspects of spallation reactions have been studied in this work using the Monte Carlo code ABRABLA07. One is influence of incident energy of protons triggering spallation-evaporation, spallation-fission or spallation-fragmentation inside of thick ISOLDE targets. The second aspect relates with different materials which possibly can improve production cross sections of lighter exotic nuclei such as n-rich isotopes of Li, Na, Mg, Si or Ca.

  Simulation with 1.4 and 2.0 AGeV proton beam on thick uranium target ^{238}U(Cx) indicate that higher incident energy can improve cross section of isotopes with Z < 25 and Z > 60. These regions are characteristic for nuclei produced in spallation-evaporation and spallation-fragmentation. The highest gain was observed mainly for n-deficient isotopes, products of spallation-evaporation, and intermediate mass fragments, originating in spallation-fragmentation. As for fission products, higher incident energy does not lead to higher production rate.

  Enhancement of cumulative production cross sections in spallation of light targets of ^{12}C, ^{28}Si, ^{40}Ca and ^{48}Ti has been also investigated compared to uranium target ^{238}U(Cx). Especially production cross sections of elements such as O, Mg and Ar seem to be one order of magnitude over those observed in spallation of uranium target. Thus spectroscopy of some n-rich isotopes from "Island of inversion" could serve as a good motivation to use spallation targets of light isotopes such as ^{12}C, ^{28}Si, ^{40}Ca and ^{48}Ti.

- *SPALADiN experiment, ^{136}Xe + p and ^{136}Xe + ^{12}C at 1AGeV:*
  The given reactions have been studied in inverse kinematics using large-acceptance detectors of SPALADiN setup, in GSI Darmstadt. A big-aperture dipole magnet in combination with large-acceptance detectors enables to measure coincidences of final-state charged particles and fragments ($Z \geq 2$) and neutrons. Excitation energies of pre-fragments were estimated, and multiplicity of neutrons as a function of excitation energy and atomic number of pre-fragments was studied as well. The cumulative or elemental production cross

sections were compared with available data and theoretical models.

The light fragment (Z < 25) from the reaction ^{136}Xe + ^{12}C were identified for the first time [Gor19]. Heavier fragment data from this reaction and data from the reaction ^{136}Xe + p have already existed and were compared with available data. SPALADiN data are also confronted with theoretical models. Intra-nuclear cascade model INCL++ is combined with one of the three statistical models for calculation of de-excitation phase, i.e. ABLA07, GEMINI++ and SMM. A good agreement of INCL++ in a pair with given statistical models was observed for fragments Z > 30 in the reaction ^{136}Xe + p. Cumulative cross sections for intermediate mass fragments, mainly with Z = 10 – 30, are reproduced reliably only by GEMINI++ and other two models are in better compliance with the data measured by Napolitani et al. [Nap07]. On the other hand, such a level of agreement between models and SPALADiN data was not achieved in the second reaction ^{136}Xe + ^{12}C. In this case, SMM model can only describe experimental data of heavier fragments, Z > 40, and at lower atomic numbers one can see significant discrepancies. ABLA07 and GEMINI++ provide less reliable results over whole range of atomic numbers. Therefore, some model improvements are necessary for all studied statistical models, but this is beyond the scope of this thesis. Some enhancement is requested also for INCL++ model, as we observed discrepancies related with low neutron multiplicity for pre-fragments with lower excitation energy. From the analysis of experimental data from SPALADiN experiment, evaporation de-excitation channel is still dominant, what was confirmed in both reactions.

Simulations provided in this thesis allow to constrain equation of state of nuclear matter using a new methodology, where experimentally measured fusion probabilities from reactions leading to production super-heavy element are used for the first time [Ves16], [Kli19]. Within our systematic study of fusion hindrance in synthesis of super-heavy elements, we observed to a strong sensitivity of surface and neck region of di-nuclear system on parameters equation of state K_0, γ, respectively. Besides properties of nuclear matter, this thesis provides guidance for promising mechanism of exotic nuclei production, i.e. spallation and deep-inelastic transfer reactions, which are currently used or may be utilized in order for production of exotic nuclei far from stability. Finally, theoretical models used for calculation in spallation/fragmentation reactions are confronted with recently measured experimental data.

Publications in refereed articles

1. **Constraining the equation of state of nuclear matter from competition of fusion and quasi-fission in the reactions leading to production of the superheavy elements**
   M. Veselský, J. Klimo, Yu-Gang Ma, G. A. Souliotis
   Phys. Rev. C. **94**, 064608 (2016)

2. **Simulation of fusion and quasi-fission in nuclear reactions leading to production of superheavy elements using the Constrained Molecular Dynamics model**
   J. Klimo, M. Veselský, G. A. Souliotis, A. Bonasera
   Nucl. Phys. A **992**, 121640 (2019)

3. **Study of the reaction mechanisms of ^{136}Xe + p and ^{136}Xe + ^{12}C at 1 AGeV with inverse kinematics and large-acceptance detectors**
   Thomas Gorbinet, Orlin Yordanov, Jean-Eric Ducret, Thomas Aumann, Yassid Ayyad, Sébastien Bianchin, Olga Borodina, Alain Boudard, Christoph Caesar, Enrique Casarejos, Bronislav Czech, Stanislav Hlavac, Jozef Klimo, Nikolaus Kurz, Christoph Langer, Tudy Le Bleis, Sylvie Leray, Jerzy Lukasik, Davide Mancusi, Piotr Pawlowski, Stéphane Pietri, Christopher Rappold,
   Marie-Delphine Salsac, Haik Simon, and Martin Veselsky
   Eur. Phys. J. A **55,** 11 (2019)

4. **New systematic features in the neutron-deficient Au isotopes**
   M. Venhart, J. L. Wood, M. Sedlák, M. Balogh, M. Bírová, A. J. Boston, T. E. Cocolios, L. J. Harkness-Brennan, R-D Herzberg, L. Holub, D. T. Joss, D. S. Judson, J. Kliman, J. Klimo, L. Krupa, J. Lušnák, L. Makhathini, V. Matoušek, Š. Motyčák, R. D. Page, A. Patel, K. Petrík, A. V. Podshibyakin, P. M. Prajapati, A. M. Rodin, A. Špaček, R. Urban, C. Unsworth and M. Veselský
   J. Phys. G: Nucl. Part. Phys. **44,** 074003 (2017)

5. **Identification of a 6.6μs isomeric state in ^{175}Ir**
   S. A. Gillespie, A. N. Andreyev, M. Al Monthery, C. J. Barton, S. Antalic, K. Auranen, H. Badran, D. Cox, J. G. Cubiss, D. O' Donnell, T. Grahn, P. T. Greenlees, A. Herzan, E. Higgins, R. Julin, S. Juutinen, J. Klimo, J. Konki, M. Leino, M. Mallaburn, J. Pakarinen, P. Papadakis, J. Partanen, P. M. Prajapati, P. Rahkila, M. Sandzelius, C. Scholey, J. Sorri, S. Stolze, R. Urban, J. Uusitalo, M. Venhart, and F. Weaving
   Phys. Rev. C **99**, 064310 (2019)

Other publications

1. **Opportunities for nuclear reaction studies at future facilities**
   Martin Veselský, Jozef Klimo, Nikoleta Vujisicova and Georgios A. Souliotis
   Conference Istros 2015, arXiv:1604.01961

2. **Direct measurement of fission barrier height of unstable heavy nuclei at ISOL facilities**
   J. Klimo, M. Veselský, R. Raabe, A. N. Andreyev, M. Huyse, P. Van Duppen, F. Renzi, K. Nishio, H. Makii, I. Nishinaka, S. Chiba, G. Souliotis, T. Grahn, P. T. Greenlees, J. Pakarinen, P. Rahkila, M. Venhart, J. Kliman, S. Hlavac, V. Matousek, L. Krupa, I. Sivacek, D. Klc, M. Sedlak, E. Rapisarda, the ACTAR TPC Collaboration
   Proceedings of the HNPS2018, the 27th Annual Symposium of the Hellenic Nuclear Physics Society

3. **EoS studies in nucleus-nucleus collisions: from Coulomb barrier to LHC**
   M. Veselsky, J. Klimo, G. A. Souliotis, X. G. Deng, Y. G. Ma, M. Ploskon
   Proceedings of the 4th Workshop on New Aspects and Perspectives in Nuclear Physics, May 5-6, 2017 - Ioannina, Greece

Bibliography

[Abb17] B. P. Abbott et al., Phys. Rev. Lett. 119, 161101 (2017).

[Abd01] H.A. Abderrahim et al., Nucl. Instrum. Methods A 463, 487 (2001).

[Ada97] G. G. Adamian et al., Nucl. Phys.A 618, 176 (1997).

[Ada97] G. G. Adamian et al., Nucl. Phys. A 627, 361 (1997).

[Ada98] G. G. Adamian et al., Nucl. Phys. A 633, 409 (1998).

[Ago03] S. Agostinelli et al., Nucl. Instrum. Meth. A 506, 250 (2003).

[Aic91] J. Aichelin, Phys. Rep. 202, 233 (1991).

[Ari12] Y. Aritomoet et al., Phys. Rev. C 85, 044614 (2012).

[Art02] A. G. Arthuk et al., Nucl. Phys. A 701, 96c-99c (2002).

[Arm04] P. Armbruster et al., Phys. Rev. Lett. 93, 212701 (2004).

[Aud05] Audouin et al., arXiv nucl-ex/0503021.

[Bar85] E. Baron et al., Nucl. Phys. A 4.40, 744 (1985); Phys. Rev. Lett. 55, 126 (1985).

[Bas93] S. A. Bass et al., Phys. Rev. Lett. 71, 1144 (1994).

[Ben98] J. Benlliure et al., Nucl. Phys. A 628, 458 (1998).

[Ber03] M. Bernas et al., Nucl. Phys. A 725, 213 (2003).

[Ber06] M. Bernas et al., Nucl. Phys. A 765, 197 (2006).

[Ber71] H. W. Bertini et al., Nucl. Phys. A 169, 670 (1971).

[Ber88] G. F. Bertsch et al., Phys. Rep. 160, No. 4, 189-233 (1988).

[Bin87] W.R. Binns et al.,Phys. Rev. C 36, 1870 (1987).

[Ble99] M. Bleicher et al., J. Phys. G: Nucl. Part. Phys. 25, 1859 (1999).

[Boc82] R. Bocket et al., Nucl. Phys. A 388, 334 (1982).

[Boh39] N. Bohr et al., Phys. Rev. 56, 426 (1939).

[Bon91] A. Bonasera et al., Phys. Rep. 202, 233 (1991).

[Bon94] A. Bonasera, Phys. Rep. 243, 1-124 (1994).

[Bon95] J. P. Bondorf et al., Phys. Rev. 257, 133 (1995).

[Bou02] A. Boudard et al., Phys. Rev. C 66, 044615 (2002).

[Bou13] A. Boudard et al., Phys. Rev. C 87, 014606 (2013).

[Cat03] R. Catherall et al., The ISOLDE Collaboration, Nuclear Instruments and Methods in Physics Research B204, 235-239 (2003).

[Cha88] R. J. Charity et al., Nucl. Phys. A 483, 371 (1988).

[Cha10] R. J. Charity et al., Phys. Rev. C 82, 014610 (2010).

[Che07] P. Chesny et al., SPALADiN target user and safety report (2007).

[Cho14] R. K. Choudhury et al., Phys. Lett. B 731, 168 (2014).

[Cor04] L. Corradi, et al., Nucl. Phys. A 734, 237 (2004).

[Cug81] J. Cugnon et al., Nucl. Phys. A 352, 505 (1981).

[Cug03] J. Cugnon et al., Eur. Phys. J. A 16, 393-407 (2003).

[Cun02] A. Cunsolo et al., Nucl. Instrum. Meth. A 481, 48 (2002).

[Dav11] J.C. David et al.,in SATIF 10 Workshop Proceedings (OECD Publishing, 2011) p. 273.

[Enq01] T. Enqvist et al., Nucl. Phys. A 686, 481 (2001).

[Enq02] T. Enqvist et al., Nucl. Phys. A 703, 435 (2002).

[ESS] https://europeanspallationsource.se, The European Spallation Source.

[Fer05] Fernandez-Dominguez et al., Nucl. Phys. A 747, 227-267 (2005).

[Gai91] J.-J. Gaimard et al., Nucl. Phys. A 531, 709 (1991).

[GEANT] GEANT4 Collaboration, http://geant4.cern.ch.

[Gen08] E. Le Gentil et al., Phys. Rev. Lett. 100, 022701 (2008).

[Gia69] M. Giacomelli et al., Phys. Rev. C 6, 1-11 (1969).

[Gia13] G. Giardina et al., Nucl. Scie. Tech. 24, 050519 (2013).

[Gle00] N. K. Glendenning, Compact stars, 2nd edition, Springer-Verlag, (2000).

[God19] K. Godbey et al., arXiv:1906.07623v1.

[Gol09] C. Golabek et al., Phys. Rev. Lett. 103, 042701 (2009).

[Gor19] T. Gorbinet et al., Eur. Phys. J. A 55, 11 (2019).

[Got14] A. Gottberg et al., Experimental tests of an advanced proton-to-neutron converter at ISOLDE-CERN, Nuclear Instruments and Methods in Physics Research B336, 143-148 (2014).

[Gro75] D. H. E. Gross et al., Phys. Rep. 45, 175 (1975).

[Gro97] D. H. E. Gross et al., Phys. Rep. 279, 119 (1997).

[Gut68] M. P. Guthrie et al., Nucl. Instrum. Meth. 66, 29 (1968).

[Han51] O. Kofoed-Hansen et al., Phys. Rev. 82, 96 (1951).

[Hel03] K. Helariutta et al., Eur. Phys. J. A 17, 181 (2003).

[Hau52] W. Huaser et al., Phys. Rev. 87, 366 (1952).

[Hof98] S. Hofmann, Rep. Prog. Phys. 61, 639 (1998).

[Hub91] J. Hubele et al., Z. Phys. A 340, 263 (1991).

[IAE08] https://www-nds.iaea.org/publications/indc/indc-nds-0530/
Proceedings of the Advanced Workshop on Model Codes for Spallation Reactions, ICTP Trieste, Italy, 4-8 February 2008. D. Filges et al., IAEA INDC(NDS)-530, Vienna, August 2008.

[ISO12] ISOLDE yield database, http://isoyields-classic.web.cern.ch/query_tgt.htm

[Itk03] M.G. Itkis et al., Yad. Fiz. 66, 1154 (2003), Phys. At. Nucl. 66, 1118 (2003).

[Itk07] M. G. Itkis et al., Nucl. Phys. A787, 150 (2007).

[Jun98] A. R. Junghans et al., Nucl. Phys. A 629, 635 (1998).

[Jur03] B. Jurado et al., Phys. Lett. B 533, 186 (2003).

[Kad17] Y. Kadi et al., Proceedings of IPAC2017, Copenhagen, Denmark.

[Kad18] Y. Kadi et al., CERN Yellow Reports: Monographs, Vol 1 (2018), CERN-2018-002-M.

[Kau80] S. B. Kaufman et al., Phys. Rev. C 22(1), 167 (1980).

[Kel08] A. Kelič et al., J. Phys. G 35, 035104 (2008).

[KEL08] A. Kelic et al.,in Joint ICTP-IAEA Advanced Workshop on Model Codes for Spallation Reaction (IAEA, Trieste, Italy, 2008) p. 181.

[Kel09] A. Kelic et al., arXiv:0906.4193.

[Kli19] J. Klimo et al., Nucl. Phys. A 992, 121640 (2019).

[Kny08] G. N. Knyazheva et al., PEPAN Lett. 5, 40 (2008).

[Koe02] U. Koester, Eur. Phys. J. A 15, 255 (2002).

[Kot95] A.A. Kotov et al., Nucl. Phys. A 583, 575 (1995).

[Koz10] E. M. Kozulin et al., Phys. Lett. B 686, 227(2010).

[Kre03] P. Kreutz et al., Nucl. Phys. A 556, 672 (1993).

[Kur12] J. Kurcewicz et al., Phys. Lett. B 717, 371-375 (2012).

[Lat07] J. M. Lattimer et al., Phys. Rep. 442, 109 (2007).

[Ler11] S. Leray et al., Phys. Soc. 59, 791 (2011).

[Ler13] S. Leraz et al., J. Phys. Conf. Series 420, 012065 (2013).

[Li93] G.Q. Li et al., Phys. Rev. C 48, 1702 (1993).

[Li94] G.Q. Li et al.,Phys. Rev. C 49, 566 (1994).

[Lui12] R. Luis et al., Eur. Phys. J. A 48, 90 (2012).

[Man14] D. Mancusi et al.,Phys.Rev. C 90, 054602 (2014).

[Mar02] T. Maruyama et al., Eur. Phys. J. A 14, 191 (2002).

[Mor75] L. G. Moretto, Nucl. Phys. A 247, 211 (1975).

[Nap04] P. Napolitani et al., Phys. Rev. C 70, 054607 (2004).

[Nap07] P. Napolitani et al.,Phys. Rev. C 76, 064609 (2007).

[NapPhD] P. Napolitani, PhD thesis, (Universite de Paris XI, France, December 2003).

[Nat02] J.B. Natowitz et al.,Phys. Rev. C 65, 034618 (2002).

[Nis10] K. Nishio et al., Phys. Rev. C 82, 044604 (2010).

[Nör74] W. Nörenberg, Phys. Lett. 53 B, 289 (1974).

[Nör75] W. Nörenberg, Z. Phys. A 274, 241 (1975).

[NNDC] https://www.nndc.bnl.gov/

[Nun15] J. Alcántara-Núñez et al.,Phys. Rev. C 92, 054602 (2015).

[Obe14] V. E. Oberacker et al., Phys. Rev. C 90, 054605 (2014).

[Oga04] Y.T. Oganessian et al., Phys. Rev. C 69, 054607 (2004).

[oga04] Y.T. Oganessian et al., Phys. Rev. C 70, 064609 (2004).

[Oga06] Y.T. Oganessian et al., Phys. Rev. C 74, 044602 (2006).

[Oga07] Y.T. Oganessian et al., Phys. Rev. C 76, 011601 (R) (2007)

[Oga12] Y.T. Oganessian et al., Phys. Rev. Lett. 109, 162501 (2012).

[Oga13] Y.T. Oganessian et al., Phys. Rev. C 87, 014302 (2013).

[Oga13] Y.T. Oganessian et al., Phys. Rev. C 87, 054621 (2013).

[Pap01] M. Papa et al., Phys. Rev. C 64, 024612 (2001).

[Pap05] M. Papa et al., J. Comp. Phys. 208, 403 (2005).

[Par88] S. Parker, Nucl. and Part. Phys. Source Book, NY: McGraw-Hill, 1988.

[Per19] A. Pergo et al., arXiv:190307898.

[Pro08] E. Prokhorova et al., Nucl. Phys. A 802, 45 (2008).

[PSB12] https://indico.cern.ch/conferenceDisplay.py?confId=194629,
40years anniversary of PSB, Oct 2012.

[Put19] M. van Putten et al., Monthly Notices of the Royal Astronimical Society: Letters. 482 (1): L46-L49 (2019); arXiv:1806.02165.

[Ran78] J. Randrup, Nucl. Phys. A 307, 319-348 (1978).

[Ran79] J. Randrup, Nucl. Phys. A 327, 490-516 (1979).

[Rei68] R. V. Reid, Annals of Physics 50, 411–448 (1968).

[Ric06] M. V. Ricciardi et al., Phys. Rev. C 73, 014607 (2006).

[Rie13] R. du Rietz et al., Phys. Rev. C 88, 054618 (2013).

[Sav99] H. Savajols et al., Nucl. Phys. A 654, 1027c (1999).

[Sek16] K. Sekizawa et al., Phys. Rev. C 93, 054616 (2016).

[Sie85] A. Sierk, Phys. Rev. Lett. 55, 582 (1985).

[Sie87] P. Siemens, Nature 305, 410 (1983) .

[Sch91] K.-H. Schmidt et al., Nucl. Phys. A 531, 709 (1991).

[Sch02] K.-H. Schmidt et al., Nucl. Phys. A 710, 157 (2002).

[Sha88] M. M. Sharma et al., Phys. Rev. C 38, 2562 (1988).

[Sou02] G.A. Souliotis, et al., Phys. Lett. B 543, 163 (2002).

[Sou03] G.A. Souliotis, et al., Phys. Rev. Lett. 91, 022701 (2003).

[Stef02] A.M. Steanini et al., Nucl. Phys. A 701, 217 (2002).

[Sto86] R. Stock, Phys. Rep. 135, 259 (1986).

[Sum00] K. Summerer et al., Phys. Rev. C 61, 34607 (2000).

[Tai03] J. Taieb et al., Nucl. Phys. A 724, 413 (2003).

[Tas91] L. Tassan-Got et al., Nucl. Phys. A 524, 121-140 (1991).

[Ves00] M. Veselsky, et al., Phys. Rev. C 62, 064613 (2000).

[Ves02] M. Veselsky, Nucl. Phys. A 705, 193 (2002).

[Ves06] M. Veselsky et al., Nucl. Phys. A 765, 252-261 (2006).

[Ves11] M. Veselsky et al., Nucl. Phys. A 872, 1-12 (2011).

[Ves13] M. Veselsky, Acta Physica Slovaca, vol. 63, no. 1&2, Nuclear reactions wih heavy ion beams.

[Ves16] M. Veselsky et al., Phys. Rev. C 94, 064608 (2016).

[Vil03] C. Villagrasa-Canton, PhD thesis (Universite de Paris XI, France, September 2004).

[Von15] N. Vonta et al., Phys. Rev. C 92, 024616 (2015).

[Wak14] A. Wakhle et al., Phys. Rev. Lett. 113,182502 (2014).

[Wan02] N. Wang et al., Phys. Rev. C 65, 064608 (2002).

[Wan13] N. Wang et al., Nucl. Scie. Tech. 24, 050520 (2013).

[Wat13] Y. X. Watanabe et al., Nucl. Instr. Meth. B 317, 752 (2013).

[Web90] F. Weber, Pulsars as Astrophysical Laboratories for Nuclear and Particle Physics, IOP Publishing (1990).

[Wei40] V.F. Weisskopf et al., Phys. Rev. 57, 472 (1940).

[Won82] C.Y. Wong, Phys. Rev. C25, 1460 (1982).

[Yas10] Z. Yasin et al., Annuals of Nuclear Energy 37, 87-92 (2010).

[Yar81] Y. Yariv et al., Phys. Rev. C 24, 488 (1981).

[You99] D. H. Youngbloo et al., Phys. Rev. Lett. 82, 691 (1999).

[Zag05] V. Zagrebaev et al., J. Phys. G 31, 825 (2005).

[Zag07] V. Zagrebaev et al., J. Phys. G 34, 1 (2007).

[Zag07] V. Zagrebaev et al., J. Phys. G 34, 2265 (2007).

[Zag11] V. I. Zagrebaev et al., Phys. Rev. C 83, 044618 (2011).

[Zha99] F. S. Zhang et al., Phys. Rev. C 60, 064604 (1999).

[Zha08] F. S. Zhanget et al., Nucl. Phys. A 802, 91 (2008).